ANALYSIS AND DESIGN OF MULTIPLE ORDER CENTRIFUGAL PENDULUM VIBRATION ABSORBERS

By

Brendan James Vidmar

A DISSERTATION

Submitted to
Michigan State University
in partial fulfillment of the requirements
for the degree of

DOCTOR OF PHILOSOPHY

Mechanical Engineering

2012

ABSTRACT

ANALYSIS AND DESIGN OF MULTIPLE ORDER CENTRIFUGAL PENDULUM VIBRATION ABSORBERS

By

Brendan James Vidmar

Impending government fuel economy standards are causing automobile manufacturers to consider innovative ways to increase the average fuel economy of their fleets. In many cases, as discussed in this study, automakers are required to push their engine operating conditions to levels not previously considered. One constraint which limits the engines to operate efficiently and salable in these conditions is torsional vibrations. Centrifugal Pendulum Vibrations Absorbers (CPVAs) are devices used to reduce the levels of these undesirable torsional vibrations without decreasing performance.

In this study, we consider nonlinear interactions in systems of order-tuned torsional vibration absorbers with sets of absorbers tuned to different orders. In all current applications, absorber systems are designed to reduce torsional vibrations at a single order; however, when two or more excitation orders are present and absorbers are introduced to address different orders, nonlinear interactions become possible under certain resonance conditions. Under these conditions, a common example of this phenomenon occurs for orders n and $2n$ where crosstalk between the absorbers, acting through the rotor inertia, can result in instabilities that are detrimental to system response. In order to design absorber systems that avoid these interactions and to explore possible improved performance with sets of absorbers tuned to different orders, we develop predictive models that allow one to examine the effects of absorber mass distribution and tuning. These models are based on perturbation methods applied to the system equations of motion ultimately yielding system response features as

a function of parameters of interest, notably absorber and rotor response amplitudes and stability. The model-based analytical results are compared with numerical simulations of the complete nonlinear equations of motion and are shown to be in good agreement. In addition, experimental absorbers at multiple orders were designed and tested on a controlled spin rig. The experimental data is found to be in good agreement with the analytical predictions, thus verifying the numerical and analytical studies. These results are useful for the selection of absorber parameters to achieve desired performance. For example, they allow for approximate closed form expressions for the ratio of absorber masses at the two orders that yield optimal performance. It is also found that utilizing multiple order absorber systems can be beneficial for system stability, even when only forcing at one order.

In a related study, we develop relatively simple predictive formulations describing the absorber and rotor dynamics. We do this by assuming specific forms about the absorber response in order to simplify the steady state analysis of absorber systems. Utilizing these assumptions, along with physically relevant scalings, the harmonics in the system can be balanced and thus yield these predictive closed form expressions. Although unable to capture all of the subtle system instabilities, these expressions are found to accurately capture both the steady-state absorber response as well as the harmonically rich rotor response for a wide range of absorber configurations, as confirmed by both numerical and experimental data. This analysis provides accurate and simple descriptions of the system dynamics. These descriptions are useful for selection of important system parameters when designing such systems and are generalized to account for single or multiple order absorber systems.

ACKNOWLEDGMENTS

The five and a half years I have spent as a graduate student at MSU has been both a gratifying, and at times, trying experience. I would not have been to able to get through it without the support of my advisors, Steve Shaw and Brian Feeny. Professor Shaw is not only a master of dynamical systems, but someone whose advice I would heed in all aspects of life. Professor Feeny is one of the kindest men you will ever meet and his expertise was invaluable. I would also like to thank Professors Xiaobo Tan and George Zhu for serving on my committee.

Thanks goes Nick Miller, Scott Strachen, Pavel Polunin, Thomas Theisen and Ryan Monroe whose fruitful discussions helped form many of the ideas in this study. A special thanks must also be handed out to Abhisek Jain, who spent many a long night with me conducting experiments in the lab. Professor Alan Haddow was instrumental in setting up the experimental device, and continued to offer advice throughout the course of this study. The undergraduate assistants who Professor Shaw continually was able to pull out of his talent pool helped me in numerous ways, and if these students are representative of the aspiring engineers in this country, I am excited for the future. These students were Jelena Paripovic, Brian Rockwell, J. T. Whitman, Bara Aldasouqi, and Cody Little.

Bruce Geist of Chrysler LLC collaborated on much of this work, is a member of my committee, and our weekly meetings allowed for an insight in the practical applications of torsional vibration absorbers. I must also thank Chrysler LLC for funding throughout my time here, and Kiranmaye Aluru for helping machine the experimental absorbers.

I would also like to thank Jeff Chottiner and John Brevick at Ford Motor Company for allowing me some first-hand experience in automotive design and testing of torsional vibration absorbers as well as monetary support.

A final thanks goes out to the National Science Foundation (Grant Number CMMI-1100260) who's support funded much of the work.

TABLE OF CONTENTS

LIST OF TABLES

LIST OF FIGURES

Chapter 1

Introduction

Vibration reduction in rotating machinery has long been an area of study in both industrial and academic settings [11, 20, 21, 35]. An inherent difficulty in solving issues relating to torsional vibrations is, in many applications, the rotating inertia and associated damping are desired to be as small as possible for maximum performance. Both of these properties, although necessary for good performance, can lead to troublesome torsional vibrations. Several well-researched methods have been employed to attenuate these torsional vibrations, which include adding inertia in the form of flywheels, utilizing energy dissipation through torsional dampers, employing frequency tuned dual mass flywheels, and the use of order tuned Centrifugal Pendulum Vibration Absorbers (CPVAs). Due to the stringent efficiency demands now present in some rotating machinery, such as internal combustion engines, adding inertia and dissipating energy are not feasible. Also, as dual mass flywheels are tuned to a certain frequency, that is an engine order excitation at a specific rotational velocity, their performance is limited to very specific conditions. CPVAs dissipate very little energy, are tuned to an order, and, as will be explained in more detail further, can be very beneficial in reducing the amplitude of torsional vibrations.

CPVAS are passive devices that have been shown to significantly reduce torsional vibrations in rotating machinery that arise from engine order excitation [12, 21]. Such machinery includes internal combustion engines, helicopter rotors, turbines, and rotary aircraft engines. For several decades, CPVAs have been used in light aircraft engines and helicopter rotors [21, 25] for vibration suppression. Recently, CPVAs have been shown to be very beneficial for use in automotive engines [6, 33, 42]. As examples of CPVAs, Fig. 1.1 shows a set of four bifilar (two-point suspension) CPVAs attached to a helicopter rotor, and an experimental bifilar absorber used at MSU.

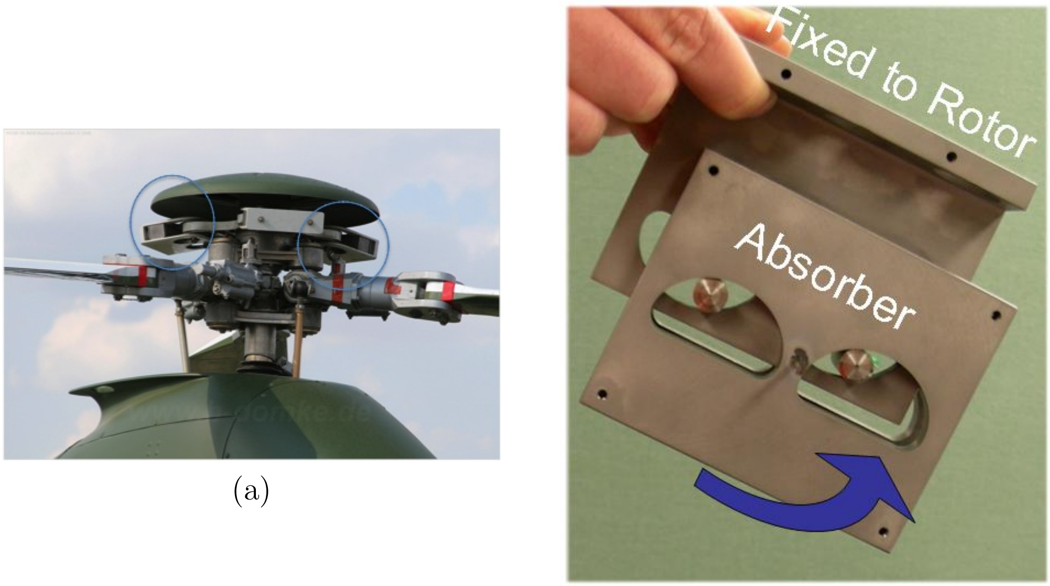

(a) (b)

Figure 1.1: (a) Bifilar Absorbers on a Helicopter Rotor. (http://www.b-domke.de /AviationImages/Rotorhead/11358.html). (b) MSU Experimental Bifilar Absorber Showing the Two-Point Suspension. For interpretation of the references to color in this and all other figures, the reader is referred to the electronic version of this dissertation.

Previous use of CPVAs in aerospace engines has been to reduce torsional vibrations of a rotor operating at a nearly constant angular velocity, in situations for which the most extreme speed and load conditions are known. These conditions allow the inertia of the absorbers to have sufficient inertia and be tuned so as to avoid the undesirable nonlinear behavior. These non-linear dynamics include instabilities such as an amplifying "jump" bifurcation for circular path absorbers, as well as non-synchronous motions for other paths that arise due to non-linear absorber coupling through the rotor, each of which are detrimental to absorber performance [3, 9, 39]. Recent research has been conducted into understanding the response and assessing the effectiveness of CPVAs for use in high efficiency automotive engines, where the mean speed of the rotor varies greatly throughout the range of operation [33,41], and for which the inertia of the entire crank shaft is desired to be as small as possible for maximum responsiveness. It should be noted that the rotary inertia of an engine powertrain has always been desired to be small, but new demands have coupled this minimization of powertrain inertia with very large engine torsional fluctuations. A crankshaft used in an experimental Ford V8 automotive engine fitted with CPVAs is shown in Fig. 1.2 [32].

Figure 1.2: Circular Path CPVA on Automotive Crankshaft.

1.0.1 Motivation

With automotive manufacturers all battling to design more fuel efficient engines, vibration suppression surprisingly plays an important role in maximizing this efficiency. The Corporate Average Fuel Economy (CAFE) standards state that passenger cars must meet a 30.5 mpg minimum and light trucks a 24.1 mpg minimum by this year. Also, by 2025, automotive manufacturers will be required to meet a combined fleet average of 54.5 mpg for cars and light trucks, as imposed by the passing of the Energy and Independence Security Act (EISA). With these impending government restrictions on fuel economy, car companies are implementing many new engine technologies, two of which, as subsequently discussed, require some sort of vibration attenuation to be as efficient and salable as possible. The first engine technology is the so-called "displacement on demand" large displacement engines, first used by General Motors in 1981 Cadillacs, modified by Mercedes-Benz in 1999, and also employed by Chrysler and Honda since 2005 [1]. These internal combustion engines vary the number of cylinders firing as engine speeds and loads change. The variable displacement engines have been found to achieve a fuel economy saving of $10 - 20\%$, mainly through the reduction of pumping losses, which occur when the engine is in its reduced cylinder mode. Using current technology however, these multi-displacement system engines cannot operate in the more efficient reduced cylinder mode for speeds below 1200 rpm, due to noise and vibration issues. Resolving these low speed vibratory problems would result in even more fuel economy improvement. The second type of new, more efficient engine technology is very small displacement, usually turbo-charged, high torque engines, for example the Ford "Fox I-3" engine . Running these engines at low speeds and high torques, that is, in the so-called "lugging" mode, is very efficient, but results in very high levels of torsional vibrations. These vibrations, which are felt by the operator and passengers, currently make these engines unsuitable for the marketplace. CPVAs have recently come to the forefront in the automotive industry to reduce these torsional vibrations.

In most applications there exists a dominant source of engine order vibration, and absorbers are tuned to that order. In fact, all previous studies known to the author have investigated the use of CPVAs tuned to attenuate torsional vibrations at a single order. However, it is known that when absorbers are pushed to large amplitudes, where nonlinear effects come into play, instabilities can occur, and the absorbers generate higher order torsional vibrations on the rotor. In this work we extend upon these studies and analyze the use of multiple-order CPVAs in order to reduce vibrations at multiple engine orders. The goal is to develop a fundamental understanding of the interplay between absorbers at different orders, and use this knowledge to develop design strategies for systems of absorbers with groups of absorbers tuned to different orders.

1.0.2 General Operation of CPVAs

CPVAs are masses suspended from a rotor in such a way that they are free to move along a desired path, similar to that of a pendulum, and a general schematic of a rotor/CPVA system is shown in Fig. 1.3. CPVAs have several inherent properties which make them ideal for use in rotating machinery. First, they have a natural frequency that is proportional to the mean rotational speed of the rotor, thus corresponding to a given order of rotation. This follows since the effective stiffness on the absorbers is due to centrifugal effects, and this property makes them effective over a continuous range of rotor speeds. Referring to the dimensions in Figure 1.3, one can find that when the rotor spins at a constant rate Ω, the natural frequency of the absorber is $\Omega\sqrt{R_{0i}/\rho_0 - 1}$, where ρ_0 is the radius of curvature of the absorber path at the path's vertex. The natural frequency of the absorber will be subsequently referred to as $\tilde{n}\Omega$ where $\tilde{n}$ is referred to as the absorber tuning order.

When tuned to the correct value of $\tilde{n}$, the absorbers oscillate in a manner that counteracts the corresponding order component of the fluctuating applied torque acting on the rotor. The engine excitation orders, $n,\ 2n, ...$ are inherent to a given machine. For example, in a four stroke internal combustion engine, each cylinder fires once every two revolutions of the crankshaft. This implies for an N cylinder engine, the dominant engine order is at $N/2 = n$, but orders $2n,\ 3n$ and higher are also generally present, although often at a much smaller amplitude. In fact, if there is significant cylinder-to-cylinder variation, one-half orders, such

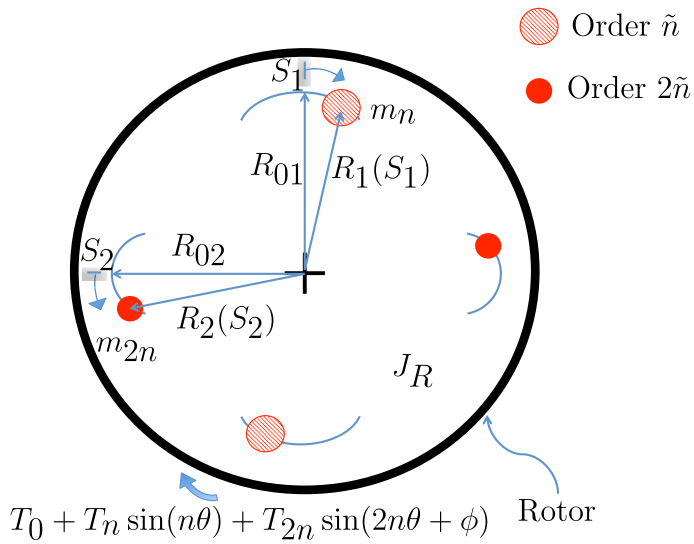

Figure 1.3: Schematic of a rigid rotor fitted with absorbers tuned to $\tilde{n}$ and $2\tilde{n}$.

as $n/2$, $3n/2$, etc. can also be present. With this knowledge, we can model the forcing from a four stroke internal combustion as a Fourier series in θ with frequency (order) n, for example, with a leading order term of $T\sin(n\theta)$, where the forcing order, n is equal to $N/2$, this is the so called *order n* excitation. For some multiple displacement engines, as previously described, the fluctuating torques applied when the engine is in "full" and "reduced' cylinder mode can both cause undesirable vibration effects. This results in vibration amplitudes at two different orders which need to be attenuated. Also, in the high compression, small displacement engines being developed, higher order harmonics can be of substantial magnitude. For example, the oscillating torque for an engine which produces a torque in which the first *two* harmonics are large can be modeled as $T_1 \sin(n\theta) + T_2 \sin(2n\theta + \phi)$. In general, the torque can be expressed as a Fourier series in terms of the base order n. Previous investigations have analyzed the performance of CPVAs tuned to a single order, when subjected to a single order torque. This work extends upon those previous investigations by both predicting the response of a system containing a rotor equipped with multiple order CPVAs subjected to multiple order torques, as well as by developing methods to design such systems for optimal performance.

As mentioned above, it is desired keep the total rotational inertia of the rotor/CPVA system at a minimum to maintain good responsivity of the engine, that is, how quickly it reacts to shifts in torque, for example, during vehicle launch. This requires using as small an absorber mass m, and absorber distance from the center of rotation R_{0i}, as possible. The absorber works by using a combination of its mass, the distance from the center of rotation, and the absorber amplitude S, to counteract the applied torque, and thus a minimization of the first two quantities results in a large absorber amplitude. This implies that an understanding of the large amplitude, nonlinear dynamic behavior of the entire system is essential for an effective design. It turns out that the path that the absorber center of mass follows $R_i(S_i)$, is very important to large amplitude behavior of the system [14, 39]. Also, if more than one absorber is employed, nonlinear inter-absorber interactions can occur due to kinematic coupling through the rotor. It will be shown that it is essential to consider the effects of this inter-absorber coupling when designing multiple order absorber systems for large amplitude behavior. In fact, if one has sufficient absorber inertia to keep amplitudes small, and the system response can be described by a linear dynamic system model, then one can use superposition to design the system, since there will be no interaction between absorbers at different orders.

1.0.3 Background

We now turn to a summary of past contributions to our knowledge about CPVAs, and less specifically, contributions to non-linear vibration absorbers. As will be shown, original studies investigated the steady-state linear response of CPVAs, slowly moved into the nonlinear steady-state response for circular paths, went on to look at non-circular path steady-state nonlinear analysis, and finally to transient non-linear analysis; all for single order CPVAs.

Frequency tuned vibration absorbers have long been understood and used as a means to reduce vibrations, and are commonly found in undergraduate vibrations textbooks, e.g., [45]. Around the early 1930's, the basic operational principles of *order* tuned vibration absorbers were first brought to light in separate patents by Salomon and Sarazin [37, 38], which were motivated by the need to alleviate crankshaft torsional vibrations in aircraft engines. A thorough description of the problems associated with aircraft engine torsional vibrations, as well as the development of the pendulum type vibration absorber, is presented in [26]. Shortly after the Salomon and Sarazins' patents, Chilton of Curtiss-Wright employed a bifilar CPVA and E. S. Taylor designed a "puck" type pendulum absorber, both to alleviate propellor snapping issues in 9 cylinder aircraft engines [26].

Shortly after Curtiss-Wright hired E. S. Taylor to become their principal vibration consultant, Pratt & Whitney decided to hire another M.I.T professor as its vibration consultant, J. P. Den Hartog. Den Hartog was the first to investigate how damping and detuning (the difference between forcing and absorber tuning orders) of a CPVA effects its linear steady-state response, and he extended on this to show that large amplitude oscillations of a circular path CPVA cause a detuning that arises from nonlinear effects [12, 13]. Den Hartog's Ph.D. student, D. Newland, first investigated the dangerous amplifying "jump" bifurcation that can occur for circular path absorbers (resulting from a saddle-node bifurcation), and recommended overtuning the absorbers (that is, making $\tilde{n} > n$) to alleviate this bifurcation. Overtuning the absorbers does increase the torque level that causes this instability, although the absorbers are less effective at reducing torsional vibrations when overtuned. Further investigations have validated Newland's ideas with controlled experiments, and extended upon the analysis through the inclusion of Coulomb friction in the system model [34, 47].

This dangerous amplifying instability seen in circular path absorbers motivated research into alternative path designs. It was known that this jump bifurcation is only possible for softening nonlinearities (frequency decreasing as a function of amplitude), motivating Madden to propose a cycloidal path [25], which, in fact, induces a slight hardening nonlinearity. The cycloidal path is the solution of the tautochrone problem in a gravitational field, described as follows: a particle released from any point on a cycloid will reach the vertex (the bottom of the curve) at the exact same time in a gravitational field. In fact, the equation of motion for a particle on this curve is a simple linear harmonic oscillator, that is, the response has the same frequencies for all amplitudes. Huygens solved the corresponding tautochrone problem in a centrifugal field, and found epicycloids to be the solution, but it wasn't until Denman in 1992 [14] that epicycloids were proposed for use in CPVAs. A special epicycloid, known as the "tautochronic epicycloid," renders the absorber frequency independent of amplitude (for constant rotor speed), thus making the absorber motion that of a linear harmonic oscillator [14]. Denman was able to formulate the equations of motion for bifilar absorbers, including the rollers, for a quite general path and was able to represent these paths as a two parameter family of curves defined by their radius of curvature $\rho^2 = \rho_0^2 - \lambda^2 S^2$, where ρ_0 is the curvature at the vertex, which fixes the absorber's linear tuning, and a parameter λ that controls the large amplitude behavior of the curve. Monroe and Shaw [29] generalized Denman's results to include the inertial effects of the rollers used in bifilar absorbers, and showed that a tautochrone exists for this system. Lee and Shaw [24] investigated the counteraction of applied torques through epicycloidal absorbers and found that, along with applying a counteracting torque at the desired order, these absorbers produced higher order harmonics back onto the rotor. As previously mentioned, epicycloidal paths yield a simple harmonic oscillator when the rotor speed is constant, yet there exists a nonlinear coupling between the absorbers and the rotor which produces these higher harmonics. Lee and Shaw interestingly found that epicycloidal absorbers tuned to one half of the forcing torque would undergo a subharmonic resonance which resulted in a pure harmonic torque applied to the rotor. Chao and Shaw [7] incorporated design guidelines for systems with absorbers that had small imperfections as well as systems of identical, subharmonic absorbers.

The cycloidal and tautochronic epicycloidal path absorbers avoid the dangerous jump bifurcation encountered by circular path absorbers, but can still give rise to non-synchonous response bifurcations for systems with multiple absorbers, including the aforementioned subharmonic bifurcation. In general, these symmetry breaking bifurcations are detrimental to system performance, as the absorbers no longer work together effectively acting as a single large inertia. Chao et al. [8, 9] showed that a critical torque level exists which will cause tautochronic absorbers to become non-synchronous. Shaw and Geist [39] subsequently generalized those results to include linear and nonlinear detuning of the tautochrone, showing where non-synchrounous and jump instabilities occur in the path parameter space, thus allowing one to select absorber paths that avoid these instabilities. The authors showed that both instabilities can be alleviated through overtuning the absorbers. Alsuwaiyan and Shaw [5] provided conditions on this non-sychrounous bifurcation for non-tautochronic paths, and also showed that overtuning the absorbers is beneficial to performance, although for circular path absorbers, the jump bifurcation can still occur. All the aforementioned studies consider only the steady-state response for CPVAs. Monroe and Shaw [27, 28] recently categorized the transient response of CPVAs for a general range of paths. It was found that an approximate value for the percent overshoot of a single absorber could be calculated analytically, in terms of the absorber tuning, damping, and system nonlinearity. The only studies known to the author that consider systems composed of absorbers tuned to multiple orders are those where some absorbers are tuned to orders $n \pm 1$ in order to reduce shaking order n shake forces [6,10]. The only study that considers multiple order torques is that of Lee and Shaw [23], who considered how a pair of identical order n absorbers can simultaneously address torques of order n and $2n$ through nonlinear effects.

It is the goal of this PhD dissertation to extend upon these previous studies through a comprehensive study of systems with multiple order CPVAs subjected to multi-order torques. As explained in more detail in the next sections, the system nonlinearites, specifically the nonlinear absorber/rotor coupling, play an important role in the dynamics of CPVAs at multiple orders, and must be considered in order to achieve optimal performance of such systems.

1.0.4 Dissertation Organization

The dissertation is organized as follows:

- **Steady-State Dynamics of Multiple Order CPVA Systems.** Chapter 2 analyzes the steady-state dynamics of multiple order CPVAs through the use of numerical simulations, perturbation methods, and numerical continuation. System stability as a function of the applied torques and other relevant parameters is investigated. Optimal inertia ratios between the two order absorbers are obtained.

- **Experimentation.** Chapter 3 introduces the experimental setup utilized and provides experimental validation of the previous analytical treatments. Synchronous and non-synchronous multiple-order absorber responses are investigated.

- **Harmonic Balance Methods Applied to CPVA Systems.** Chapter 4 presents an analysis on the dynamics of CPVAs through the use of harmonic balance methods.

The harmonic balance approximations are compared to numerical simulations as well as experiments for a wide array of absorber systems.

- **Conclusions.** The final chapter reviews the work completed in this dissertations and gives some recommendations for some future areas of study.

Chapter 2

Modeling and Prediction of System Response

The equations describing the motion of a rigid rotor equipped with multiple order pendulum absorbers are derived in this chapter. These complicated, nonlinear equations are then non-dimensionalized and the non-dimensional parameters are scaled based on practical limits for the ranges of these parameters. Perturbation methods are then applied to the scaled equations of motion, and are shown to accurately capture the both the stable steady-state dynamics as well as the instabilities present in the system. All analytical results are compared to simulations of the fully coupled nonlinear equations of motion.

2.1 Equations of Motion

For the present investigation, we model the system at hand as a rigid rotor spinning about a fixed axis with masses attached that move along pre-described paths relative to the rotor, as shown in Fig. 2.1. The figure exhibits two different paths that the masses can follow, defined by the distance from the center of the rotor to the center of the masses, referred to as $R_i(S_i)$, where S_i is the masses' arc length position relative to the rotating frame. The characteristics of these curves, along with their distance from the center of the rotor determine the linear and nonlinear tuning of the masses. The general system has N_1 absorbers tuned to an order,

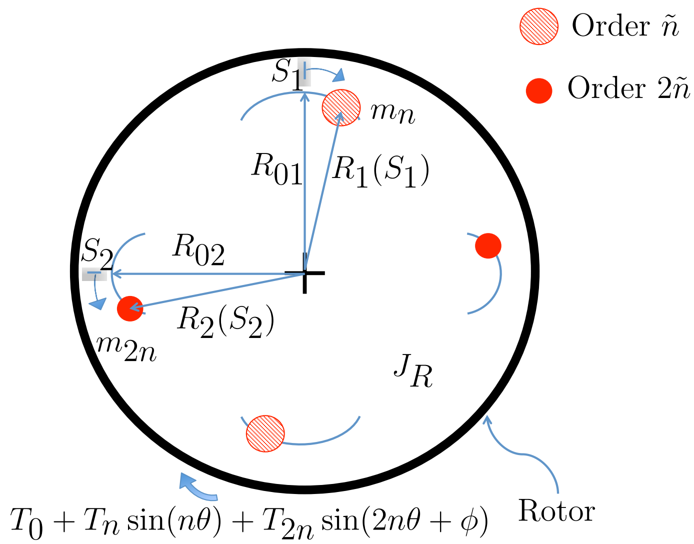

Figure 2.1: Schematic of a rigid rotor fitted with absorbers tuned to $\tilde{n}$ and $2\tilde{n}$.

$\tilde{n}_1$, as well as N_2 absorbers tuned to order $\tilde{n}_2$. For convenience it is assumed that $N_1 = N_2$ and that the order $\tilde{n}_1$ absorbers are indexed from $1 : N_1$ and the order $\tilde{n}_2$ absorbers indexed from $N_1 + 1 : N_1 + N_2$, where we define $M = N_1 + N_2$. The masses of the absorbers at their respective order are assumed to be equal, i.e.,

$$
\begin{aligned}
m_i &= m_n \qquad && 1 \leq i \leq N_1 \\
m_i &= m_{2n} \qquad && N_1 + 1 \leq i \leq M
\end{aligned}
$$

In order to motivate the modeling of the engine torque, a sample schematic of gas pressure torques for a four-stroke, in-line, four cylinder engine is shown in Fig. 2.2.

This torque can be modeled as

$$
T(\theta) = T_0 + T_n \sin(n\theta) + T_{2n} \sin(2n\theta + \phi)
$$

in which T_0 is the DC torque, $T_{n,2n}$ are the fluctuating components of the torque, and ϕ is the phase between the harmonics. With the above information, the kinetic energy for the

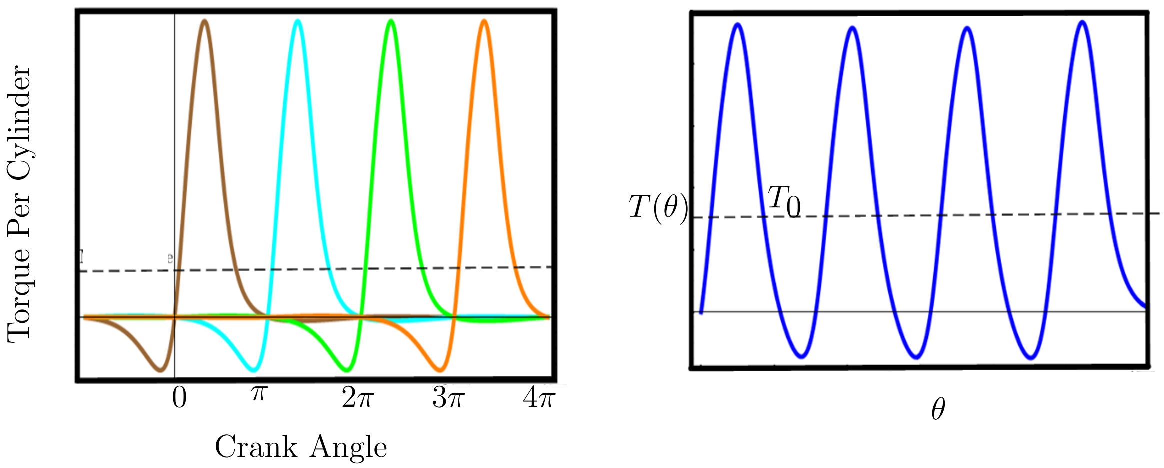

(a) (b)

Figure 2.2: (a) Torques generated from individual cylinders, calculated by converting a characteristic gas pressure force acting on a piston to crank torques. (b) Summed torque, which is dominated by a DC term and second order harmonic. Higher order harmonics are also evident.

rotor/CPVA system can be found to be

$$
\begin{aligned}
T_t = \frac{1}{2}(J_R\dot{\theta}^2 + \sum_{i=1}^{N_1}(m_i(X_i(S_i)\dot{\theta}^2 + \dot{S}_i + 2G_i(S_i)\dot{\theta}\dot{S}_i)) \\
+ \sum_{i=N_1+1}^{M}(m_i(X_i(S_i)\dot{\theta}^2 + \dot{S}_i + 2G_i(S_i)\dot{\theta}\dot{S}_i)))
\end{aligned}
\tag{2.1}
$$

where

$$X_i(S_i) = R_i^2(S_i),$$

and

$$G_i(S_i) = \sqrt{X_i(S_i) - \frac{1}{4}(\frac{dX_i}{dS_i}(S_i))^2}.$$

In order to obtain the differential equations describing the dynamics of the system we use Lagrange's method. The generalized forces are found to be

$$\delta W = -c_{a,i}\dot{S}_i\delta S - (c_0\dot{\theta} - T_0 - T(\theta))\delta\theta,$$

and performing the steps in Lagrange's method yields $N_1 + N_2 + 1$ equations of motion, found to be:

$$m_i[\ddot{S}_i + G_i(S_i)\ddot{\theta} - \frac{1}{2}\frac{dX_i}{dS_i}(S_i)\dot{\theta}^2] = -c_{ai}\dot{S}_i \qquad 1 \leq i \leq M, \tag{2.2}$$

for the i^{th} absorber and

$$\begin{aligned} &J_R\ddot{\theta} + \sum_{i=1}^{N_1}(m_i(\frac{dX_i}{dS_i}(S_i)\dot{S}_i\dot{\theta} + X_i(S_i)\ddot{\theta} + G_i(S_i)\ddot{S}_i + \frac{dG_i}{dS_i}(S_i)\dot{S}_i^2)) \\ &+ \sum_{i=N_1+1}^{M}(m_i(\frac{dX_i}{dS_i}(S_i)\dot{S}_i\dot{\theta} + X_i(S_i)\ddot{\theta} + G_i(S_i)\ddot{S}_i + \frac{dG_i}{dS_i}(S_i)\dot{S}_i^2)) \\ &= -c_0\dot{\theta} + T_0 + T_n\sin(n\theta) + T_{2n}\sin(2n\theta + \phi) \end{aligned} \tag{2.3}$$

describing the dynamics of the rotor.

In order to get the equations of motion in a form suitable for non-linear analysis methods, we non-dimensionalize the variables and change the independent variable from time to the rotor angle, θ following the work of Chao et. al. [8]. To change the independent variable a new dimensionless dependent variable y, is defined as

$$y = \frac{\dot{\theta}}{\Omega}$$

This variable is used to then define relationships between derivatives with respect to time and θ as follows:

$$\ddot{\theta} = \frac{dy}{d\theta}\frac{d\theta}{dt}\Omega = y'y\Omega^2$$

$$\dot{(\ )} = \frac{d(\ )}{d\theta}\frac{d\theta}{dt} = (\ )'y\Omega$$

and

$$\ddot{(\ )} = \frac{d^2(\ )}{d\theta^2}\left(\frac{d\theta}{dt}\right)^2 + \frac{d(\ )}{d\theta}\frac{d^2\theta}{dt^2} = (\ )''y^2\Omega^2 + (\ )'y'y\Omega^2$$

In summary, we have the following relationships, where $(\ )' = \dfrac{d(\ )}{d\theta}$,

$$\ddot{\theta} = \Omega^2 yy' \quad \dot{(\ )} = \Omega y(\ )' \quad \ddot{(\ )} = \Omega^2 yy'(\ )' + \Omega^2 y^2(\ )''$$

This process transforms the equations of motion, Eqs. (2.2) and (2.3) into a set of periodically forced, non-autonomous equations, and thus the nonlinearity, $T_n \sin(n\theta)$+higher harmonics, into a forcing term. The equations of motion are then rearranged into a non-dimensional form as follows,

$$ys_i'' + (s_i' + g_i(s_i))y' - \frac{1}{2}\frac{dx_i}{ds_i}(s_i)y + \mu_{ai}s_i' = 0 \qquad 1 \leq i \leq M \tag{2.4}$$

$$\begin{aligned}
&\epsilon\Big(\frac{1}{N_1(1+\alpha)}\Big(\sum_{i=1}^{N_1}\Big[\frac{dx_i}{ds_i}s_i'y^2 + x_i(s_i)yy' + g_i(s_i)(s_i'yy' + s_i''y^2) \\
&+ \frac{dg_i}{ds_i}s'^2y^2\Big]\Big) + \frac{\alpha}{N_2(1+\alpha)}\Big(\sum_{i=N_1+1}^{M}\Big[\frac{dx_i}{ds_i}s_i'y^2 + x_i(s_i)yy' \\
&+ g_i(s_i)(s_i'yy' + s_i''y^2) + \frac{dg_i}{ds_i}s'^2y^2\Big]\Big)\Big) \\
&+ yy' = -\mu_0 y + \Gamma_0 + \Gamma_n\sin(n\theta) + \Gamma_{2n}\sin(2n\theta + \phi)
\end{aligned} \tag{2.5}$$

in which $(\,)' = \frac{d(\,)}{d\theta}$. The parameters $x_i(s_i) = R_i^2(s_i)/R_{i0}^2$ and $g_i(s_i) = \sqrt{x_i(s_i) - \frac{1}{4}(\frac{dx_i(s_i)}{ds_i})^2}$ are path-related functions, described in detail in the next section, and the other variables and parameters are defined and described in Table 2.1. While many of these parameters have been considered in previous CPVA studies, the absorber inertia ratio α is of special interest here, since it dictates the distribution of absorber inertia between the two orders for a fixed amount of absorber inertia, that is, for a fixed value of ϵ. These equations form the basis of the analysis that follows.

Table 2.1: Definition of non-dimensional variables in Eqns. (2.4-2.5).

Non-dimensional parameter	Definition	Description
y	$\frac{\dot{\theta}}{\Omega}$	Angular velocity of the rotor normalized by the rotor mean speed, Ω
ϵ	$\frac{N_1 m_n R_0^2(1+\alpha)}{J_R}$	Inertia ratio of absorbers to rotor
s_i	$\frac{S_i}{R_0}$	Absorber arc length normalized by its distance from the rotor center
$\mu_{a,i}$	$\frac{c_{a,i}}{m_i \Omega}$	Normalized absorber viscous damping
μ_0	$\frac{c_o}{J_R \Omega}$	Normalized rotor viscous damping
Γ_0	$\frac{T_0}{J_R \Omega^2}$	Mean engine torque normalized by twice the rotor's kinetic energy
$\Gamma_{n,2n}$	$\frac{T_{n,2n}}{J_R \Omega^2}$	Fluctuating component of the engine torque normalized by twice the rotor's kinetic energy
α	$\frac{m_{2n}}{m_n}$	Ratio of masses at each order

2.1.1 Absorber Paths

In order to smooth out torsional vibrations with minimal absorber inertia under the most severe fluctuating loads, the absorbers will move at large amplitudes, requiring careful selection of the absorber paths, which are specified by the functions x_i in the equations of motion. Denman [14] conveniently represented these paths as a two parameter family of curves defined by their radius of curvature $\rho^2(S) = \rho_0^2 - \lambda^2 S^2$, where ρ_0 is the curvature at the vertex, which fixes the absorber's linear tuning order $\tilde{n}$, and λ controls the large amplitude behavior of the curve, thereby dictating the absorbers' nonlinear dynamics. Typically, the absorber tuning is taken to be slightly above the dominant engine order, for example, for an N-cylinder four-stroke engine, the dominant engine order is $n = N/2$, and absorber tuning is taken to be $\tilde{n} = N(1+\sigma)/2$, where the detuning parameter σ is a few percent. The tradeoff is that smaller values of σ make the absorber work better, but it also makes the absorber amplitudes large, inducing nonlinear effects, including the generation of higher harmonics that can result in crosstalk among absorbers.

Selection of the nonlinear path parameter is more complicated. Basically, the nonlinear part of the path dictates whether the absorber frequency (order) increases or decreases as a function of absorber amplitude, and the degree to which this nonlinear detuning occurs [3,39]. There exists a special value, λ_{te}, corresponding to the tautochronic epicycloid, which renders this detuning zero, that is, selection of this path makes the absorber dynamics essentially linear out to large amplitudes [14,39]. Figure 2.3 shows three curves for the same linear tuning value, $\tilde{n} = 1.5$, with nonlinear path parameters of $\lambda = 0$ (circle), $\lambda = \lambda_{\mathrm{te}}$, and $\lambda = 1$ (cycloid).

Conservative absorber designs select relatively large values of the detuning σ, keeping the

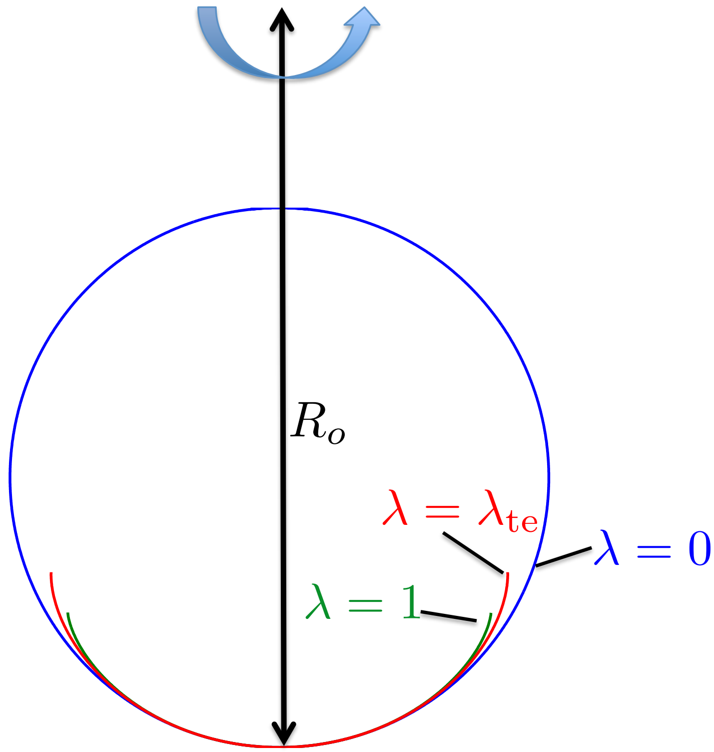

Figure 2.3: Absorbers paths which produce a linear tuning of $\tilde{n} = 1.5$, for three different nonlinear path parameters, $\lambda = 0, \lambda_{\rm te}, 1$.

absorber response away from its resonance, and therefore linear [3, 36, 39]. More aggressive designs, with improved performance for smaller absorber inertia, keep σ small and account for nonlinear behavior, typically by taking $\lambda \approx \lambda_{te}$. In this study, following the work of Shaw and Geist [39], we define the path as a perturbation of the tautochronic epicycloid, which allows for the analysis of different path types. This path can be easily described through the radial distance from the rotor center to the absorber location along it's arc length as,

$$x_i(s_i) = 1 - \tilde{n}s_i^2 + \epsilon h_i(s_i).$$

The paths of each absorber at the different orders are assumed to be identical,

$$x_i(s_i) = x_n(s_i) \qquad 1 \leq i \leq N_1$$
$$x_i(s_i) = x_{2n}(s_i) \qquad N_1 + 1 \leq i \leq M,$$

and the perturbation of the path away from the tautochronic epicycloid is described by $h_i(s_i)$. The form of the deviation from tautochronic paths is defined to be

$$h_i(s_i) = \sum_{j=1}^{N} \varphi_j s_i^{2j+2} \tag{2.6}$$

This is due to the symmetric nature of the curves and the fact that the second order corrections can be captured in the quadratic term already used tautochronic path formulation. The exact form for φ_1 has been found to be as follows,

$$\varphi_i = (\frac{1}{12})(\tilde{n}_i^2 + 1)^2(\tilde{n}_i^2 - \lambda_i^2(1 + \tilde{n}_i^2)),$$

where the complete path derivation and details can be found in Shaw and Geist [39]. The higher order coefficients of the amplitude expansions can easily be found performing a series expansion in s of $x_i(s_i)$.

As mentioned above, the design of absorber systems must account for various types of instabilities that may occur. These instabilities arise since CPVA systems have multiple elements with identical natural frequencies, or, for the present study, natural frequencies in 2 : 1 ratios, low damping, and they are driven near resonance. One type of instability encountered is a jump, due to absorber detuning (specifically, softening) at large amplitudes, resulting in the absorber transitioning into a vibration amplifier (since its phase shifts such that it adds to the fluctuating torque). This is a common problem with circular path absorbers, and it is avoided in practice by selecting large detuning [3, 36]. Another, more subtle, instability occurs for systems comprised of multiple identical absorbers. When aggressively tuned, these absorbers experience cross-talk through the rotor inertia, resulting in an instability of the desired synchronous response, and this occurs even for tautochronic absorbers, that is, when the absorbers are designed to be as linear as possible. This instability can also be avoided by detuning, which is accomplished by proper selection of the absorber path, and analysis indicates how one can tune for optimal performance without encountering this instability [39]. The issue of imperfections among absorbers is also detrimental to performance, and tuning strategies to account for these effects, at least for small absorber amplitudes, are also known [4].

2.2 Motivating Simulation Results

With the full equations of motion developed for CVPA systems with absorbers tuned to orders n and $2n$, one can begin to qualitatively map out the stability of the absorber response using numerical simulations. Shown in Fig. 2.4 is the normalized order n and $2n$ torque space, Γ_n and Γ_{2n}, exhibiting some of the instabilities that can occur for zero relative phase between the torque harmonics, $\phi = 0$. This system has 4 absorbers, 2 each at orders n and $2n$, that is, the absorbers are tuned to exactly match the torque orders. The mass ratio between the different order absorbers is taken to be $m_{2n}/m_n = 0.1$.

Synchronous responses correspond to both sets of absorbers acting in relative unison, as desired; these occur, for example, at points W and Y in Fig. **??**. As the torque amplitudes are increased, instabilities can occur, and these are quite rich if there are multiple absorbers

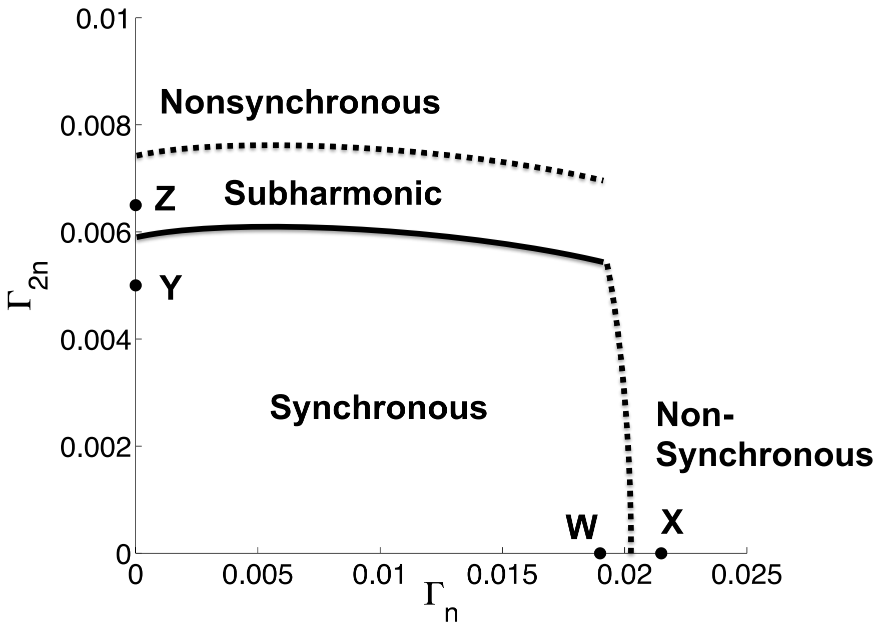

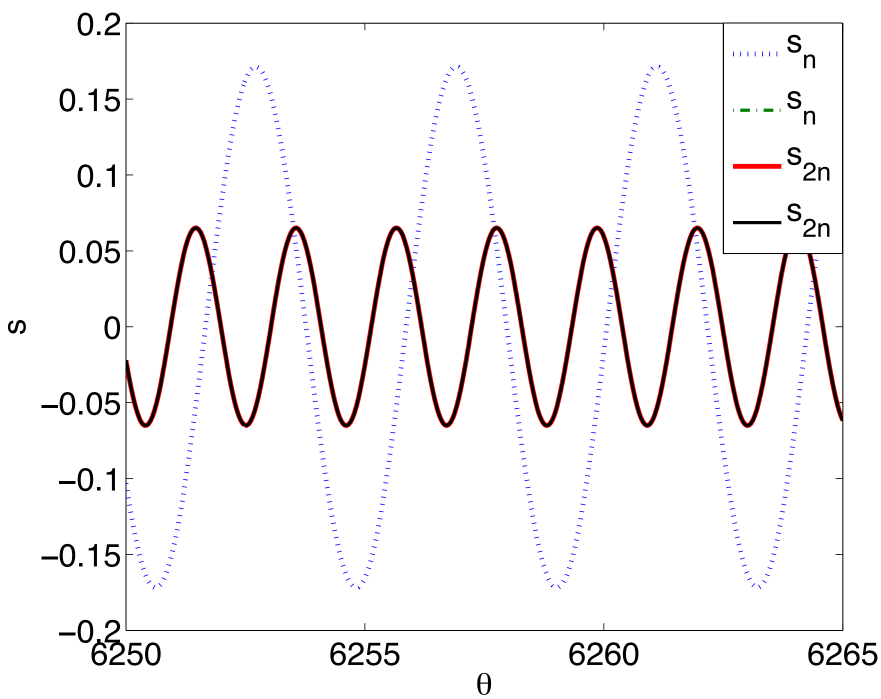

(b)

Figure 2.4: Simulated responses of a system composed of four tautochronic absorbers, two each at orders 1.5 (s_n) and order 3 (s_{2n}), subjected to a torque composed of a linear combination of orders 1.5 and 3. Note the different scales used for depicting the responses. (a) Torque harmonic amplitude space, Γ_3 vs. $\Gamma_{1.5}$, with boundaries of the desired synchronous response indicated schematically; solid line depicts a subharmonic instability boundary, dotted (dashed) line depicts a symmetry-breaking instability boundary to nonsynchronous responses of the order 1.5 (3) absorbers. (b) Mutually synchronous response at point W.

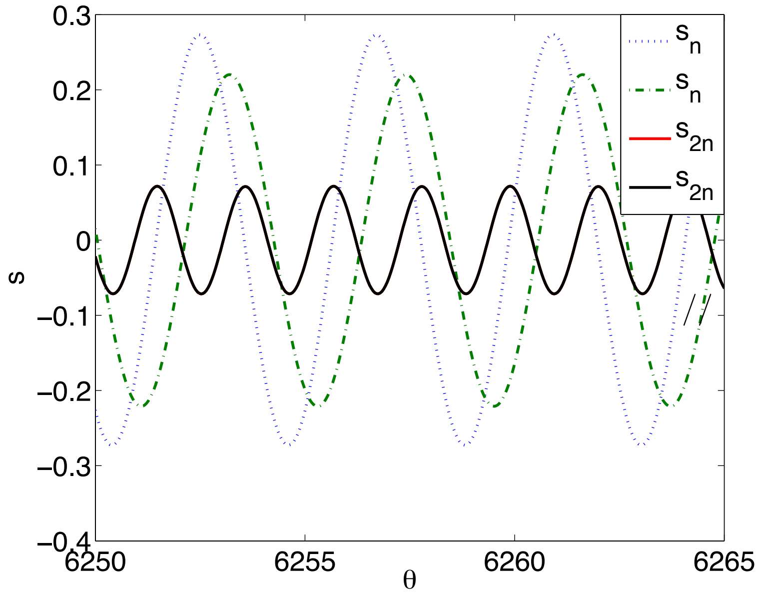

(c)

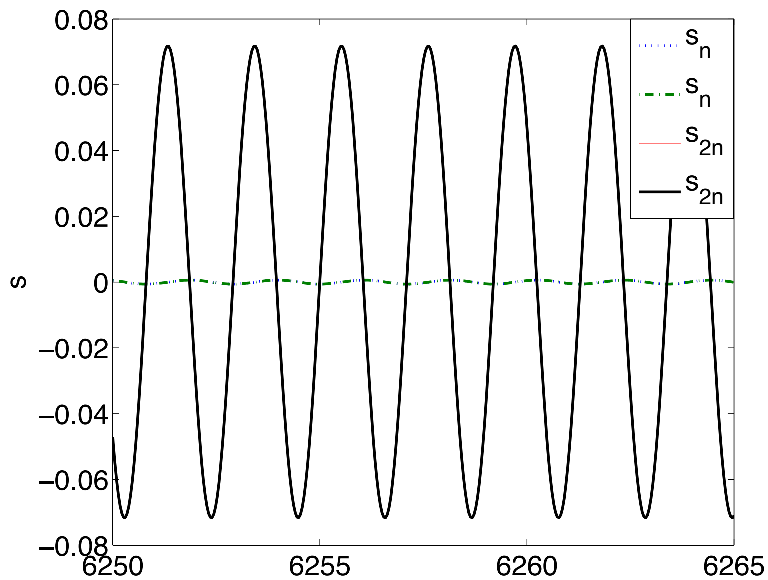

(d)

Figure 2.5: (c) Response at point X; the order 1.5 absorbers have become nonsynchronous and are in a transition towards their amplitude limits. (d) Response at point Y; similar to W, only with reversed relative amplitudes.

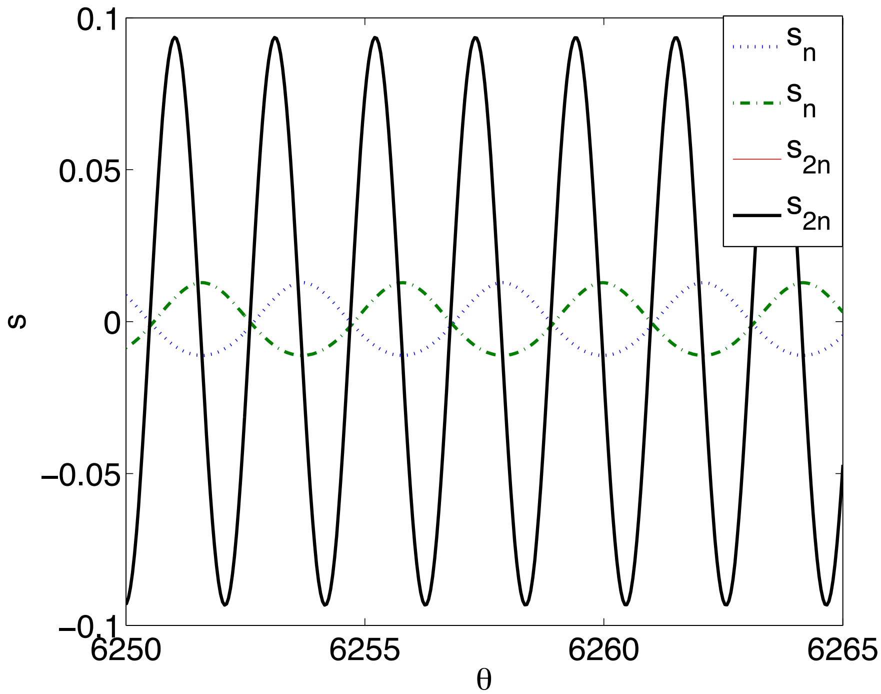

(e)

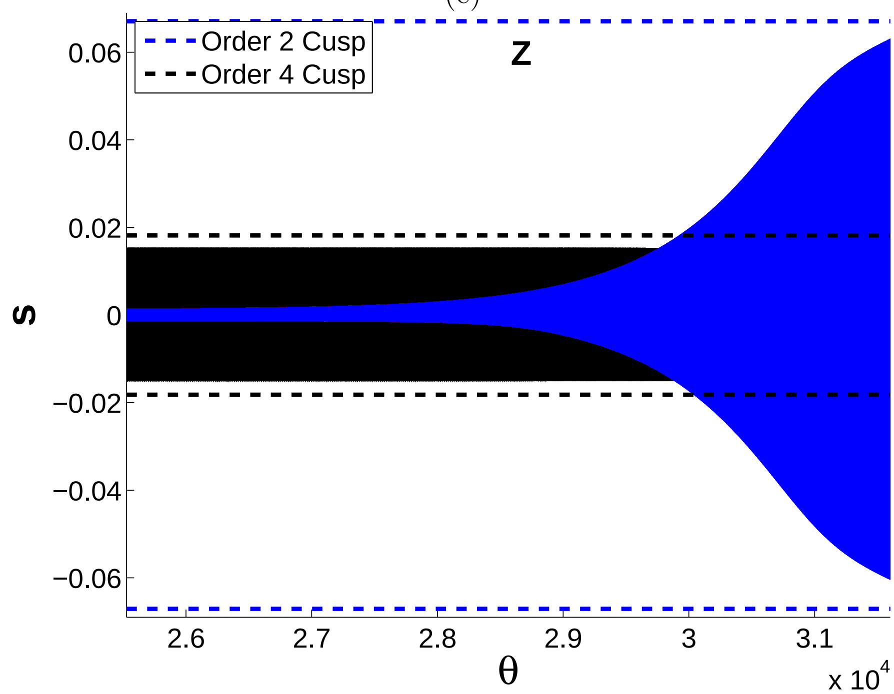

(f)

Figure 2.6: (e) Response at point Z; the order 1.5 absorbers have become subharmonic and are in transition toward their amplitude limits, as shown in (f). (f) Response at point Z, depicted over a long time interval; the order n absorber instability eventually results in large amplitude motion; the cusp amplitudes are the maximum possible amplitudes for these absorbers.

at each order. Three types of instabilities are indicated. The solid line represents the order 4 absorbers undergoing a subharmonic transition [22,30] in which they go out of phase and respond at order 2, an example of which occurs at point Z in Fig. 2.4. The dashed-dotted line represents the order 2 absorbers becoming nonsynchronous with an amplitude and phase shift, but remaining at order 2; such a response occurs at point X. The dashed line represents a condition for which the order 4 absorbers become nonsynchronous (not encountered here). Note that this instability is seen to occur beyond the subharmonic transition of the order two absorbers for the present system, but this may not always be the case. Each of these instabilities is detrimental to system performance, since the absorber amplitudes grow and reach physical limits, imposed by either hardware or the mathematics of the tautochronic absorber paths [39]. These preliminary results provide a general overview of the behavior of multiple order CPVA systems, and the analytic results developed below will provide a method for carrying out parameter studies of this behavior, to which we now turn.

2.3 Perturbation Analysis

In order to make the equations of motion suitable for analytical investigation, specifically by perturbation methods, we follow a scaling similar to that of Chao [8]. Taking advantage of a small dimensionless inertia ratio ϵ allows one to scale the responses, expand the equations of motion, and ultimately uncouple the rotor dynamics from those of the absorbers to leading order in ϵ. In the subsequent analysis, it is assumed that the following non-dimensional quantities are small, specifically $O(\epsilon)$: the torque amplitudes at orders n and $2n$, the absorber and rotor damping coefficients, and the absorber detunings $(\tilde{n}_i - kn)/(kn)$ for $k = 1, 2$. These conditions are met in applications, and perturbation analyses following this scaling have proven useful for matching experimental results [27, 40, 47] and for absorber system design [3, 27, 39].

This scaling results in a system for which the rotor runs at nearly constant speed with small fluctuations, that is, $y = 1 + \epsilon w$, where y is the rotor speed normalized by its mean value. Solving the rotor equation of motion, Eqn. (2.5), for yy' and performing expansions in ϵ, the rotor acceleration can be expressed as $yy' = \epsilon w'$, where

$$\begin{aligned} w' &= \tilde{\Gamma}_n \sin(n\theta) + \tilde{\Gamma}_{2n} \sin(2n\theta + \phi) \\ &\quad + \frac{1}{N_1(1+\alpha)} \left[\sum_{i=1}^{N_1} (2\tilde{n}_i^2 s_i s_i' + \tilde{n}_i^2 s_i g_{i0} - s_i'^2 g_{i0}') \right. \\ &\quad \left. + \sum_{N_1+1}^{M} \alpha (2\tilde{n}_2^2 s_i s_i' + \tilde{n}_2^2 s_i g_{i0} - s_i'^2 g_{i0}') \right], \end{aligned} \tag{2.7}$$

where $g_{i0}(s_i) = \sqrt{1 - \tilde{n}_i^2(1 + \tilde{n}_i^2) s_i^2}$. Inserting w' into the absorber equations, Eqn. (2.4), utilizing the above the scalings and expanding in ϵ yields M equations for the absorbers in which the rotor dynamics has been eliminated to leading order. These equations have the following form, convenient for application of standard perturbation methods:

$$s_i'' + \tilde{n}_i^2 s_i = \epsilon f_i(s_1, .., s_M, s_1', .., s_M', \mu_i, \tilde{n}_i, \lambda, T(\theta)) + O(\epsilon^2), \tag{2.8}$$

where

$$f_i = 3\varphi_i s_i^3 - \tilde{\mu}_{ai} s_i' + [s_i' + g(s_i)][\frac{1}{N_1}(\sum_{i=1}^{N_1} \frac{1}{1+\alpha}(-2n_i^2 s_i s_i' - n_i^2 g(s_i) s_i$$
$$+ \frac{dg(s_i)}{ds_i} s'^2_i) + \sum_{i=N_1+1}^{M} \frac{\alpha}{1+\alpha}(-2n_i^2 s_i s_i' - n_i^2 g(s_i) s_i \tag{2.9}$$
$$+ \frac{dg(s_i)}{ds_i} s'^2_i)) - \tilde{\Gamma}_n \sin(n\theta) - \tilde{\Gamma}_{2n} \sin(2n\theta + \phi)].$$

Note that the absorber amplitudes are not scaled to be small in this analysis, since the absorber path is taken to be close to the tautochrone, which yields a linear oscillator equation for the absorber motion out to large amplitudes. Thus, the equations of motion allow for large amplitude absorber motions, but their motion is sufficient to counteract the applied torque, resulting in attenuation of rotor vibration. The order ϵ terms in the absorber equations capture, to leading order, the effects of absorber damping, and the coupling between the absorbers' through the rotor dynamics, which is driven by the applied torque and the dynamics of the other absorbers. Once solutions of Eq. (2.8) are known, the rotor response, which is the quantity of principle interest for vibration reduction, can be reconstructed using Eq. (2.7). Perturbation analysis can be performed on Eq. (2.8), in order to obtain approximate solutions of the absorbers' amplitudes and phases as a function of θ. In this study, we employ the method of multiple scales (MMS) [31] to construct these approximate solutions.

As is common for capturing dynamics near resonances, we introduce detuning parameters which allow for small deviations of the absorbers' orders relative to their respective forcing orders, as well for variations in the 2 : 1 relationship between the absorbers. For forcing at orders $n_1 = n$ and $n_2 = 2n$ the detuning parameters are defined as,

$$n = \tilde{n}_1 + \epsilon\sigma_1$$

$$2n = \tilde{n}_2 + \epsilon\sigma_2$$

In order to make the equations for amplitudes and phases autonomous, we use the standard MMS coordinate change, $\phi_i = \beta_i - \epsilon\sigma_i$. Using these assumptions, the results of MMS produce $2M$ equations representing the slow time dynamics of the amplitudes and phases, a_i and ϕ_i, of the absorbers. These complicated expressions capture the nonlinear absorber interactions, and are given in a condensed form here in order to demonstrate their general form,

$$\begin{aligned} a_i' = \epsilon[&-\frac{\mu_i}{2}a_i + \frac{\Gamma_n}{n_1}\cos(\phi_i)F_1(a_i) \\ &- \frac{\Gamma_{2n}}{4}a_i\sin(2\phi_i) + P_i] \qquad 1 \leq i \leq N_1 \end{aligned} \tag{2.10}$$

$$\begin{aligned} \phi_i' = \epsilon[&-\sigma_1 - \frac{3}{4}\varphi_i a_i^3 - \frac{\Gamma_n}{n_1 a_i}\sin(\phi_i)F_2(a_i) \\ &- \frac{\Gamma_{2n}}{4}a_i\cos(2\phi_i) - \frac{1}{N_1(1+\alpha)}(\frac{n_1^5 a_i^2}{4} - \frac{n_1}{2}) + R_i] \\ &1 \leq i \leq N_1 \end{aligned} \tag{2.11}$$

$$\begin{aligned} a_i' = \epsilon[&-\frac{\mu_i}{2}a_i \\ &+ \frac{\Gamma_{2n}}{n_2}\cos(\phi_i)F_1(a_i) + V_i] \qquad N_1 + 1 \leq i \leq M \end{aligned} \tag{2.12}$$

$$\begin{aligned} \phi_i' = \epsilon[&-\sigma_2 - \frac{3}{4}\varphi_i a_i^3 - \frac{\Gamma_{2n}}{n_2 a_i}\sin(\phi_i)F_2(a_i) \\ &- \frac{\alpha}{N_1(1+\alpha)}(\frac{n_2^5 a_i^2}{4} - \frac{n_2}{2}) + X_i] \qquad N_1 + 1 \leq i \leq M \end{aligned} \tag{2.13}$$

where the functions (P_i, R_i, V_i, X_i) contain the coupling terms, which depend on all absorber amplitudes and phases, and are found to be:

$$P_i(a_i, a_j, \phi_{ji}) = \frac{1}{N_1(1+\alpha)} \sum_{j=1}^{N_1} [-\frac{1}{4} n_1^3 a_i a_j^2 \sin(2(\phi_j - \phi_i))$$

$$+ n_1 a_j G_1 + n_1(n_1^2 + n_1^4) a_j^3 H_1]$$

$$+ \frac{\alpha}{2N_2(1+\alpha)} \sum_{j=N_1+1}^{M} [a_i a_j n_2^2 \cos(2\phi_i - \phi_j) F_1(a_j)]$$

$$R_i(a_i, a_j, \phi_{ji}) = \frac{1}{N_1(1+\alpha)} \sum_{j=1}^{N_1} [\frac{1}{4} n_1^3 a_j^2 \cos(2(\phi_j - \phi_i))$$

$$+ n_1 \frac{a_j}{a_i} G_2 + n_1(n_1^2 + n_1^4) \frac{a_j^3}{a_i} H_2]$$

$$- \frac{\alpha}{2N_2(1+\alpha)} \sum_{j=N_1+1}^{M} [a_j n_2^2 \sin(2\phi_i - \phi_j) F1(a_j)]$$

$$V_i(a_i, a_j, \phi_{ji}) = \frac{\alpha}{N_2(1+\alpha)} \sum_{j=N_1+1}^{M} [-\frac{1}{4} n_2^3 a_i a_j^2 \sin(2(\phi_j - \phi_i))$$

$$+ n_2 a_j G_1 + n_2(n_2^2 + n_2^4) a_j^3 H_1]$$

$$- \frac{1}{2N_2(1+\alpha)} \sum_{j=1}^{N_1} [a_j^2 n_1^3 \cos(2\phi_j - \phi_i)(F_1(a_i) + F_2(a_i))]$$

$$X_i(a_i, a_j, \phi_{ji}) = \frac{\alpha}{N_2(1+\alpha)} \sum_{j=N_1+1}^{M} [\frac{1}{4} n_2^3 a_j^2 \cos(2(\phi_j - \phi_i))$$

$$+ n_2 \frac{a_j}{a_i} G_2 + n_2(n_2^2 + n_2^4) \frac{a_j^3}{a_i} H_2]$$

$$- \frac{1}{2N_2(1+\alpha)} \sum_{j=1}^{N_1} [\frac{a_j^2}{a_i} n_1^3 \sin(2\phi_j - \phi_i)(F_1(a_i) + F_2(a_i))]$$

Where the H_i and G_i terms are integrals defined below.

$$G_1(a_i, a_j, \phi_{ji}) = \frac{1}{2\pi} \int_0^{2\pi} \cos(x) \sin(x - \phi_j + \phi_i)[1 - n_i(1$$
$$+ n_i^2) a_j^2 \cos^2(x)]^{(1/2)} [1 - n_i(1 + n_i^2) a_i^2 \cos^2(x - \phi_j + \phi_i)]^{(1/2)} dx$$

$$G_2(a_i, a_j, \phi_{ji}) = \frac{1}{2\pi} \int_0^{2\pi} \cos(x) \cos(x - \phi_j + \phi_i)[1 - n_i(1$$
$$+ n_i^2) a_j^2 \cos^2(x)]^{(1/2)} [1 - n_i(1 + n_i^2) a_i^2 \cos^2(x - \phi_j + \phi_i)]^{(1/2)} dx$$

$$H_1(a_i, a_j, \phi_{ji}) = \frac{1}{2\pi} \int_0^{2\pi} \cos(x) \sin^2(x) \sin(x - \phi_j + \phi_i)$$
$$\left[\frac{1 - n_i(1 + n_i^2) a_i^2 \cos^2(x - \phi_j + \phi_i)}{1 - n_i(1 + n_i^2) a_j^2 \cos^2(x)} \right]^{(1/2)} dx$$

$$H_2(a_i, a_j, \phi_{ji}) = \frac{1}{2\pi} \int_0^{2\pi} \cos(x) \sin^2(x) \cos(x - \phi_j + \phi_i)$$
$$\left[\frac{1 - n_i(1 + n_i^2) a_i^2 \cos^2(x - \phi_j + \phi_i)}{1 - n_i(1 + n_i^2) a_j^2 \cos^2(x)} \right]^{(1/2)} dx$$

The functions F_1 and F_2, which are related to the individual absorber nonlinear behavior, are defined as [39]:

$$F_1(a_i) = \frac{1}{2\pi} \int_0^{2\pi} \sin^2(x)[1 - n_i^2(1 + n_i^2) a_i^2 \cos^2(x)]^{(1/2)} dx$$

$$F_2(a_i) = \frac{1}{2\pi} \int_0^{2\pi} \cos^2(x)[1 - n_i^2(1 + n_i^2) a_i^2 \cos^2(x)]^{(1/2)} dx.$$

Nonlinear interactions arise from the fact that the absorbers are driven near their individual resonances at orders n and $2n$ (as required for good performance) and, in addition, the fact that nonlinearities in the absorber motions result in combinations of harmonics that promote crosstalk, as shown below. These nonlinear interactions become important at large absorber amplitudes, and thus the nearly tautochronic scaling is required to capture these effects; that is, this coupling does not appear at leading order if one considers amplitude expansions for the absorbers, as is done for circular paths [3]. We now turn to results derived from this analysis, and compare them with direct simulations.

2.4 Synchronous Responses

In order to exhibit the basic effects that the different order absorbers have on each other, we first assume the absorbers at their respective order behave in a mutually synchronous manner. This is dynamically equivalent to a system with only two absorbers, one at each order; however, the use of a single absorber at each order is seldom realizable in practice due to space and balance issues. Assuming a synchronous response, the perturbation equations, Eqs. (2.10) to (2.13) above are simplified through the removal of the summations across multiple absorbers as well the complicated non synchronous expressions.

As a motivating example, Fig. 2.7 shows the amplitudes of both absorbers, as obtained from the perturbation equations along with simulation results, versus the amplitude of the order n applied torque, with the order $2n$ torque taken to be zero; this corresponds to sweeping along the horizontal axis in Fig. 2.4(a). This is of interest to situations when the order $2n$ absorbers are used to address the second harmonic in the rotor response induced by the nonlinear dynamics of the order n absorbers. We initially assume a stable response in the perturbation equations for Fig. 2.7, but, as will be shown, nonsynchronous responses can occur.

It is of interest to note that although the system is being excited only at order n, the order $2n$ absorbers actually reach their cusp amplitude at a torque level much below that

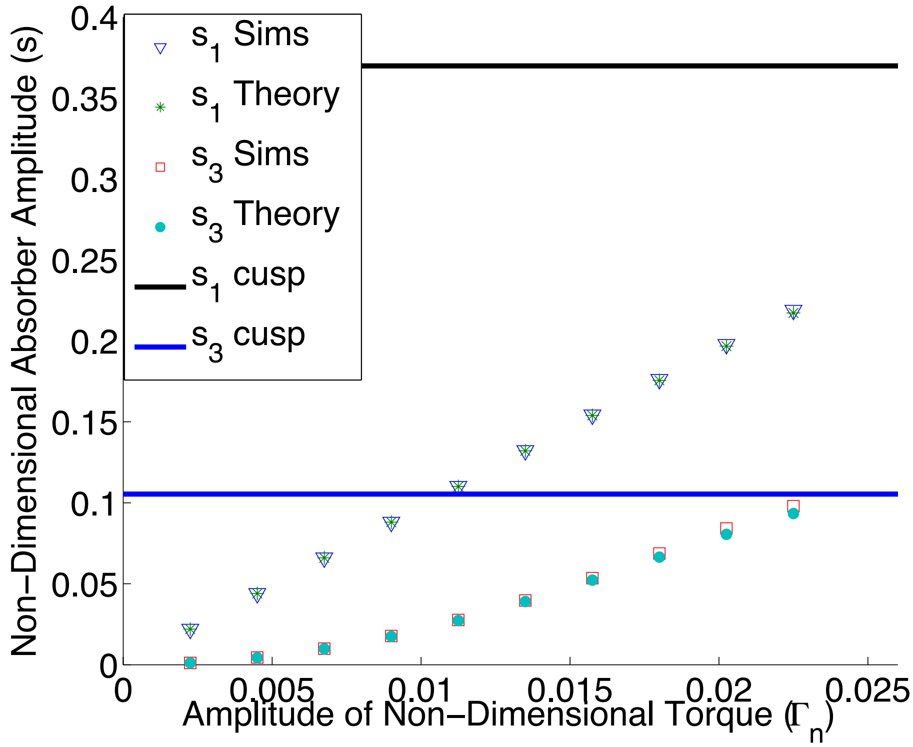

Figure 2.7: Predicted and simulated steady-state absorber amplitudes as a function of the order n torque amplitude; the order $2n$ torque amplitude is zero. The cusp values are amplitude limits set by hardware constraints. System parameters: $m_3/m_{1.5} = 0.1$, $\epsilon = 0.05$.

which causes the order n absorbers to reach their amplitude limit. This is a result of the non-linear interaction between the absorbers, specifically the fact that the order n absorbers impart a harmonically rich torque on the rotor, composed primarily of orders n (used to address the order n torque), $2n$, and $3n$. It is clear from these results that the order $2n$ absorbers do not have sufficient inertia for these loading conditions. If one were to analyze this system using linear response theory, which ignores the nonlinear interactions, the results would show the order $2n$ absorbers to have a much smaller amplitude, since the order $2n$ absorbers are being driven well away from their resonance. Thus, the growth of the order $2n$ absorbers as the order n torque is increased is clear evidence of the importance of nonlinear effects. One goal of the present work is to provide a tool for determining the appropriate inertia balance, described by the parameter α, for such sets of absorbers.

As the main goal of the absorbers is to reduce torsional fluctuations of the rotor, one can investigate how well they perform by looking at the angular acceleration amplitude of the rotor. This is shown in Fig. 2.8, for the same conditions as Fig. 2.7.

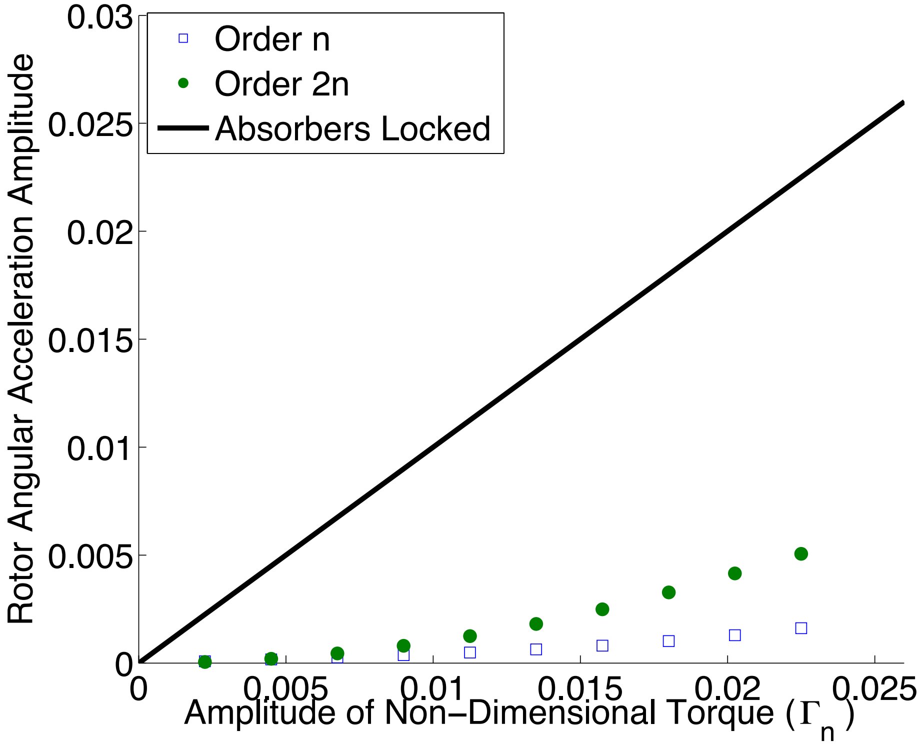

Figure 2.8: Order n and $2n$ harmonic components of the rotor angular acceleration as a function of the order n applied fluctuating torque amplitude, for the same conditions as Fig. 2.7. The solid line is the reference response for the absorbers locked.

In order to benchmark the effectiveness of the absorbers, one considers the rotor response with the absorbers locked in place, so as to account for their added flywheel inertia, but not their dynamic effects; this torsional vibration level is represented by the solid line in Fig. 2.7. As seen from Fig. 2.8, the absorbers significantly reduce the order n component of the rotor torsional vibrations, as desired. It is also interesting to note that, even though the rotor is being driven only at order n, order $2n$ torsional vibrations are present, as described above. In fact, these would be even more prominent if not for the presence of the order $2n$ absorbers. For all results to follow, the rotor vibration results are very similar to those of Fig. 2.8, and are thus not shown.

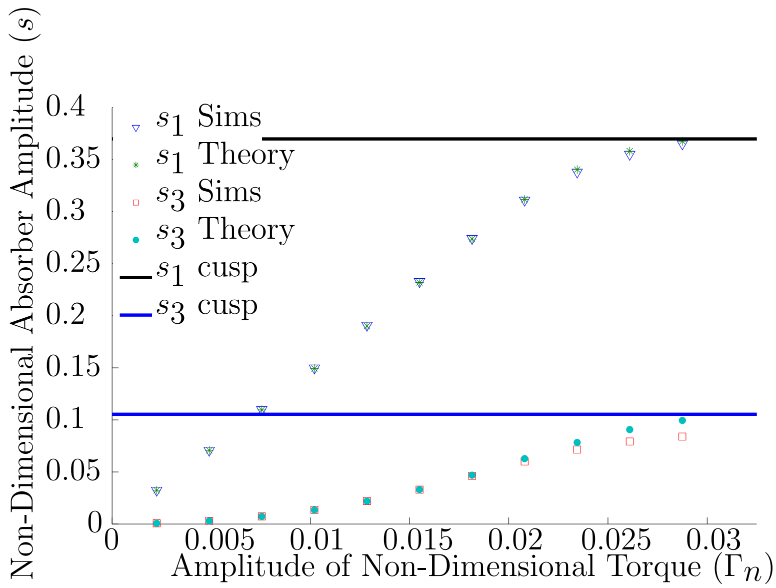

Figure 2.9: Absorber amplitudes as a function of order n fluctuating torque amplitude; the order $2n$ torque amplitude is zero. System parameters: $m_3/m_{1.5} = 0.62$, $\epsilon = 0.05$. The absorbers reach their respective cusps at approximately the same level of excitation.

The results of Fig. 2.7 show that this design does not have appropriate inertia balance between the order $n = 1.5$ and $2n = 3$ absorbers, since the order 1.5 absorber is not near its limits at a torque level where the order 3 absorber reaches its limits. An ideal design would have the absorbers reach their limits at the same torque level. In fact, the perturbation equations offer an analytical prediction for the mass ratio that provides this condition, determined as follows using the steady-state perturbation equations. First, damping is taken to be zero, so that the absorber response phases are all zero or π, and then the absorber amplitudes are set to be at their respective cusp values, or some percentage thereof (which are functions of only their tuning orders $\tilde{n}$ [14, 39]). This results in a pair of equations that involve the following parameters: the absorber mass ratio, the peak torque level (corresponding to the value when both absorbers reach their cusps, $\tilde{\Gamma}_{n,m}$ and $\tilde{\Gamma}_{2n,m}$), the two forcing orders and the values of the absorber detunings. These equations provide a very useful tool for selecting important absorber design parameters, and determining the maximum torque level the resulting system can handle. These equations are given by:

$$\tilde{\Gamma}_n = -\frac{a_{1,m}n_1}{4F_2(a_{1,m})(1+\alpha)}\Big(-2n_1 + a_{1,m}^2 n_1^5 \\ +2a_{2,m}F_1(a_{2,m})n_1^2\alpha + 4\sigma_1(1+\alpha) - \tilde{\Gamma}_{2n}(1+\alpha)\Big),$$

and

$$\alpha = \frac{a_{1,m}^2(-2(F_1(a_{1,m}) + F_2(a_{1,m})))n_1^3 - 4(a_{2,m}n_1\sigma_2 + F_2(a_{2,m})\tilde{\Gamma}_{2n})}{a_{2,m}^3 n_1^6 + a_{2,m}n_1(-2n_1 + 4\sigma_2) + 4F_2(a_{2,m})\tilde{\Gamma}_{2n}},$$

where, for the tautochronic epicycloids, the maximum absorber amplitude is defined as:

$$a_{i,m} = \frac{1}{\tilde{n}_i\sqrt{\tilde{n}_i^2+1}}.$$

Fig. 2.9 repeats the conditions shown in Fig. 2.7 with the same total absorber inertia, but with a different ratio of absorber inertias. Here the absorber inertia ratio is calculated so that both sets of absorbers reach their maximum values at the same torque level for the given absorber tuning, specifically, $\alpha = 0.62$, a surprisingly large value given the fact that there is no applied torque at order $2n$. Note that the corresponding maximum torque level is predicted to be $\Gamma_{n,max} = 0.025$, closely matching the value found by simulations. These results demonstrate the utility of the perturbation predictions. Note that the optimal mass ratio can also be obtained when both orders of excitation are present, but one must assume some relationship between the different forcing order amplitudes, and found by solving the above equations simultaneously.

The above results show the effects of the multiple absorbers on each other, as well as the dependency of the system response on the ratio of the absorber inertias. The matter of how these parameters affect torsional vibration levels will be considered after we describe non-synchronous responses.

2.5 Non-Synchronous Responses

We now turn to some instabilities that can occur when multiple absorbers are used at each order. It should be noted than in order to carry out an analytical study on the stability of the synchronous response, one must compute the Jacobian of the set of the non-synchronous perturbation equations, evaluate this Jacobian on the synchronous solution, and then calculate the eigenvalues of this matrix. This, in fact, is not a trivial task for single order absorber systems [8, 39], and may perhaps be impossible for sets of multiple order absorbers due to the fact that an analytical synchronous response solution is not evident to the author. With this in mind, the stability calculations done in this study are carried out using numerical continuation software, and prove to be computationally inexpensive and very accurate.

Using the full, nonsynchronous perturbation equations for a system of four absorbers (two at each order), a numerical continuation study using AUTO [15, 16] is carried out for the conditions used in Fig. 2.7. The order n torque is swept until the bifurcation to nonsynchronous response of the order n absorbers is found, in which the absorber response is similar to that in Fig. 2.5 (c). This instability is then investigated as both the order n and order

$2n$ torque amplitudes are varied. As clear from Fig. 2.10, the nonsynchronous response of the order n absorbers, caused by the order n torque, is actually due to the same bifurcation as the subharmonic response of the order n absorbers when driven primarily by an order $2n$ torque. Thus, the solid and dashed-dotted bifurcation lines depicted in Fig. 2.4(a) are actually a single curve, bounding synchronous and nonsynchronous responses of the order n absorbers, although the character of these nonsynchronous responses appears different in the two limiting cases, $\Gamma_n = 0$ and $\Gamma_{2n} = 0$. Note that in all these simulations the order $2n$ absorbers remain mutually synchronous. The maximum (cusp) amplitude of the absorbers is shown in Fig. 2.10 as well, and it is clear that this instability occurs near the maximum absorber amplitudes. Simulations of the full non-linear equations confirm the accuracy of these bifurcation curves, as shown in Fig. 2.10. Also shown in Fig. 2.10 are contours of the root mean square (RMS) values of the rotor response, generated from analytical approximations by inserting the absorber amplitudes obtained from the perturbation equations into the scaled rotor response assumption, Eqn. 2.7. One can see that at torque levels above this instability line, the rotor response increases dramatically in amplitude, as the absorbers go unstable and grow towards their amplitude limits.

The curve in Fig. 2.10 provides very useful guidelines for designing multiple order absorber systems, as one must design the system to be in the stable regime, and desires to minimize the rotor vibration amplitudes. Typically, one would have a range of the two torque amplitudes along with their relative phase, and one would select absorber parameters so that the synchronous response was stable for all operating conditions. Examples of this situation are not presented here, but are straightforward to obtain using the tools developed herein.

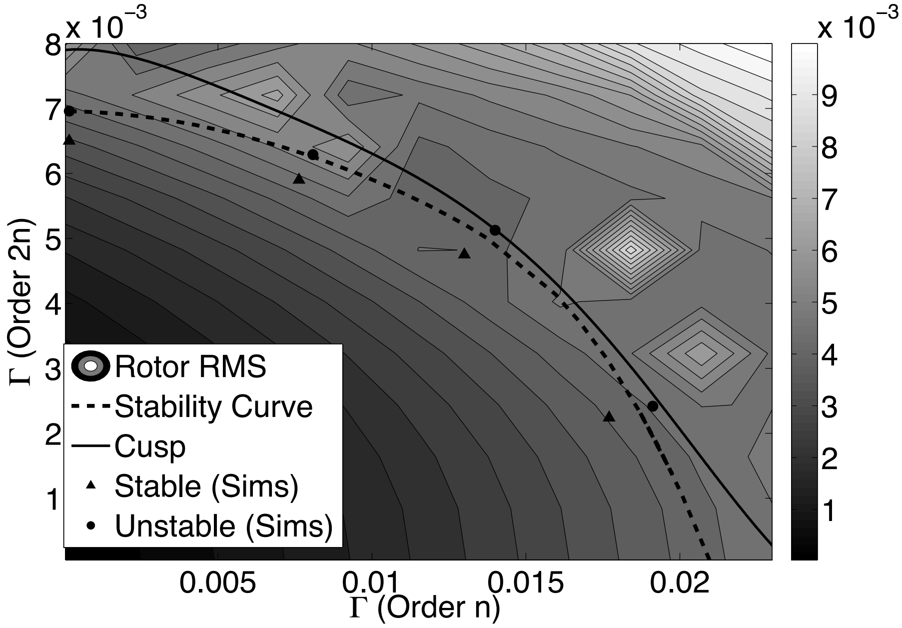

Figure 2.10: Order $n = 1.5$ absorber synchronous response stability boundary as a function of the driving torques, for $\phi = 0$. Torques outside the range of this curve result in nonsynchronous responses of the order n absorbers.

2.5.1 Minimizing Torsional Vibration

In order to attenuate torsional vibrations at multiple orders, CPVA's tuned to the multiple orders must be used. Interestingly, it was shown above that if only the order n torsional vibration is desired to be decreased, a system using multiple orders of CPVA's can be more effective than using only absorbers tuned to order n (we used $2n$ absorbers in addition to n, but further adding $3n$ might offer even more benefit). In this part of the study we keep the total inertia of all absorbers constant as α (defined in Table 2.1) is varied, which makes the performance comparisons meaningful, since one expects to get better performance if more total absorber inertia is added. Of particular interest here is the level of torsional vibration, since its reduction is the ultimate goal of the absorber systems. This is computed from the perturbation results for the absorber amplitudes, specifically using the scaled rotor angular acceleration, w', after the absorber amplitudes have been determined using Eqns. (2.10)-

(2.13). The measure we use for the rotor torsional vibration is percent correction, defined as the ratio of the order n component of rotor angular acceleration amplitude when the absorbers are locked to that when they are free.

As α is varied the limiting mechanisms of the absorbers depend on the arrangement of absorbers. If one has only a single absorber at order n, the limiting factor is the cusp amplitudes of the absorbers and the results of Section 2.4 apply; in this section these limits are depicted in the Figures that follow as dashed-dot curves for the limit of the order n absorbers and as solid curves for the limit of the order $2n$ absorbers. If there are multiple absorbers at order n, the limiting factor will be the instability of the synchronous response, and the critical value Γ_n^* is depicted as a dotted curve in the Figures, as calculated by numerical continuation of the perturbation equations using AUTO.

To illustrate the main points of this section, Figure 2.11 shows a contour plot of the torsional vibration amplitude as a function of the order n torque amplitude Γ_n and the mass ratio α, where the absorbers are assumed to remain synchronous, which is analogous to having a single absorber at each order, and there is no torque at order $2n$ ($\Gamma_{2n} = 0$). In this case the order n absorbers reach their cusps along the dashed-dot line, and the order $2n$ absorbers reaching cusps along the solid line. Note that these two conditions meet at $\alpha \approx 0.62$, which is the optimal value found in the analysis of Section 2.4. For reference, Γ_n^* is shown as the dotted curve in Fig. 2.11, although it is not relevant to this case. This indicates that the limiting condition is the loss of stability of the synchronous response when multiple absorbers are used at order n, which will be considered below. As is evidenced in Fig. 2.11, when desiring to attenuate vibrations at order n only and assuming a synchronous absorber response, using all the available inertia towards order n absorbers yields the largest correction. The addition of order $2n$ absorbers decreases the correction, although only by a small amount, and will be shown to provide a benefit in the stabilization of the order n absorbers when the stable response assumption is lifted.

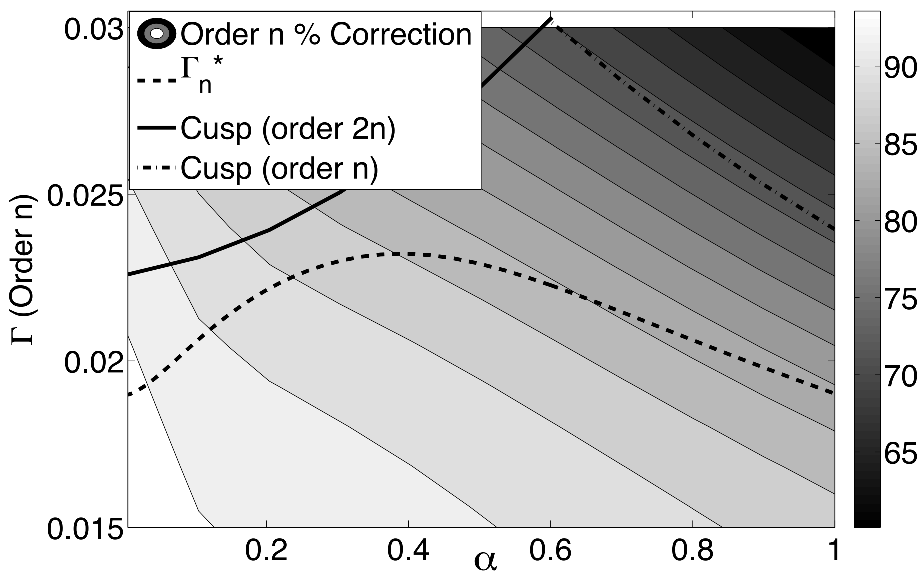

Figure 2.11: Order n applied torque versus the mass ratio of the different order absorbers, when assuming a synchronous response.

Fig. 2.12 shows the contours of torsional vibration correction for the same conditions as Fig. 2.11, but with two absorbers at order n. Note that the limiting condition here is Γ_n^*, and that the loss of stability causes a sharp increase in the torsional vibrations at the limit, which is well below the cusp limits. In the stable regime, the contours of the percent correction are exactly the same as those in Fig. 2.11, although different contour lines are labeled. This clearly indicates the importance of the stability of the synchronous response. An interesting, and surprising, observation is the fact that the order $2n$ absorbers provide a 23.5% increase in the order n operating torque range, that is, the order $2n$ absorbers actually stabilize the synchronous response of the order n absorbers. In this case the optimal value of α for maximizing the torque range is approximately 0.4. This is well below the "equal cusp" value of 0.62, but still a significant distribution of absorber inertia at order $2n$, given the fact that the torque is purely order n. Considering the contours, one obtains a better correction for small values of α, but α allows for a significant increase in the torque operating range. Practically, this trend allows the tuning on the order n absorbers to be much more aggressive (closer to the torque order), and thus results in better performance in reducing the order n torsional vibrations.

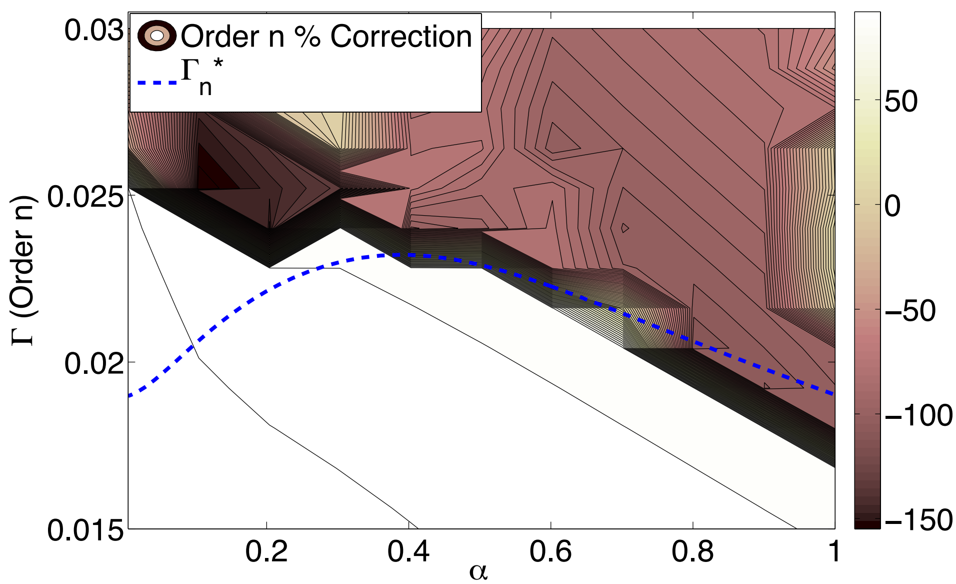

Figure 2.12: Order n applied torque versus the mass ratio of the different order absorbers. As evident, using a small amount of order $2n$ absorbers can stabilize the order n absorbers.

2.6 Non-Tautochronic Paths

All of the previous analysis was conducted for a tautochronic path, which renders the absorber motion linear out to large absorber amplitudes. Previous researchers have conducted extensive analysis on the dynamics of non-tautochronic path absorbers [3, 34, 36, 47], specifically circular and cycloidal path absorbers, all for single order absorber systems. In order to conduct analysis on these non-tautochronic paths, one must scale the absorber amplitudes to be small, which is not required for perturbation analysis of the tautochronic path absorbers. Since the torque generated by the absorbers onto the rotor becomes harmonically rich at larger absorber amplitudes, this amplitude scaling results in perturbation equations which fail to capture the non-linear multiple order absorber crosstalk to leading order of the small parameter. As mentioned earlier, and detailed in [39], a perturbation at leading order away from the tautochrone can be implemented in order to analytically investigate absorber paths which deviate from the tautochrone without having to assume small absorber amplitudes. The question that then remains is if this $O(\epsilon)$ correction to the path can accurately capture the system's dynamics throughout the range of curves possible using the two-parameter family of paths as explained above. In order to answer this question, the two extremes of the family of curves are investigated, specifically circular and cycloidal paths. Referring back to Fig. 2.3, one can see that, strictly geometrically speaking, the cycloidal path does not differ greatly from the epicycloidal path, and in fact can almost be exactly replicated by keeping terms to $O(s^8)$ in the perturbation away from the tautochrone, $h_i(s_i)$, as shown in Fig. 2.13. It is also noteworthy that, as fully derived in [14], the nonlinear path parameter which yields a tautochronic epicycloid, λ_{te}, can be expressed in terms of the absorber tuning as,

$$\lambda_{\text{te}} = \sqrt{\frac{\tilde{n}^2}{\tilde{n}^2 + 1}}.$$

Recalling that $\lambda = 1$ yields a cycloidal path, as $\tilde{n} \to \infty$ the tautochronic epicycloid approaches a cycloid. One then expects the absorber tuning order to effect the accuracy of the results, causing a general formulation of the dynamics non-tautochronic path absorbers to be difficult.

We begin by the analysis on a single order absorber/rotor system in order to asses both

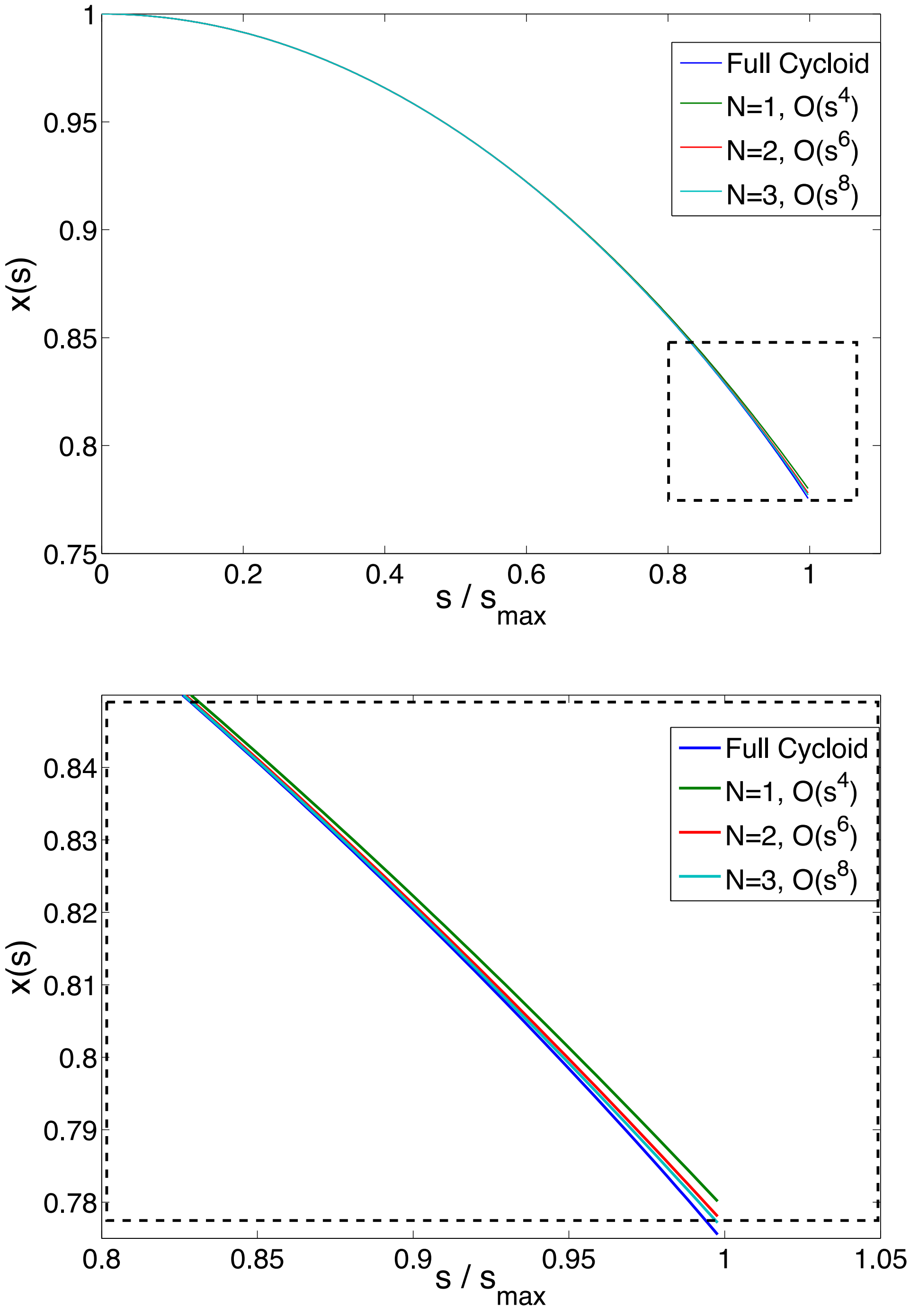

Figure 2.13: Normalized rotor center to absorber COM length as a function of absorber arc length for different numbers of truncations of the absorber path.

the ability of the perturbation equations to accurately estimate the dynamics of the system, as well the effect of the absorber tuning on this ability. Shown in Fig. 2.14 are the percent difference in absorber amplitudes obtained from the perturbation equations to those found by numerically integrating the full equations of motion versus the absorber tuning order for cycloidal paths. It is know from previous researchers, and can be confirmed by numerical simulations, that the cycloidal path causes the the absorber frequency to increase with amplitude, a so-called hardening nonlinearity. We therefore perform the comparisons between the perturbation equations and the numerical simulations at a torque level which produces an absorber amplitude equal to 90% of it's cusp amplitude, as found from simulations. It is clear from Fig. 2.14 that using the tautochronic path scaling to capture the dynamics of cycloidal path absorbers is yields large errors as compared to numerical simulations at large absorber amplitudes, although these errors are decreased as the absorber tuning order is increased. It is therefore necessary to perform a "strongly" nonlinear analysis in to accurately predict the dynamics of cycloidal path absorbers for a general tuning order. This analysis would require the use of action/angle coordinates and could be quite involved. For this reason, further investigation of multiple order, cycloidal path absorber systems is not undertaken in this study.

A similar analysis on the ability to analytical investigate circular path absorbers is not given here, as previous research has shown the detrimental instabilities that can occur for such paths [34,36,47]. Circular path absorbers are only beneficial in their ease of implantation and should only be considered as a last resort.

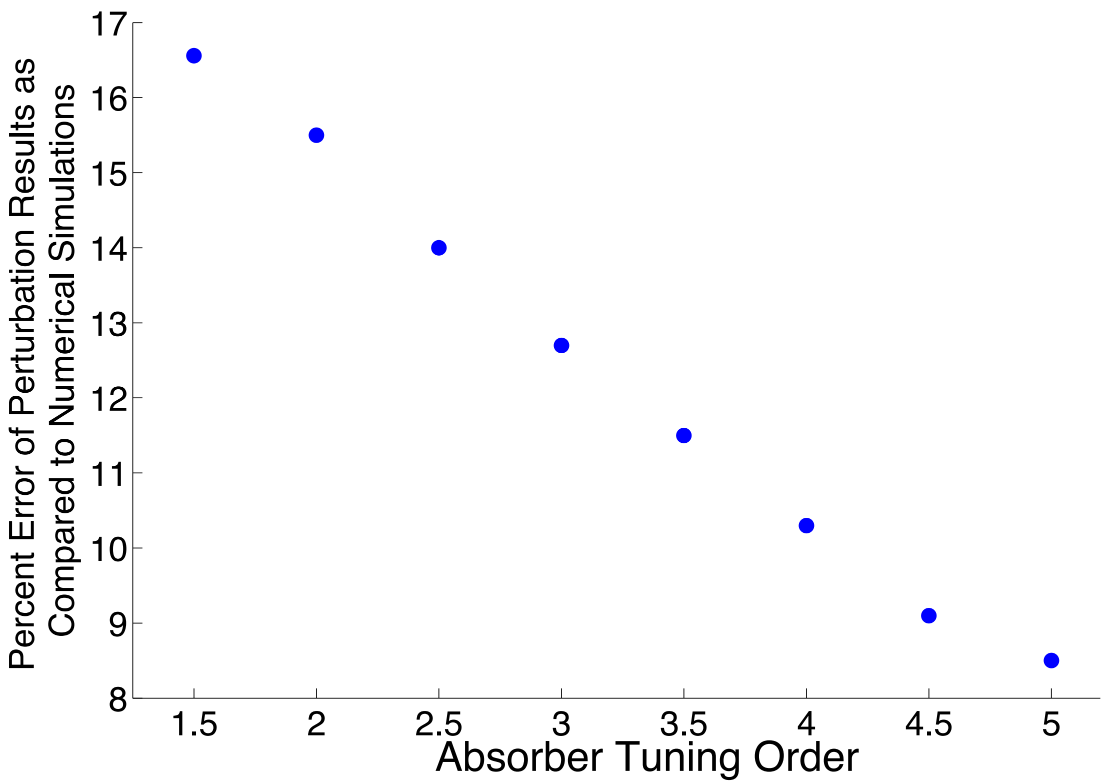

Figure 2.14: Percent error between the perturbation equations and numerical simulations for a single order cycloidal path absorber system vs. absorber tuning order.

Chapter 3

Experimental Validation

The analytical predictions presented in the previous chapter are investigated through the use of a customized experimental setup here. The experimental setup is described and a set of parameter identification tests are conducted. Synchronous, steady state experiments are performed on multiple order absorbers, as well non-synchronous stability tests. The experimental data is found to agree with the theoretical results.

3.1 Experimental Setup

The experimental rig consists of a shaft (the rotor) with a mounting section for up to four absorbers, driven by a feedback-controlled electric motor. The setup is equipped with four absorbers here, two tuned to order $\tilde{n}_1$ and two tuned to order $\tilde{n}_2$, where $\tilde{n}_2 = 2\tilde{n}_1$. For the subsequent discussion, the order $\tilde{n}_1$ absorbers are referred to as absorbers 1 and 2 and the order $\tilde{n}_2$ absorbers as 3 and 4. A schematic diagram of the experimental setup is shown in Fig. 3.1, outlining the sensors and controls, explained subsequently. A photograph of the experimental setup, equipped with the multiple-order absorbers is shown in Fig. 3.2, giving the reader a view of the actual components described below.

The instantaneous angle of the absorbers ϕ (relative to the rotor) is measured via an optical encoder. In order to compare the measured absorber angle to the analytical formulation, we must convert this angle into an arc length, S (in meters). For an epicycloidal

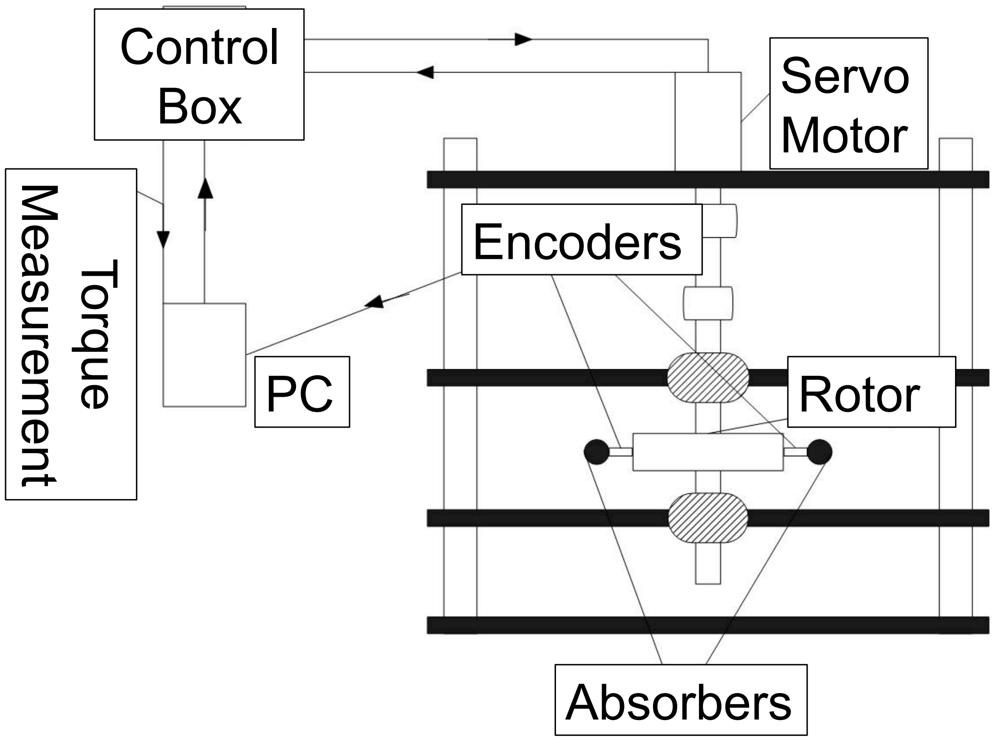

Figure 3.1: Schematic of the experimental setup.

path, this measured angle can be described in terms of the absorber arc length, as shown in Fig. 3.3, as

$$\phi = \tan^{-1}\left(\frac{x(S)}{y(S)}\right), \tag{3.1}$$

where the $x(S)$ and $y(S)$ distances for an epicycloidal path can be shown to be

$$x(S) = \frac{\rho_0}{1-\lambda^2}(\sin(\xi)\cos(\lambda\xi) - \frac{\lambda^2 S}{\rho_0}\cos(\xi)),$$

$$y(S) = L + \frac{\rho_0}{1-\lambda^2}(\cos(\xi)\cos(\lambda\xi) + \frac{\lambda^2 S}{\rho_0}\sin(\xi) - 1),$$

where $\xi = (1/\lambda)\sin^{-1}(S\lambda/\rho_0)$, which is the local tangent angle (in radians) to the pendulum COM curve with respect to the x axis , and L is the length of the encoder arm. In order to get a relationship between the measured encoder angle and the absorber arc length,

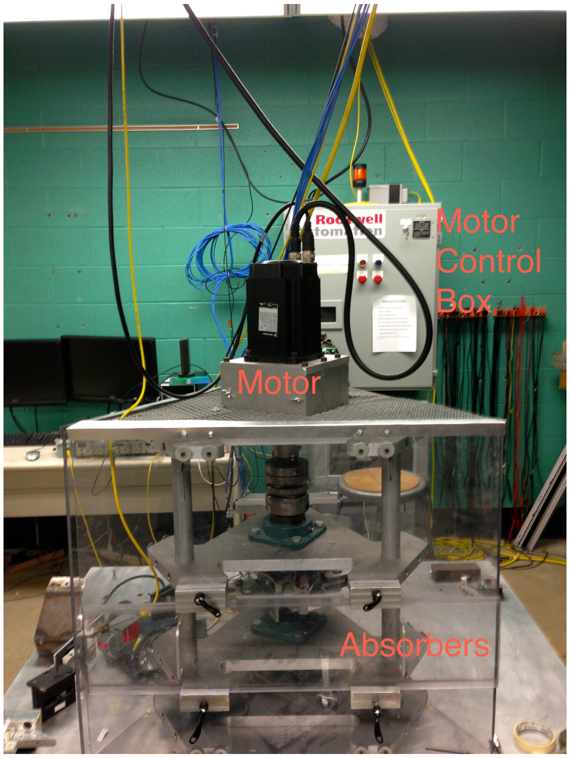

(a)

(b)

(c)

Figure 3.2: Photograph of the experimental setup. (a) The entire setup, showing the motor, rotor, and corresponding motor control and data acquisition components. (b) Multiple order experimental absorbers. (c) Self centering rollers.

Eq. (3.1) must be solved for S in terms of ϕ. This can only be done numerically, when given the values of the encoder arm length, L, non-dimensional large-amplitude path coefficient, λ, and the path vertex radius of curvature, ρ_0 (in m). These values are indeed known, and interestingly, when one plots the absorber arc length versus the encoder angle for the

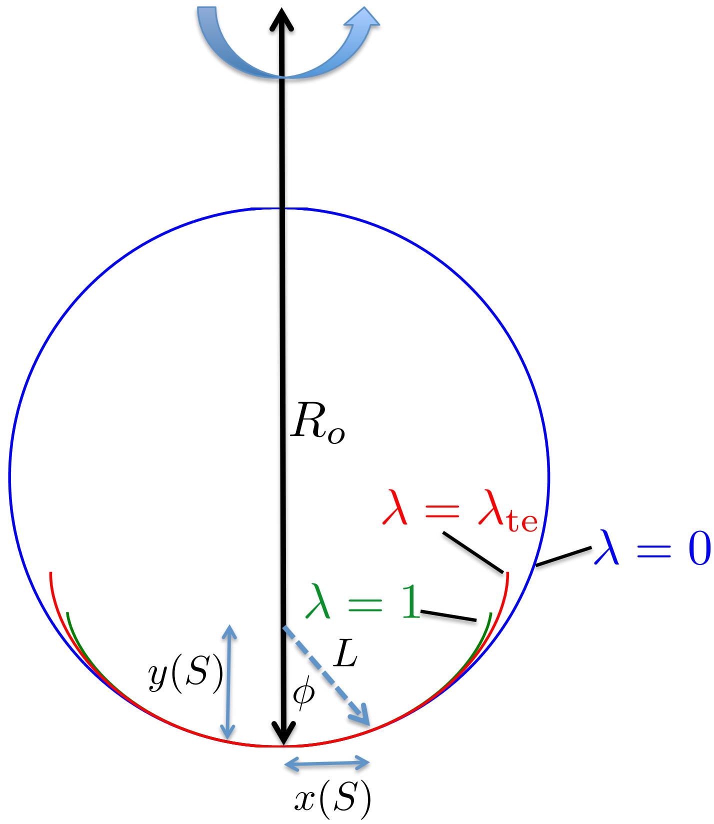

Figure 3.3: Geometrical schematic of the measured absorber angle via an optical encoder with a rotating arm of length, L (λ_{te} provides a tautochronic epicycloid and λ_1 yields a cycloid.

epicycloidal path formulation and compares this to the obtained absorber arc length for a circular path ($S = L\phi$), the differences are negligible, as shown in Fig. 3.4. In fact the error in calculating the arc length from a circular path assumption when the absorber is at its amplitude limit is only 0.112%. Thus we can use the circular path assumption in order to translate the measured encoder angle into an absorber arc length.

The instantaneous rotor speed $\dot{\theta}$ is also measured by an optical encoder, from which the mean and harmonic components, as well as the angular acceleration, can be distilled. The torque $T(\theta)$ applied to the rotor is supplied by an input voltage to the armature, and is quantified by measuring the current sent to the motor; a current to voltage conversion

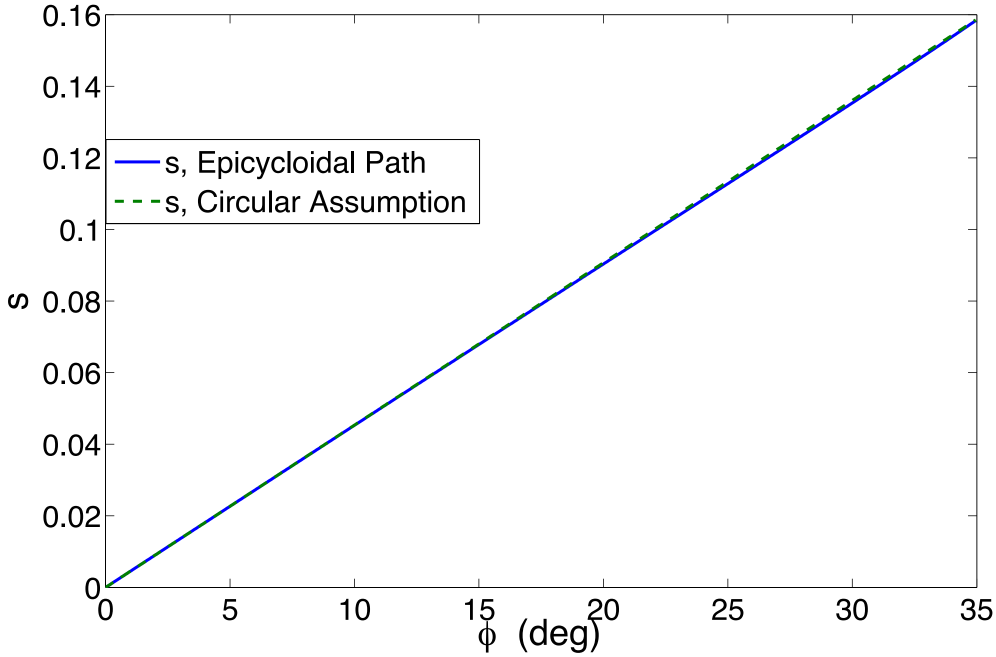

Figure 3.4: Calculated non-dimensional absorber arc length, s, versus measured encoder angle, ϕ, for epicyloidal and circular path formulations.

is set in the control box which allows the corresponding torque voltage to be displayed in LabVIEW. Using the inertial properties of the motor given by the manufacturer, the torque (in Newton-meters) can then be obtained from the voltage measurement. All three of these signals (absorber angle, rotor speed, and torque) are fed into a PC running data acquisition and control software (coded in LabVIEW), which allows for real-time viewing and post-processing of data in the time or order (frequency divided by the mean speed) domains. The custom written LabVIEW code also allows for PID feedback control of the mean rotor speed to maintain a nearly constant mean speed, upon which the fluctuating torque is applied. An error analysis has been conducted on the experimental sensors in order to obtain quantitative measures of the accuracy of the data and is presented in Appendix A.1. An important feature of this setup is that the fluctuating components of the applied torque are based on the rotational angle of the rotor, which allows for accurate engine order excitation, for which multiple engine order harmonics can be generated, and also allows for external data from, say a dynamometer, to be used to generate the torque pulses. The ability to change the applied order of the torque allows one to easily investigate the influence of mistuning between the absorber and applied torque order, without having to change the absorber hardware. Further details of this rig are described in [40].

3.2 System Parameter Values

In order to quantify certain physical parameters associated with the experimental setup that cannot be directly measured, specifically the rotor inertia, absorber tunings, and absorber and rotor damping, a set of parameterization experiments are first conducted. The unknown parameters listed above can be extracted by running the experiment under certain conditions and utilizing the available measured quantities, which will now be explained in detail.

3.2.1 Rotor Inertia

To obtain the rotor inertia, J, the attached absorbers are locked into place at their respective vertices, which reduces the equation of motion for the rotor to,

$$J\ddot{\theta} + c_0\dot{\theta} = T_0 + T\sin(n\Omega t), \tag{3.2}$$

where θ is the rotational angle of the rotor, $\dot{()} = d()/dt$, c_0 is the rotor damping, and T_0, T are the amplitudes of applied mean and fluctuating components of torque, respectively. Assuming the rotor damping force balances the mean torque, the rotor angular velocity, $\dot{\theta}$ can be measured for different levels of applied fluctuating torque, T, when applied at a constant order, n. The order n rotor angular acceleration fluctuations can then be computed from the measured velocity, and are plotted versus different values of the applied order n torque, as shown in Fig. 3.5. A line is then fit to this data and the slope of this line is $1/J_{\text{meas}}$, from which we obtain the rotor inertia. It should be noted that when measuring the inertia, the absorbers are kept on and locked instead of being removed. This is due to the fact that the bifilar absorbers do not rotate with respect to the rotor and, therefore the inertia of the absorber about their center of mass can be added to the rotor inertia. The rotor inertia used for analysis is then easily calculated from the measured inertia as

$$J = J_{\text{meas}} - \sum_{i}^{M}(m_i R_{i,0}^2).$$

The rotor inertia is different for each of the subsequent experimental investigations, as we add and remove absorbers for the different tests and the overall inertia ratio is desired to be kept the same, done by adding inertia to the rotor. Therefore this test must be repeated each time and, for this reason the obtained rotor inertia values for each experiment are presented in the corresponding experimental investigation sections below.

3.2.2 Absorber Tunings

The absorbers were designed to be tuned to a certain order, but one must experimentally verify the actual absorber tuning order. It can be shown [19] that amplitude of rotor angular acceleration, when compared against the forcing order n, for a given torque level, will have a minimum at the tuning order of the pendulum. Shown in Fig. 3.6 is the amplitude of the order n harmonic of the rotor angular acceleration divided by the measured amplitude of the applied order torque versus the order of the applied fluctuating torque for an order $\tilde{n}_1$

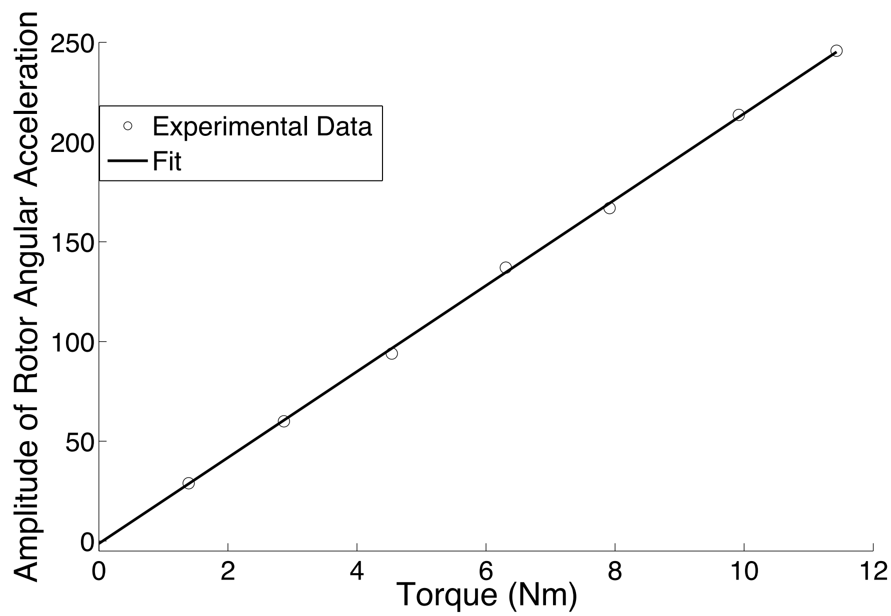

Figure 3.5: Amplitude of order n rotor angular acceleration versus the amplitude of applied order n torque, with absorbers locked.

absorber. The angular acceleration amplitude is divided by the measured applied fluctuating torque because, although the desired amplitude of torque is kept constant along the entire order range (as specified by the user), the motor may produce small fluctuations about the specified torque. From Fig. 3.6, it is seen that the absorber's tuning order is $\tilde{n}_1 = 2.3$. Similar experiments were carried out on the other three absorbers in order to quantify each absorber's tuning order, where the results are presented in Table 3.1. When performing these order sweeps, care must be given to the level of applied fluctuating torque used. All previously studied absorber paths (circles, epicycloids, cycloids) have some sort of large amplitude, non-linear behavior with circles producing a softening non-linearity and epicycloids and cycloids a hardening one. If the amplitude of fluctuating torque is too large, then these inherent non-linearities effect the measured tuning order, moving it lower or higher than the actual value, depending on the path. If the amplitude of fluctuating torque is too small, the absorbers will not overcome their frictional damping force, and thus not oscillate. It is therefore somewhat of an art form to correctly apply the right amount of fluctuating torque for generating responses that are good for estimating the tuning order.

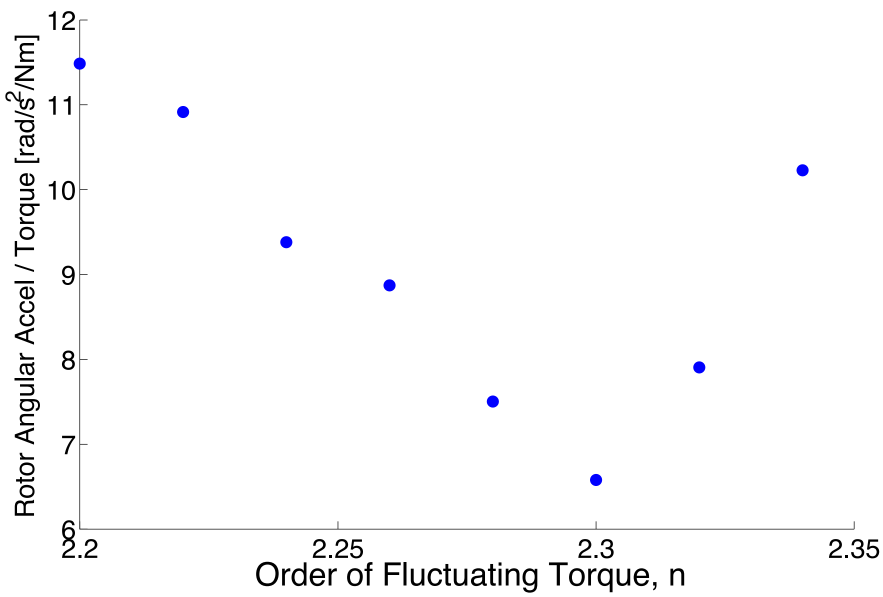

Figure 3.6: Order n amplitude of rotor angular acceleration divided by the amplitude of fluctuating torque as a function of the applied torque order, n.

3.2.3 Absorber Dampings

An equivalent viscous damping is used to model the energy dissipation mechanisms in the experimental absorbers. In order to quantify this damping, a logarithmic decrement scheme [45] is employed. In order to achieve a free vibration response experimentally, an amplitude of oscillating torque which produces an absorber amplitude of $\approx 12^\circ$ for the order $\tilde{n}_1$ absorbers and $\approx 7^\circ$ for the order $\tilde{n}_2$ absorbers is suddenly shut off, while the rotor maintains a nearly constant speed. These absorber amplitudes were chosen to allow for a sufficient amount of absorber decay time while at the same time keeping the absorbers in their linear response regime. The experimentally obtained absorber amplitudes versus there respective times of decay are shown for both order absorbers in Fig. 3.7. As commonly found in all undergraduate vibrations texts, the ratio between N peaks in a single degree of freedom, free vibration decay is given by

$$\delta = \frac{1}{N} \ln\left(\frac{x_i}{x_{i+N}}\right) = \zeta \omega_n \tau_d,$$

where ζ is the non dimensional damping ratio, $\omega_n = \tilde{n}_i \Omega$, and $\tau_d = 2\pi/\omega_n\sqrt{1-\zeta^2}$. One can then solve for the non-dimensional damping ratio from

$$\zeta = \frac{\delta}{\sqrt{\delta^2 + 4\pi^2}}.$$

In order to overcome the quantization error inherent in the optical encoders, as well as to calculate the average viscous damping coefficient over the entire decay, nn x_i near the beginning of the decay is used with an x_{i+N} near the end of the decay in order to get an average damping value.

The obtained non-dimensional damping values for each absorber are presented in Table 3.1, for a mean rotor speed of 300 RPM, as the non-dimensional damping is defined as $\mu_{a,i} = c_a/(m\Omega)$, where $\zeta_{a,i} = \mu_{a,i}/(2\tilde{n}_i)$.

3.2.4 Rotor Damping

The analytical treatment of the system at hand involves an assumption that the rotor damping force balances with the mean torque, $T_0 = c_0\Omega$, which eliminates the effect of the rotor damping in the first order of ϵ. The rotor damping effect is included in the numerical simula-

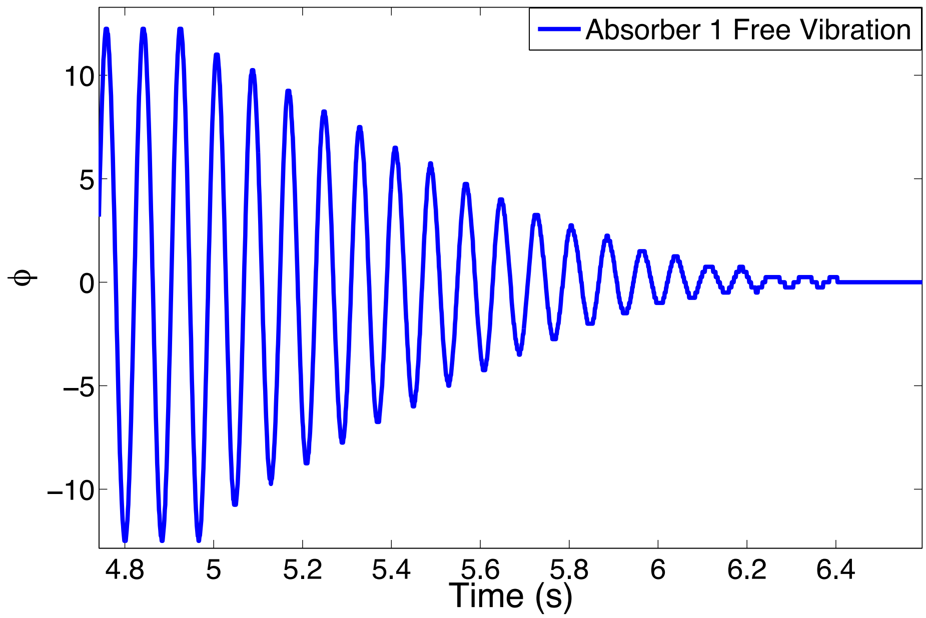

(a)

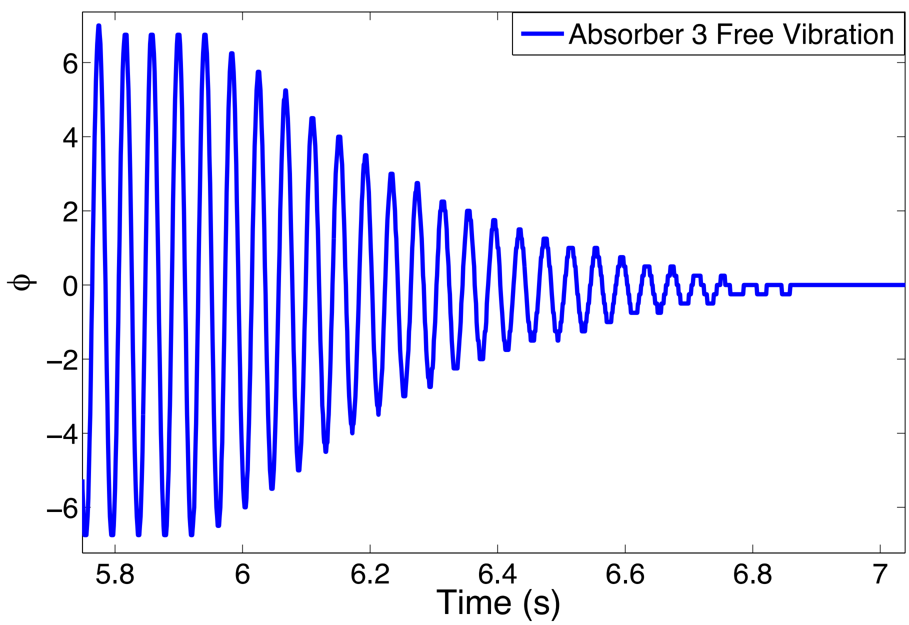

(b)

Figure 3.7: Free vibration response of both order absorbers. (a) Order $\tilde{n}_1$ absorber. (b) Order $\tilde{n}_2$ absorber.

tions, though, which requires the quantification of the experimental rotor damping. In order to accomplish this, we run the rotor at multiple constant speeds with the absorbers locked and measure the applied mean torque required to obtain these speeds. When the rotor spins at a constant speed, Ω, Eq. (3.2) reduces to

$$c_0 \Omega = T_0.$$

The measured mean speed is then plotted against the measured mean torque for a range of speeds, as shown in Fig. 3.8. If the rotor damping force is not a function of mean speed, then the data should be linear in the mean torque with a slope of $1/c_0$. Looking at Fig. 3.8, the data is not precisely linear, but a linear assumption suffices here, as the rotor damping has a small effect on the system dynamics. The dimensional value of this damping is in Table 3.1.

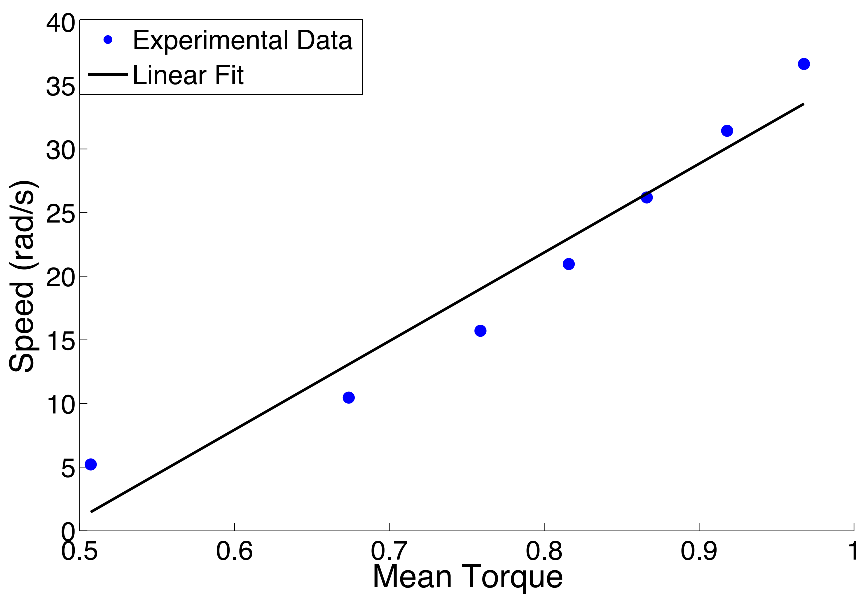

Figure 3.8: Rotor mean speed, Ω vs. the mean torque applied, T_0.

All of the experimental parameters obtained by the methods described above are presented in Table 3.1.

Table 3.1: Values of Experimental Parameters.

Parameter	Definition	Value
$m_{1,2}$	absorber 1 and 2 mass	0.4312 kg
$m_{3,4}$	absorber 3 and 4 mass	0.0482 kg
α	inertia ratio between multiple order absorbers	0.106 kg
$R_{1,0}$	rotor center to absorber 1 and 2 COM	0.12316 m
$R_{3,0}$	rotor center to absorber 3 and 4 COM	0.123 m
$\tilde{n}_1$	absorber 1 tuning order	2.3
$\tilde{n}_2$	absorber 2 tuning order	2.3
$\tilde{n}_3$	absorber 3 tuning order	4.6
$\tilde{n}_4$	absorber 4 tuning order	4.6
$\mu_{a,1}$	absorber 1 viscous damping	0.1
$\mu_{a,2}$	absorber 2 viscous damping	0.1054
$\mu_{a,3}$	absorber 3 viscous damping	0.191
$\mu_{a,4}$	absorber 4 viscous damping	0.186
c_0	rotor damping	0.0144 Nms

3.3 Steady-State Experimental Results

Utilizing the experimental setup described above, steady-state absorber and rotor responses as functions of the amplitude of applied fluctuating torque were tested for sets of multiple order absorbers. Synchronous and non-synchronous absorber responses are compared against the perturbation results derived in the previous chapter (Eqs. (2.10) to (2.13)). The experimental rotor angular acceleration fluctuations are compared with predictions obtained by extracting the first three rotor harmonics from the scaled and expanded form of the rotor angular acceleration, as given in Eq. (2.7). Numerical simulation results are also presented for each experimental investigation.

3.3.1 Synchronous Response

To experimentally test the synchronous response of multiple order absorbers, one absorber at each order is unlocked and free to oscillate. The amplitude of the fluctuating torque, applied at $n = 2.29$, is varied and the response of the absorbers at each order is measured through optical encoders. Shown in Fig. 3.9 is the experimentally obtained non-dimensional absorber amplitudes versus the amplitude of applied order n torque, along with the predictions obtained through the perturbation equations (labeled as theory) and numerical simulations.

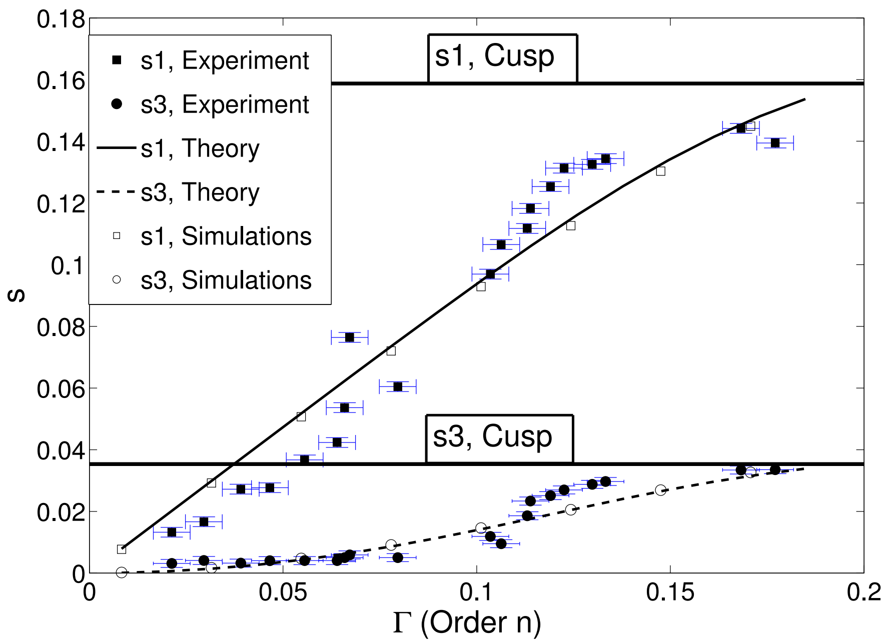

Figure 3.9: Experimental absorber amplitudes, s, vs. the amplitude of applied order n torque, Γ_n, with perturbation and numerical simulation predictions. ($n = 2.29$, $\epsilon = 0.18486$)

As visible from Fig. 3.9, the perturbation equations accurately predict the amplitudes of both order absorbers for the entire torque range. The internal $2:1$ resonance, which drives the order $\tilde{n}_2$ absorber is accurately captured in the experimental data, as the forcing is directly resonating the order $\tilde{n}_1$ absorber. There exists a small error between the predictions and the experimental results at low torque levels, most likely due to the absorber damping having features that are not included the model, explained subsequently. First, the level of absorber damping generally is a function of its amplitude [47], whereas a single effective value is used for all amplitudes in the present study, in order to match the analytical models. In fact, it is known that some level of nonlinear damping is present in the system, and this has been investigated in detail for the Coulomb friction aspects of the circular path absorbers [47]. In general, the motion of bifilar absorbers involves frictional rubbing between the absorber and flange, as well as rolling resistance of the rollers. The rubbing is particularly problematic when the rotor axis is vertical and the rotor is run at low speeds, since gravity will promote rubbing. (In fact, gravity is an important effect when running the system with a horizontal rotation axis at the speeds feasible with this equipment [44]). In order to overcome some of the difficulties associated with these effects, self-centering rollers are implemented for the tautochronic bifilar absorbers as shown in Fig. 3.2(c) [2]. In order to center the bifilar absorber with respect to the flange with these rollers, the absorbers must oscillate, and this requires a certain threshold of oscillating force acting on the absorber, thus giving a physical explanation to the damping as a function of absorber amplitude. In fact, this low amplitude effect is similar to the dry friction measured for circular path absorbers [47]. Also, as detailed in Section 3.2.3, the absorber damping coefficient used for experimental data is measured by performing a logarithmic decrement on the absorber response when the oscillating part of the applied torque is suddenly switched to zero from an amplitude that causes the absorber to oscillate at an amplitude of about 12°. The decrement is performed over the entire absorber decay, and the method assumes a single degree of freedom system ($\epsilon \rightarrow 0$), whereas the actual dynamics involve coupled oscillations of the rotor and absorber.

Looking at the corresponding experimental rotor harmonics, as shown in Figs. 3.10 and 3.11, the predictions again accurately match the data. The experimental order n rotor harmonic deviates a small amount from the predictive results at low levels of applied fluctuating torque. This is due to the fact that the experimental absorber amplitude at this level is smaller than the predictions, thus not absorbing as much of the torsional oscillations as the model predicts. The order $2n$ and $3n$ experimental data match the predictions across the entire range of torque, and this deviation of accuracy in the order n harmonic due to the absorber amplitude error at small torque levels is not observed. Most likely, this is due to the amplitudes of the higher harmonics being relatively small at these low levels of torque. Overall, the synchronous multiple order predictions track the experimental data throughout the range of applied fluctuating torque, confirming the accuracy of the analytical and numerical predictions.

3.3.2 Non-Synchronous Response: Order $\tilde{n}_1$ Absorbers Only

For the following experimental results, both order $\tilde{n}_1 = 2.3$ absorbers are unlocked, and the order $\tilde{n}_2$ absorbers are removed, yielding an inertia ratio of $\epsilon = 0.226$. Combinations of two orders of applied fluctuating torque at orders $n = 2.3$ and $2n = 4.6$ are applied. The applied torque is increased until the non-synchronous bifurcations captured analytically in Section 2.5 are experimental observed. Four points covering the $\Gamma_{n,2n}$ surface are investigated, as shown in Fig. 3.12.

As visible from Fig. 3.12(a), the analytical stability curve, generated from a numerical continuation of the perturbation equations, accurately predicts the torque amplitudes which cause the absorber instabilities. The points labeled (1) in Fig. 3.12(a) exhibit the synchronous and non-synchronous absorber responses generated from a torque at order n only. The square data point corresponds to the experimental torque which causes the non-synchronous response. It can be seen from Fig. 3.12(b) that their is phase difference between the two absorbers, and in some cases, this instability causes an absorber to increase in amplitude and reach it's corresponding amplitude limit. The period doubling, sub-harmonic bifurcation is labeled as the square point (4) in Fig. 3.12(a), and arrises when the applied torque is at order $2n$ only. This bifurcation causes a drastic increase in the absorbers amplitudes, and they quickly reach their amplitude limits, as visible from Fig. 3.12(c). This sub-harmonic bifurcation results in the absorbers oscillating completely out of phase with each other, as captured in Fig. 3.12(d), which exhibits a short time recording of the sub-harmonic response.

3.3.3 Non-Synchronous Response: Order $\tilde{n}_1$ and $\tilde{n}_2$ Absorbers

For the next set of experimental results, all four of the experimental absorbers are unlocked (two at each order). As in the previous section, the absorber instabilities in the $\Gamma_{n,2n}$ torque space are experimentally compared to the analytical results obtained in Section 2.5. For an accurate comparison to the previous section, the ratio of the absorber inertia to that of the rotor was desired to be the same value. In order to accomplish this, due to the added inertia of the order $\tilde{n}_2$ absorbers, inertial weights were added to the rotor. The corresponding measured inertia ratio was found to be, $\epsilon = 0.218$. This is a 3% decrease in the inertia ratio used in the previous section and will suffice for our investigation.

Figure 3.14 exhibits the theoretical stability boundary as a function of the two applied fluctuating torque orders, with experimental results for stable and unstable absorbers responses. The experimental data agrees with the analytical prediction, with the order $\tilde{n}_1$ absorber bifurcations being the same as detailed in the previous section. Interestingly, the addition of the order $\tilde{n}_2$ absorbers does not increase the level of fluctuating torque which causes the absorber bifurcations. In fact, the experimental results motivated further study into this phenomenon.

It was found that both the inertia ratio, ϵ, as well as the absorber damping effect the stabilization of the order $\tilde{n}_1$ absorbers through the use of higher order absorbers. Specifically, as the inertia ratio between the absorbers and rotor changes, the optimal inertia ratio of different order absorbers changes as well. The optimal different order absorber inertia ratio of ≈ 0.38 given in Section 2.5 is valid for the specific inertia ratio of absorbers to rotor used in that case ($\epsilon = 0.05$). The absorber damping plays an important role in the stabilization as well, and if the absorber damping is too large, the addition of order $\tilde{n}_2$ absorbers will decrease the torque level which causes the non-synchronous response of the order $\tilde{n}_1$ absorbers. For the experimental parameters used, it was found that a non-dimensional damping ratio coefficient, ζ, of 0.018 was the damping threshold which caused the order $\tilde{n}_2$ absorbers to no longer increase in the stabilization of the order $\tilde{n}_1$ absorbers. The absorbers used in this study have a damping ratio of $\zeta \approx 0.2$, for which no apparent benefit in terms of system stabilization is gained. This does not render the results in Chapter 2 practically unattainable however. The damping ratio in the experimental absorbers used in this investigation should be much larger than that used in applications, specifically automotive, for two reasons. First, the spin rig used in this study spins in the vertical plane, causing the effects of dry friction to be larger than in an horizontally spun rotor. Second, the damping ratio is a function of the rotor mean speed, Ω, for which the tests conducted in this study are at a much lower speed than in most applications.

3.4 Conclusions

The experimental setup utilized to investigate the dynamics of multiple order absorber systems has been detailed. The indirect measurement of the parameters associated with this setup that cannot be directly calculated is detailed. Experimental results are shown to agree with the theoretical predictions given in the previous chapter. Specifically, synchronous multiple order experimental absorber responses are shown to closely match the theoretical and numerical predictions. Experimental non-synchronous responses for sets of order $\tilde{n}_1$ absorbers quantitatively match the stability boundaries calculated through the use of a numerical continuation of the perturbation equations. The experimental bifurcations of the order $\tilde{n}_1$ absorbers are then investigated with the addition of order $\tilde{n}_2$ absorbers. The experimental and theoretical results are again found to be in agreement, proving the utility of the analytical predictions for use in absorber design.

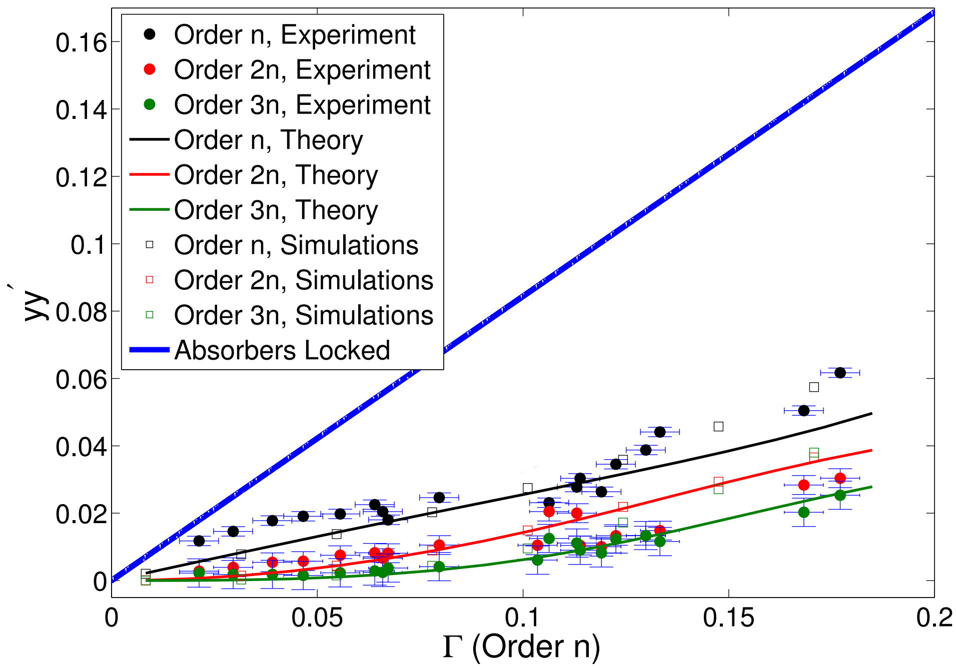

(a)

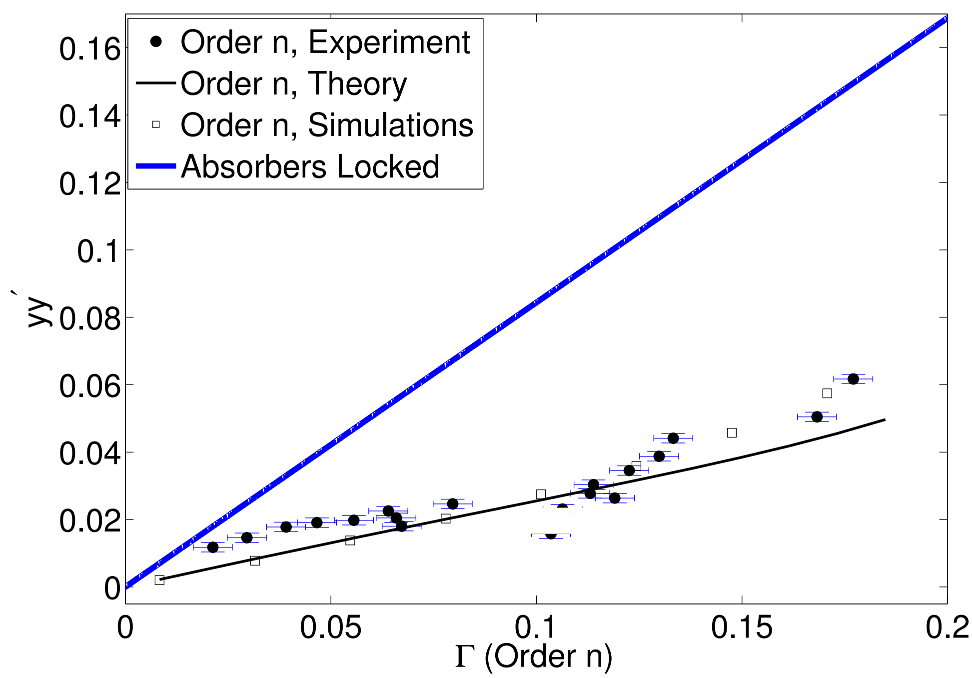

(b)

Figure 3.10: Experimental rotor angular acceleration, yy' vs. Γ_n for multiple order epicycloidal absorbers compared against the perturbation and numerical predictions ($n = 2.29$, $\epsilon = 0.18486$). (a) First three rotor response orders, n, $2n$, $3n$. (b) Order n.

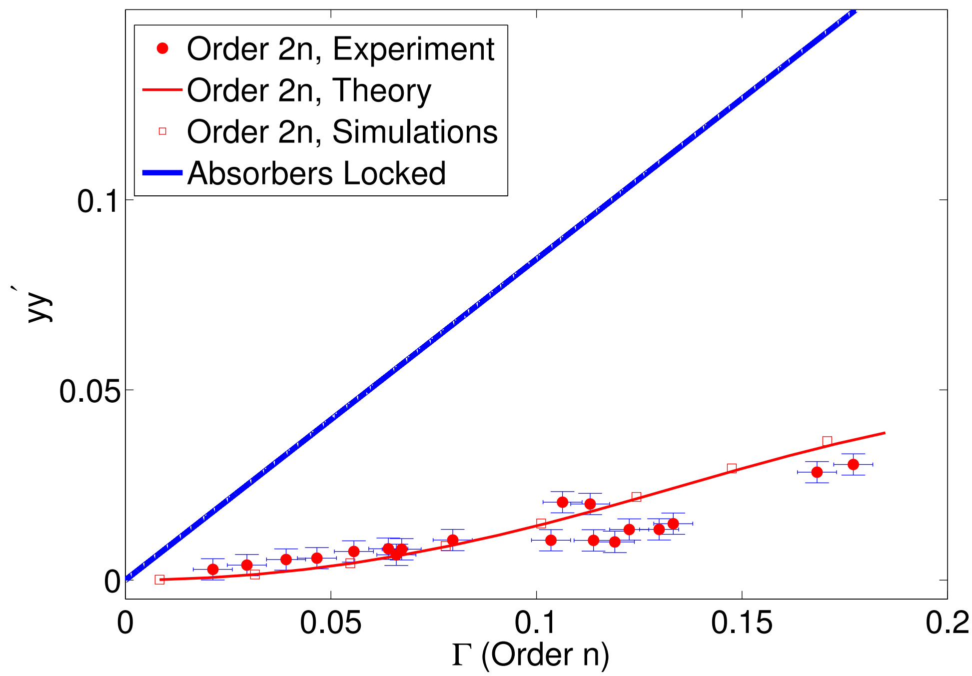

(c)

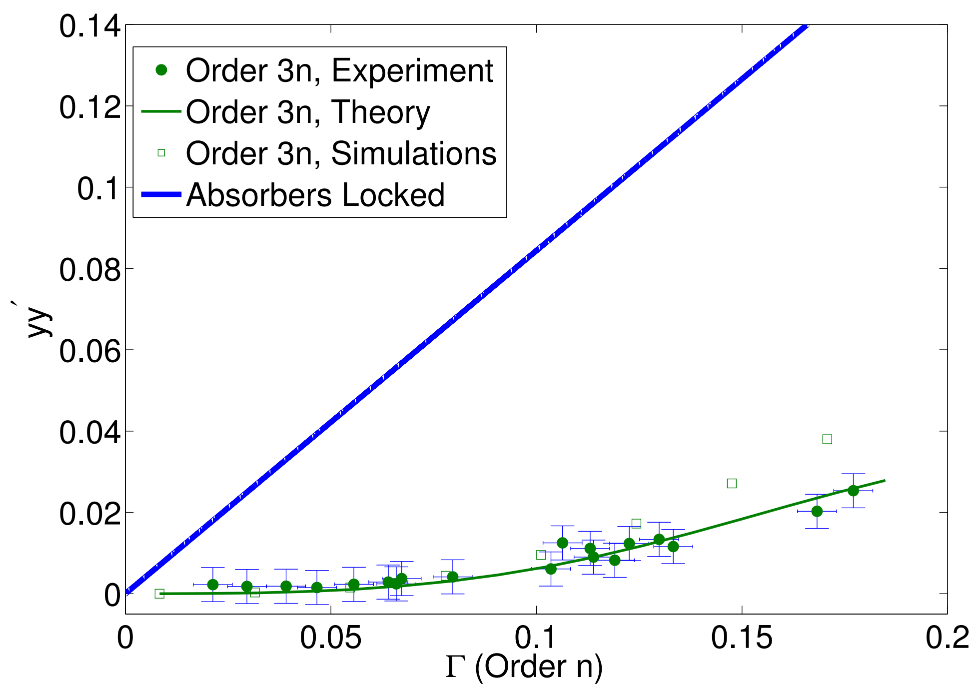

(d)

Figure 3.11: (c) Order $2n$. (d) Order $3n$.

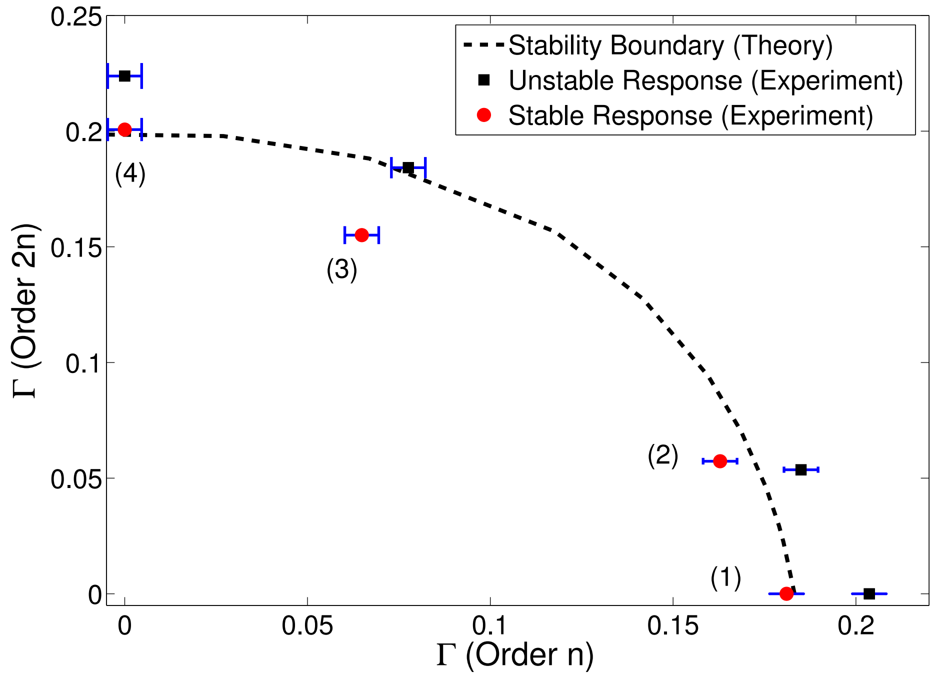

(a)

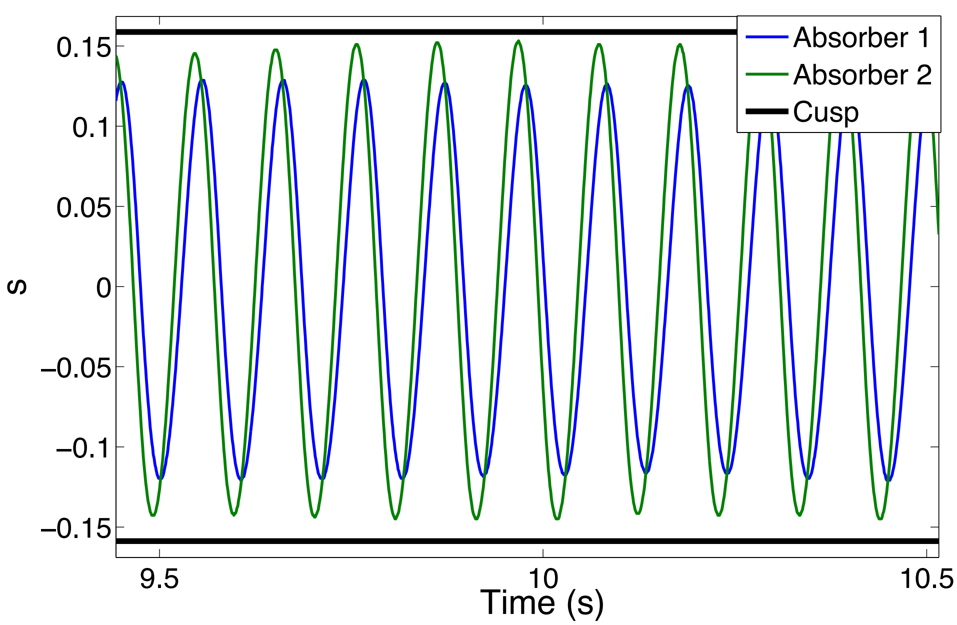

(b)

Figure 3.12: Experimental stability results for a pair of order $\tilde{n}_1$ absorbers. (a) Theoretical stability boundary with a sample of stable and unstable experimental data points. (b) Experimental time response of the non-synchronous absorber response corresponding to the data point labeled (1).

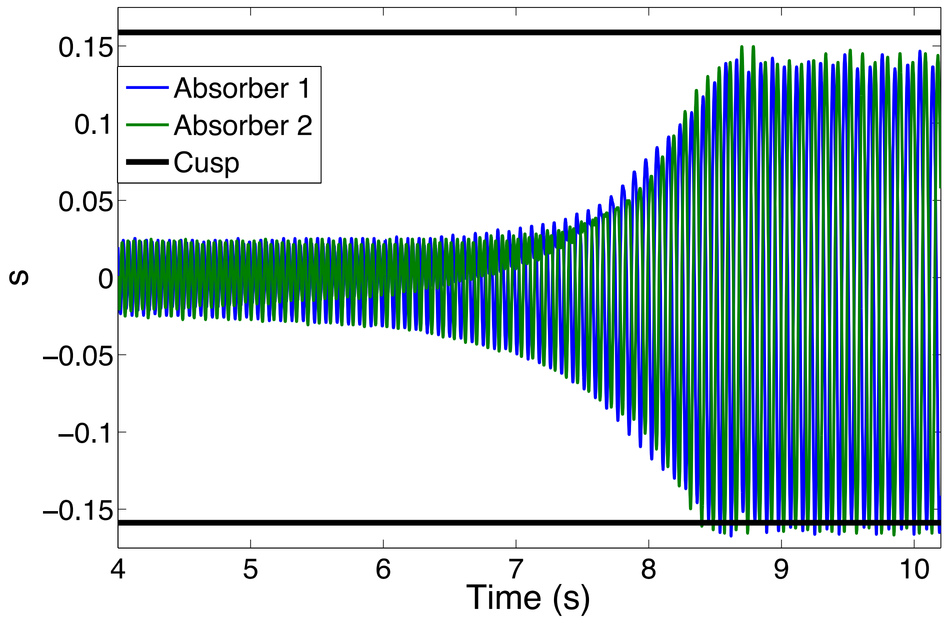

(c)

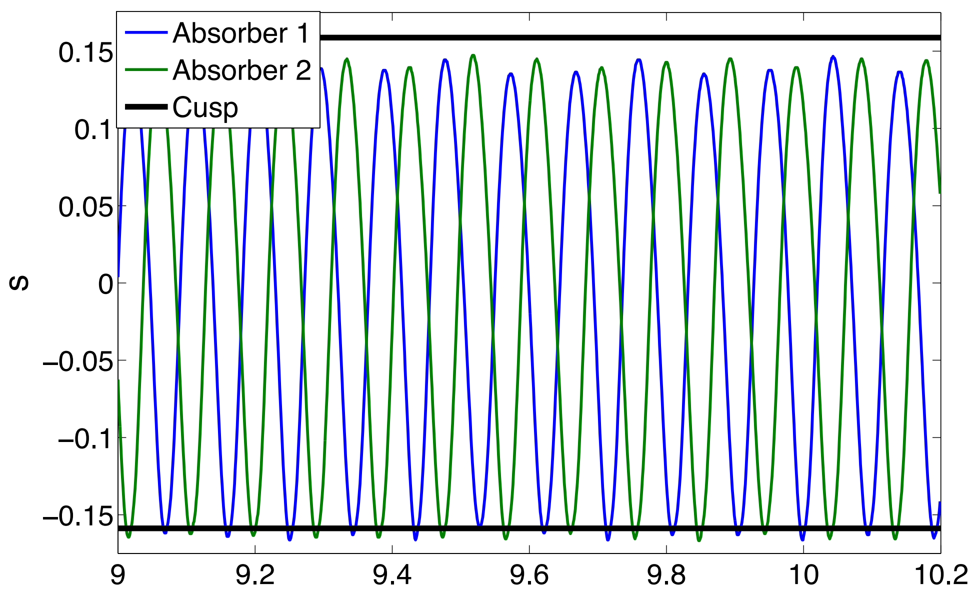

(d)

Figure 3.13: (c) Experimental time response of the sub-harmonic absorber response corresponding to the data point labeled (4) in Fig. 3.12. (d) Short time sample of the sub-harmonic instability, showing the out of phase absorber motion.

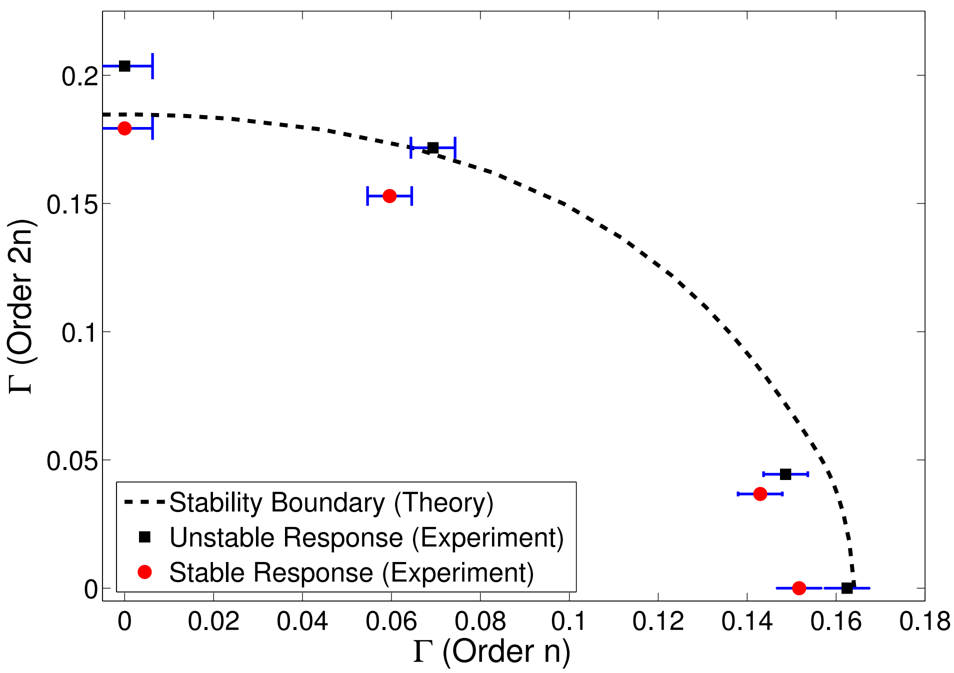

Figure 3.14: Experimental absorber amplitudes, s, vs. the amplitude of applied order n torque, Γ_n, with perturbation and numerical simulation predictions. ($n = 2.29$, $\epsilon = 0.18486$)

Chapter 4

A Harmonic Balance Approach to the Dynamics of CPVAs

In this chapter harmonic Balance (HB) methods are applied to the scaled equations of motion Eqs. (2.7) and (2.8) as given in Section 2.3. The purpose of this analysis is that it provides explicit formulas that predict the steady-state system response, including its harmonic content, although without stability information. Two assumptions about the form of the absorber amplitudes are used in the approximations, and relatively simple formulas are derived which accurately predict absorber amplitudes and corresponding rotor response. Predictions are validated using numerical simulations and experimental data.

4.1 General Harmonic Balance

The rotor/absorber system is dynamically complicated, as inherent nonlinearities in the absorber motion and the absorber/rotor coupling do not allow for a closed form solution for the system dynamics. Current methods of analyzing CPVAs involve numerical simulations and perturbation analysis. The perturbation methods do allow for accurate studies of the system dynamics as a function of system parameters, and can capture the detrimental nonlinear instabilities inherent in the system [3, 8, 39]. For example, when the absorber path is a circle, the absorbers behave similar to a simple pendulum and become detuned at large amplitudes. This detuning can cause a jump bifurcation in the pendulum's amplitude, which is accompanied by a phase shift in the absorber response causing amplification of the rotor vibrations [3, 36]. Denman [14] grouped a set of absorber paths into a two parameter family of curves, one parameter controlling the linear tuning of the absorber and the other controlling the large amplitude nonlinear behavior. The two extremes of this family of curves, in terms of the nonlinear parameter, are circles (softening path) at one end and cycloids (hardening path) at the other. Between these two extremes is a family of epicycloids, one of which is the so called tautochronic epicyloid, which renders the absorber motion, when decoupled from the rotor, linear over all feasible amplitudes (that is, out to the cusp on the curve). Implementing non-circular paths can alleviate the jump bifurcation, but non-synchronous absorber responses can still occur, due to the multiple harmonics imparted onto the rotor from the absorber/rotor nonlinear coupling [3, 8, 39, 46]. One important aspect of these nonlinear interactions is that the second harmonic ($2n$) can cause, through parametric coupling terms, subharmonic instabilities in the system.

The perturbation methods referenced above provide an accurate representation of the system dynamics, but involve quite complicated calculations and resulting expressions [9,39, 46]. In this chapter, we derive relatively simple formulas for the absorber amplitude and the harmonic amplitudes of the corresponding rotor angular acceleration as a function of system parameters. In order to obtain these formulas, the harmonic balance method is applied to a scaled version of the equations of motion. The harmonic balance method is an efficient way to estimate the steady-state dynamics of nonlinear systems, as commonly applied in nonlinear electric circuits [18]. We first utilize scaling techniques in order to decouple the absorber dynamics from those of the rotor, and two different assumptions about the form of the amplitude of the absorbers are used to perform the harmonic balance.

We begin by applying the harmonic balance methods to a quite general system that involves a rotor equipped with absorbers tuned to two orders and subjected to a torque composed of two orders. In the first harmonic balance method, the so-called general method, the unknown steady state amplitudes of the degrees of freedom are assumed to be unknowns and take no particular form. It will be shown that due to the complicated non-linearities inherent in the system, usable closed form solutions for the absorber amplitude and rotor angular acceleration as a function of the applied torque cannot be obtained by this method. To overcome this, the applied torque is expressed as a function of the absorber amplitudes and other parameters, which allows for accurate absorber design studies to be carried out. In the second approach, we assume the absorber amplitude to be in the form of a power series in the (non-dimensional) torque amplitude. This formulation allows for the absorber amplitude to be obtained explicitly as a function of the system parameters, by collecting harmonics of the absorber response, as well as powers of the applied torque. The utility of this method is in the fact that relatively simple formulas for absorber and rotor response can be obtained in terms of the other relevant parameters in the system. It will be shown that due to the assumption about the absorber amplitude, certain solution branches for the the absorber amplitude will not be captured, and there is some degradation in the accuracy of this theory at large absorber amplitudes.

We begin with the harmonic balance analysis of the general system consisting of absorbers tuned to two orders as well as forcing at two orders. This formulation will lead to the most general form of the approximations, which can then be greatly simplified in some special cases of interest. As previously stated, the application of harmonic balance to this system, although providing accurate predictions to the steady-state dynamical response of the absorbers and rotor, will fail to capture instabilities of the system response [3, 8, 23, 39]. For this reason, for this investigation we assume a response of the absorbers in which each group is mutually synchronous, implemented by grouping the inertia of all the absorbers at each order into a single effective absorber, thus simplifying Eqs. (2.7) and (2.8) into the form

$$
\begin{aligned}
w' &= \Gamma_n \sin(n\theta) + \Gamma_{2n} \sin(2n\theta + \phi) \\
&\quad + \frac{1}{1+\alpha} \Big[(2\tilde{n}_1^2 s_1 s_1' + \tilde{n}_1^2 s_1 g_{10} - s_1'^2 g_{10}') \\
&\qquad + \alpha (2\tilde{n}_2^2 s_2 s_2' + \tilde{n}_2^2 s_2 g_{20} - s_2'^2 g_{20}') \Big] ,
\end{aligned}
\tag{4.1}
$$

$$
s_j'' + \tilde{n}_j^2 s_j = \epsilon f_j(s_j, s_j', .., s', \mu, \tilde{n}_j, n_j, \lambda, T(\theta)) + O(\epsilon^2) \quad j = 1, 2, \tag{4.2}
$$

where,

$$
\begin{aligned}
f_j &= h_j'/2 - \tilde{\mu}_{a,j} s_j' + [s_j' + g_{0j}(s_j)][\frac{1}{1+\alpha}(-2n_1^2 s_1 s_1' - n_1^2 g_{01}(s_1) s_1 \\
&+ \frac{dg_{01}(s_1)}{ds_1} s_1'^{\,2} + \alpha(-2n_2^2 s_2 s_2' - n_2^2 g_{02}(s_2) s_2 + \frac{dg_{02}(s_2)}{ds_2} s_2'^{\,2})) \\
&- \tilde{\Gamma}_n \sin(n\theta) - \tilde{\Gamma}_{2n} \sin(2n\theta + \phi)],
\end{aligned}
$$

in which $\epsilon w' = yy' = \dfrac{\ddot{\theta}}{\Omega^2}$ is the non-dimensional rotor angular acceleration, which we use as the measure to quantify rotor torsional vibration. Also, due to the complicated nature of the path functions, specifically $g_i(s_i)$, which is explained in detail in Chapter 2 [1], one must expand Eqs. (4.1) and (4.2) in the absorber arc length s_i in order to obtain explicit expressions; here we keep terms up to $O(s_i^5)$.

It has been previously found, from extensive simulation and experimental studies, that the motion of the absorbers is very closely resembled by a single harmonic, for all paths.

[1] This term is specifically the radial distance from the rotor center to the absorber center multiplied by the dot product of the unit vectors in the rotational direction of the vertex of the absorber path and the tangent of this curve as the absorber moves along the path.

Using this as a guideline for the harmonic approximation of the response, we assume the absorbers each respond at single harmonic, that is, they have the form,

$$s_1 = A_1 \sin(n\theta) + B_1 \cos(n\theta), \tag{4.3}$$

and

$$s_2 = A_2 \sin(2n\theta) + B_2 \cos(2n\theta). \tag{4.4}$$

Equations (4.3) and (4.4) which are inserted into Eq. (4.2) and harmonics are balanced. The balancing of harmonics results in four equations in the four unknowns, $A_{1,2}, B_{1,2}$. Commonly, the absorber amplitudes would be solved for in terms of the forcing, but in this case the nonlinearities do not allow for a closed form solution for the unknown harmonic amplitudes. However, by neglecting damping the phases are simplified such that one can eliminate the $B_{1,2}$ terms. The applied torques can then be solved for in terms of $A_{1,2}$ and other relevant system parameters as follows,

$$\begin{aligned}\tilde{\Gamma}_n = &\frac{-(16A_1(A_2 n^3(-8 + A_2^2(\tilde{n}_2^2 + \tilde{n}_2^4))\alpha\epsilon}{X_1}\\ &+\frac{-2\tilde{\Gamma}_{2n} n(1+\alpha)\epsilon + 2n^2(2 + 2\alpha - 2\epsilon + A_1^2\tilde{n}_1^4\epsilon)}{X_1}\\ &+\frac{-2(1+\alpha)(2\tilde{n}_1^2 - 3A_1^2\varphi_1\epsilon)))}{X_1},\end{aligned} \tag{4.5}$$

$$\begin{aligned}\tilde{\Gamma}_{2n} = &\frac{-(8(-8A_2(\tilde{n}_2^2(1+\alpha) + 4n^2(-1+\alpha(-1+\epsilon)))}{X_2}\\ &\frac{-8A_1^2 n\tilde{n}_1^2\epsilon + 3A_1^2A_2^2 n\tilde{n}_1^2\tilde{n}_2^2(1+\tilde{n}_2^2)\epsilon}{X_2}\\ &\frac{4A_2^3(4n^2\tilde{n}_2^4\alpha + 3(1+\alpha)\varphi_2)\epsilon))}{X_2},\end{aligned} \tag{4.6}$$

where,

$$X_i = (-64 + 5A_i^4\tilde{n}_i^4(1+\tilde{n}_i^2)^2 + 24A_i^2(\tilde{n}_i^2+\tilde{n}_i^4))(1+\alpha)\epsilon$$
$$i = 1, 2.$$

The above equations, with some manipulations that are subsequently explained in further detail, allow for accurate prediction of the absorber response as a function of torque amplitudes. This is essentially accomplished by choosing amplitudes for the absorber amplitudes and then solving for the corresponding torque amplitudes. In order to gauge the effectiveness of the absorbers in terms of reducing torsional vibrations of the rotor, we consider the rotor angular acceleration, defined as w' in Eq. (4.1). While each absorber responds at single harmonic, the rotor response is composed of multiple harmonics. Observations, justified by the following analysis, shows that the rotor response can be well approximated by three harmonics. These multiple harmonics are imparted onto the rotor by nonlinear interactions with the absorbers, and they can be quantified by inserting the absorber amplitude approximations, Eqs. (4.3) and (4.4), into the rotor angular acceleration equation, Eq. (4.1), and collecting harmonics. This results in terms for the rotor angular acceleration at three different harmonic orders, with harmonic amplitudes given by,

$$w'_n = \frac{-A_1n^2(-64 + A_1^4\tilde{n}_1^4(1+\tilde{n}_1^2)^2 + 8A_1^2(\tilde{n}_1^2+\tilde{n}_1^4))}{64(1+\alpha)} + \tilde{\Gamma}_n, \tag{4.7}$$

$$\begin{aligned} w'_{2n} = &\frac{16\tilde{\Gamma}_{2n}(1+\alpha) - n(-16A_1^2\tilde{n}_1^2 + A_2n}{16(1+\alpha)} \\ &\times (-64 + A_2^4\tilde{n}_2^4(1+\tilde{n}_2^2)^2 + 8A_2^2(\tilde{n}_2^2+\tilde{n}_2^4))\alpha), \end{aligned} \tag{4.8}$$

and

$$w'_{3n} = \frac{3A_1^3n^2\tilde{n}_1^2(1+\tilde{n}_1^2)(16 + 3A_1^2(\tilde{n}_1^2+\tilde{n}_1^4))}{128(1+\alpha)}. \tag{4.9}$$

Substitution of the torques from Eqs. (4.5) and (4.6) into these equations allows one to express the rotor angular acceleration harmonics in terms of the absorber amplitudes. While the expressions are straightforward, the actual calculation is not so. Typically one specifies the system and input parameters, including the torque amplitudes, and solves for $A_{1,2}$ from Eqs. (4.5) and (4.6), using numerical methods. However, a well known approach to avoiding numerics is to vary the absorber amplitude and solve for the corresponding torque, since it is known explicitly. However, this is not possible when two torques are present. A way to perform this operation in this case is to assume a linear relationship between the two torque harmonic amplitudes and a constant relative phase between them, i.e $\tilde{\Gamma}_{2n} = \beta\tilde{\Gamma}_n$, which is a good assumption for some automotive applications [17]. With this assumption, one is still left with the problem of obtaining A_2 from Eq. (4.6), which is a cubic equation. One approach, which will be shown to be limited in accuracy, but does allow one to obtain explicit expressions, is to keep only the terms linear in A_2, which yields

$$A_2 = -\frac{\left(A_1^2 n\tilde{n}_1^2 + \tilde{\Gamma}_n(1+\alpha)\beta\right)\epsilon}{\tilde{n}_2^2(1+\alpha) + 4n^2(-1+\alpha(-1+\epsilon))}. \tag{4.10}$$

One must now only specify the range of amplitudes for A_1, and then $\tilde{\Gamma}_n$ can be obtained, from which all other results follow. This process will be presented subsequently using examples.

4.2 Harmonic Balance Using a Power Series in Torque Amplitude

We now turn to a harmonic balance approach in which the absorber amplitudes are assumed to have a special form, specifically as a power series in the applied torque amplitude. This approach works since the torque amplitudes are non-dimensionalized by the twice the rotor kinetic energy ($J\Omega^2$) and are therefore small in practice. This series expansion approach yields convenient closed form solutions for the harmonic amplitudes for the absorber and the rotor angular acceleration as a function of the applied torques and system parameters.

The absorber amplitudes are expressed as,

$$s_1 = (\sum_{i=1}^{k} C_i \tilde{\Gamma}_n^i) \sin(n\theta) + (\sum_{i=1}^{k} D_i \tilde{\Gamma}_n^i) \cos(n\theta),$$

and

$$s_2 = (\sum_{i=1}^{k} (E_i \tilde{\Gamma}_n^i + G_i \tilde{\Gamma}_{2n}^i)) \sin(2n\theta) + (\sum_{i=1}^{k} (F_i \tilde{\Gamma}_n^i + H_i \tilde{\Gamma}_{2n}^i)) \cos(2n\theta).$$

We have included the $\tilde{\Gamma}_n$ terms in the s_2 equation in order to capture the effects of the internal resonances caused by the multiple harmonics imparted onto the rotor by the absorbers. However, we do not include terms of the form $\sqrt{\Gamma_{2n}}$ in the s_1 expansions, which would be needed to capture the subharmonic vibration absorber [9, 22]. Inserting the above expressions into Eq. (4.2), collecting orders of $\tilde{\Gamma}_{n,2n}$, and balancing harmonics, linear equations for the coefficients are obtained. The terms that are linear in the applied torque, C_1, D_1,

E_1, F_1, G_1 and H_1, are found to be,

$$C_1 = \frac{4n(1+\alpha)(\tilde{\mu}_{a,1} + \tilde{\mu}_{a,1}\alpha + 2G_1\tilde{\Gamma}_{2n}n^2\alpha)\epsilon^2}{P_1} \tag{4.11}$$

$$\begin{aligned} D_1 = & \frac{1}{-P_1}(-(2(1+\alpha)\epsilon(-2\tilde{n}_1^2(1+\alpha) + 2n^2(1+\alpha-\epsilon) \\ & + 4\tilde{\Gamma}_{2n}H_1 n^3\alpha\epsilon + \tilde{\Gamma}_{2n}n(1+\alpha)\epsilon))) \end{aligned} \tag{4.12}$$

$$E_1 = F_1 = 0$$

$$G_1 = \frac{2\tilde{\mu}_{a,2}n\epsilon^2}{4\tilde{\mu}_{a,2}^2 n^2\epsilon^2 + (\tilde{n}_2^2 + n^2(-4 + \frac{4\alpha\epsilon}{1+\alpha}))^2} \tag{4.13}$$

$$H_1 = -\frac{\epsilon(\tilde{n}_2^2 + n^2(-4 + \frac{4\alpha\epsilon}{1+\alpha}))}{4\tilde{\mu}_{a,2}^2 n^2\epsilon^2 + (\tilde{n}_2^2 + n^2(-4 + \frac{4\alpha\epsilon}{1+\alpha}))^2} \tag{4.14}$$

where,

$$\begin{aligned} P_1 = & 4\tilde{n}_1^4(1+\alpha)^2 - 16\tilde{\Gamma}_{2n}^2(G_1^2 + H_1^2)n^6\alpha^2\epsilon^2 - n^2(1+\alpha) \\ & \times (8\tilde{n}_1^2(1+\alpha-\epsilon) + (\tilde{\Gamma}_{2n}^2 - 4\tilde{\mu}_{a,1}^2)(1+\alpha)\epsilon^2) + 4n^4 \\ & \times ((-1+\epsilon)^2 + \alpha^2(1 - 2\tilde{\Gamma}_{2n}^2 H_1\epsilon^2) - 2\alpha(-1+\epsilon+\tilde{\Gamma}_{2n}^2 H_1\epsilon^2)) \end{aligned}$$

Note that the above equations do not capture the perturbation away from the tautochrone, φ_i, since they capture the linear response of the absorber. Solving for the higher order expansions in $\Gamma_{n,2n}$, truncating at $k = 5$, one finds $C_{2,4}$, $D_{2,4}$, $E_{3,5}$, $F_{3,5}$, $G_{2,4}$, $H_{2,4} = 0$, and the expressions for $C_{3,5}$, $D_{3,5}$, $E_{2,4}$, $F_{2,4}$, $G_{3,5}$, and $H_{3,5}$ are complicated functions of ϵ, $\tilde{n}_{1,2}$, n, $\mu_{a,1,2}$, and $\varphi_{1,2}$. These expressions are given in Appendix B.2, and although they are complicated in their general form, they simplify in many practical cases. Also, the parameters in the expressions are always known explicitly, which allows one to simply insert values into the expressions for an accurate representation of the absorber amplitude. Once the expressions for the constants are known, the absorber amplitudes can easily be found through

$$|s|_1 = \sqrt{(\sum_{i=1}^{k} C_i \tilde{\Gamma}_n^i)^2 + (\sum_{i=1}^{k} D_i \tilde{\Gamma}_n^i)^2}, \tag{4.15}$$

$$|s|_2 = \sqrt{(\sum_{i=1}^{k} E_i \tilde{\Gamma}_n^i + G_i \tilde{\Gamma}_{2n}^i)^2 + (\sum_{i=1}^{k} F_i \tilde{\Gamma}_n^i + H_i \tilde{\Gamma}_{2n}^i)^2}. \tag{4.16}$$

With the amplitude of the absorbers known, operations similar to those above can be performed in order to get an accurate representation of the rotor response, outlined as follows: The absorbers' responses are expanded using Eq. (4.1) and powers of the applied torque as well as harmonics of each order are collected. The amplitudes of the first two harmonics of the rotor angular acceleration, w'_{lin}, when one keep only linear terms in the torque amplitudes, are given by,

$$w'_{\text{lin},n} = \tilde{\Gamma}_n \sqrt{\frac{(C_1^2 n^4 + (1 + D_1 n^2 + \alpha)^2)}{(1+\alpha)^2}} \tag{4.17}$$

$$w'_{\text{lin},2n} = \tilde{\Gamma}_{2n} \sqrt{\frac{(16\text{G}1^2 n^4 \alpha^2 + (1 + \alpha + 4\text{H}1 n^2 \alpha)^2)}{(1+\alpha)^2}}. \tag{4.18}$$

The higher harmonics that are imparted onto the rotor response by system nonlinearities obviously cannot be captured by the linear response assumption. In order to capture these higher harmonics, and obtain a more accurate representation on the order n rotor response, one must include higher orders of $\Gamma_{n,2n}$ in the approximation. The inclusion of these higher order terms yields additional terms in all orders of the rotor response; these are presented in their most general form in Appendix B.2 for reference.

4.3 Examples

The accuracy of the equations formulated in the previous section will now be investigated through some cases studies of special interest. We first look at the most general system utilizing the general form of the approximations developed above, and extend the study to include some special cases with simplifying assumptions, as well as the effects of perturbations away from the tautochronic path.

4.3.1 Absorbers and Forcing at Two Orders

Assuming the system at hand consists of two absorbers, with one absorber having a tuning twice of that of the other, as well as applied torques at each of these orders, one can use Eq. (4.5) in its presented form, along with the solution for A_2 as a function of A_1 as presented above, to capture the absorber amplitude as of function of torque. The absorber amplitude approximations derived from assuming a power series in the applied torque can also be utilized to look at the linear response assumption, done by simply truncating the series expansions at $k = 1$ in Eqs. (4.15) and (4.16). The nonlinear responses can also be used through the inclusion of the higher order terms in the expansions. For the subsequent examples, the following non-dimensional parameters are used: $\tilde{n}_1 = 1.5$ (corresponding to a three-cylinder four-stroke engine), $\tilde{n}_2 = 3$, $\alpha = 0.5$, $\mu_{a,1} = 0.1$, $\mu_{a,2} = 0.2$, $\epsilon = 0.05$, and the relationship between the multiple torques is assumed to be $\tilde{\Gamma}_n = 0.25\tilde{\Gamma}_{2n}$ with zero phase between the two torques, which act directly at the resonant frequency of the absorbers ($n = \tilde{n}_1 = 1.5$, $2n = \tilde{n}_2 = 3$). There exists a maximum amplitude for each absorber, $|s|_{\max}$, referred to as the "cusp amplitude" (since it corresponds to a cusp on many paths), which is the maximum amplitude the absorbers can achieve, due to the fact that non-circular paths becomes undefined beyond this point. This amplitude is found by solving for $|s|_{\max}$ from $g(|s|_{\max}) = 0$. In practice, stoppers are implemented at an amplitude that are typically close to, but less than this cusp amplitude. Due to the expansions in the absorber arc length that are employed, this amplitude limit is not captured in the approximations, but is evident in the numerical simulations.

We take a detour here to explain the comparisons between the two HB methods. As previously mentioned, the absorber amplitude is expanded to $O(s_i^5)$. The accuracy of the power series in the applied torque HB method does not improve with orders of torque greater than $O(\Gamma^3)$, as shown in Fig. 4.1, due to the breakdown of the amplitude expansions of $g(s)$ and other path functions near the cusp of the path.

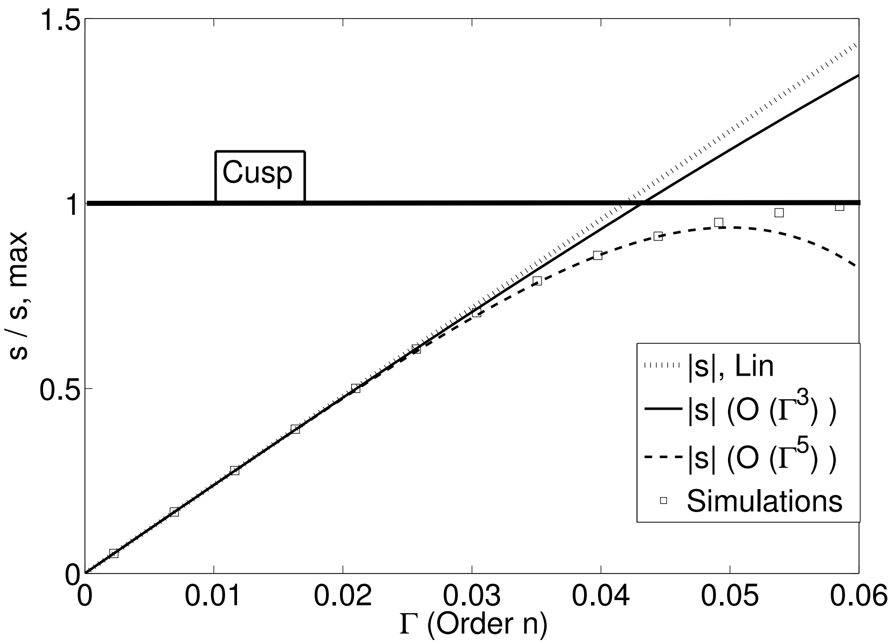

Figure 4.1: Tautochronic epicycloid absorber amplitude, $|s|$, versus amplitude of fluctuating torque, Γ_n for different numbers of truncation for the power series HB method.

Figure 4.2 exhibits the approximate absorber amplitudes as a function of the applied torques using both HB methods, with numerical simulations of the coupled, nonlinear equa-

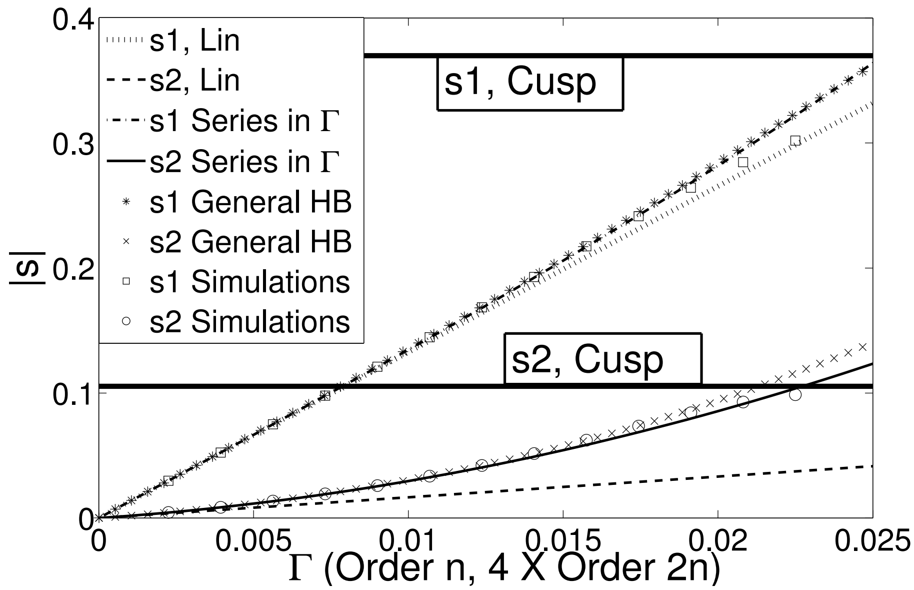

Figure 4.2: Absorber amplitudes, $|s_{1,2}|$, vs. amplitude of applied order torques, $\Gamma_{n,2n}$, from the different harmonic balance (HB) approximations, with numerical simulations, for $\varphi = 0$ (tautochronic epicycloid).

tions of motion for baseline comparison. As is visible from Fig. 4.2, both of the harmonic balance approximations provide an accurate representation of the absorber amplitude for the entire range of torque. There exists a small error between the approximations and the numerical simulations which occurs when the order $\tilde{n}_2$ absorber approaches its amplitude limit. The higher order approximations capture some of the non-linear effects of the system at larger amplitudes, which is visible from the hardening of the absorber amplitude near the cusp. Interestingly, the linear approximation is accurate for the order $\tilde{n}_1$ absorber for the torque range used here, which is due to the fact that we are using the tautochronic path, and that this absorber does not get very close to its cusp value. Below we show that the accuracy of the linear response degrades as the perturbation away from the tautochrone becomes non-zero. The accuracy of the linear approximation of the order $\tilde{n}_2$ absorbers degrades significantly even at a very small torque level. This is due to the parametric excitation of the order $\tilde{n}_2$ absorber by the order $\tilde{n}_1$ absorber, resulting from the nonlinear coupling between the absorbers and rotor. The amplitude of the parametric excitation here is the square of the order $\tilde{n}_1$ absorber amplitude, for which the linear approximation will obviously break down, but is captured by the higher order approximations.

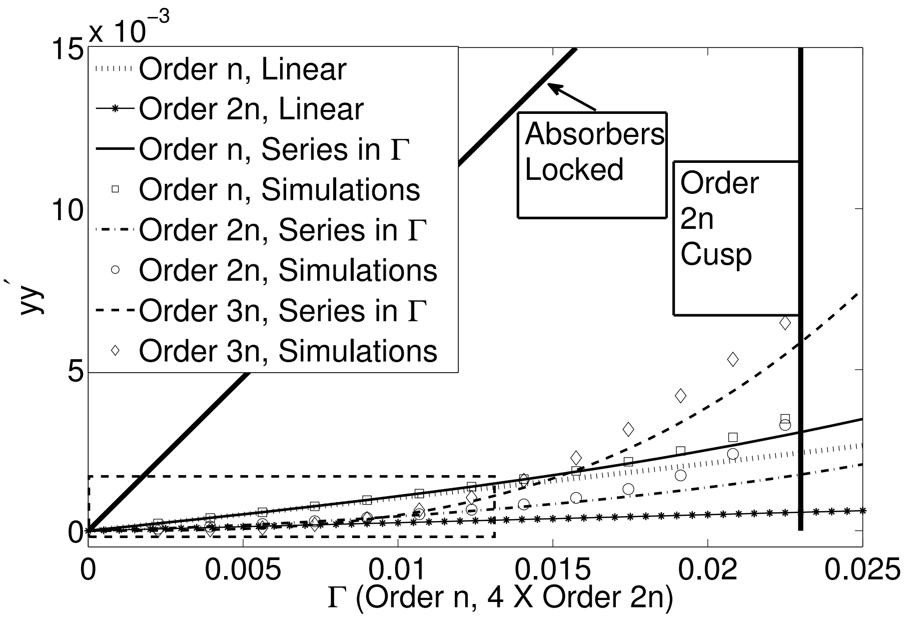

(a)

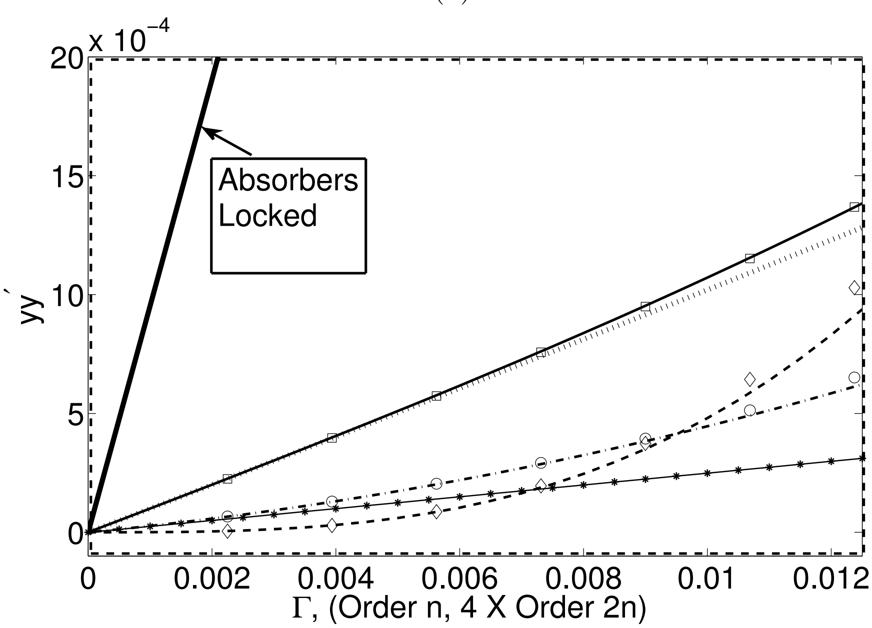

(b)

Figure 4.3: Rotor angular acceleration, yy', harmonic amplitude approximations using the amplitude expansions, vs. the amplitude of applied order torques, $\Gamma_{n,2n}$. (a) Full torque range showing approximations out to $O(\Gamma_n^3)$. (b) The zoomed in region near the origin.

The approximations of the harmonic amplitudes of the non-dimensional rotor angular acceleration, yy', versus the applied torques are shown in Fig. 4.3 for the power series HB method. The linear harmonic balance approximation for the order n torque is in good agreement with the numerical simulations for a limited torque range, which breaks down when the order $\tilde{n}_1$ absorber is at $\approx$ 50% of it's amplitude limit. Including the higher order terms in the approximation, the order n, as well as the order $2n$ and $3n$ harmonic approximations, are also in good agreement with the numerical simulations, again deviating in accuracy at the torque level which causes the absorber amplitude approximations to lose some accuracy.

Figure 4.4 exhibits the harmonic amplitudes of the rotor angular acceleration as a function of the applied torque amplitudes using the general HB method, with A_2 expressed as a function of A_1, as given in Eq. (4.10). This assumption makes this method not as accurate in predicting the rotor harmonic amplitudes. In fact, it can easily be shown that for a linearized absorber/rotor model with zero damping, the absorber counteracts all of the applied torque when perfectly tuned, resulting in only a DC response from the rotor [12]. Due to nonlinear effects, however, the rotor angular acceleration is not identically zero, and the harmonic amplitudes grow like nonlinear powers of the torque amplitudes, that is, like Γ_n^m with $m \geq 2$.

4.3.2 Multiple Absorbers with Single Order Forcing

It is of interest to consider the case of a rotor subjected to forcing at a single order and fitted with multiple order absorbers. This has automotive applications, for example, in multi-displacement engines [33]. In order to investigate the accuracy of the approximations for this situation, one can set $\tilde{\Gamma}_{2n} = 0$ in the above expressions (Eqs. (4.5), (4.6), (4.8), (4.11) and (4.12)), resulting in some simplification of the formulas. Equation (4.5) and the

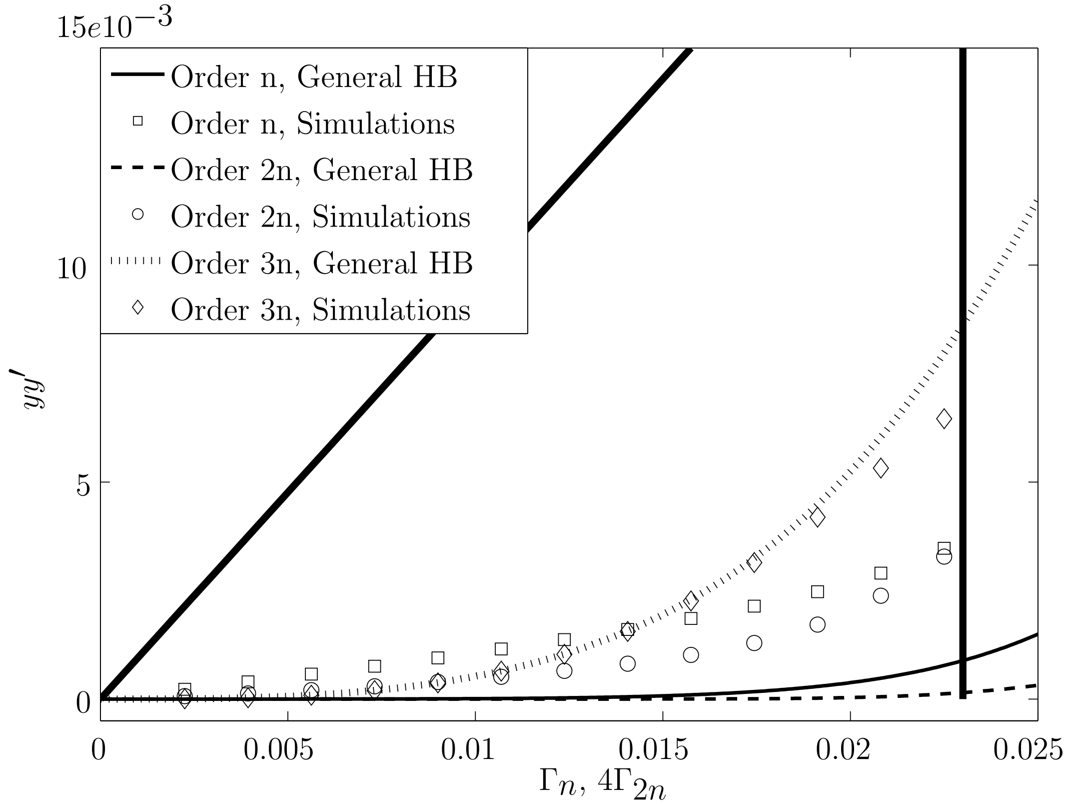

Figure 4.4: Harmonic amplitudes of the rotor angular acceleration, yy', predicted using the general HB method vs. the amplitude of applied order torques, $\Gamma_{n,2n}$. The absorber amplitudes A_1 and A_2 are assumed to satisfy Eq. (4.10).

expression for A_2 are as presented above without the $\tilde{\Gamma}_{2n}$ terms, and the linear terms in the expansions in Γ_n reduce to,

$$C_1 = \frac{\tilde{\mu}_{a,1} n \epsilon^2}{\tilde{\mu}_{a,1}^2 n^2 \epsilon^2 + \left(\tilde{n}_1^2 + n^2 \left(-1 + \frac{\epsilon}{1+\alpha}\right)\right)^2},$$

$$D_1 = -\frac{\epsilon \left(\tilde{n}_1^2 + n^2 \left(-1 + \frac{\epsilon}{1+\alpha}\right)\right)}{\tilde{\mu}_{a,1}^2 n^2 \epsilon^2 + \left(\tilde{n}_1^2 + n^2 \left(-1 + \frac{\epsilon}{1+\alpha}\right)\right)^2},$$

and the higher order terms can easily be found by setting $\tilde{\Gamma}_{2n} = 0$ in the expressions provided in the appendix. In this case the order $\tilde{n}_2$ absorber is driven only through the nonlinear crosstalk with the order $\tilde{n}_1$ absorber, and its amplitude is described through the E_2 and F_2 terms given in the appendix. An example of the absorber amplitude approximation, as a function of Γ_n, and results from simulations, are shown in Fig. 4.5. It interesting to note that the order $\tilde{n}_2$ absorber grows in amplitude and reaches its cusp limits even though the system is being forced only at $n = \tilde{n}_1$. This is due to the aforementioned nonlinear crosstalk between the multiple order absorbers, which is accurately captured by both harmonic balance methods. As in Fig. 4.2, the approximations decrease in accuracy near the cusp amplitudes, but are valid over a large torque range. The rotor responses for both HB methods (expansions in Γ_n and general) are presented in Figs. 4.6 and 4.7, and exhibit the same trends as Figs. 4.3 and 4.4. The importance of the ratio of the absorber masses as a design parameter is made evident in these figures, as both absorbers reach their respective amplitude limits for the same level of torque in Fig. 4.5. This is a desirable feature of the response, which does not hold for the example presented in Fig. 4.2.

4.3.3 Single Order Absorber with Single Order Forcing

We now turn to the simplest case, that is, a single order absorber with the rotor subjected to a single order torque. The results are obtained from the above approximations by setting $\alpha = 0$ (the mass ratio between the different order absorbers), which results in the following expressions for the linear terms in the expansions in Γ_n,

$$C_1 = \frac{\mu_a n_1 \epsilon^2}{-\mu_a^2 n_1^2 \epsilon^2 - (-n_1^2 + \tilde{n}_1^2 + n_1^2 \epsilon)^2}, \tag{4.19}$$

and

$$D_1 = \frac{\epsilon(-n_1^2 + \tilde{n}_1^2 + n_1^2 \epsilon)}{-\mu_a^2 n_1^2 \epsilon^2 - (-n_1^2 + \tilde{n}_1^2 + n_1^2 \epsilon)^2}. \tag{4.20}$$

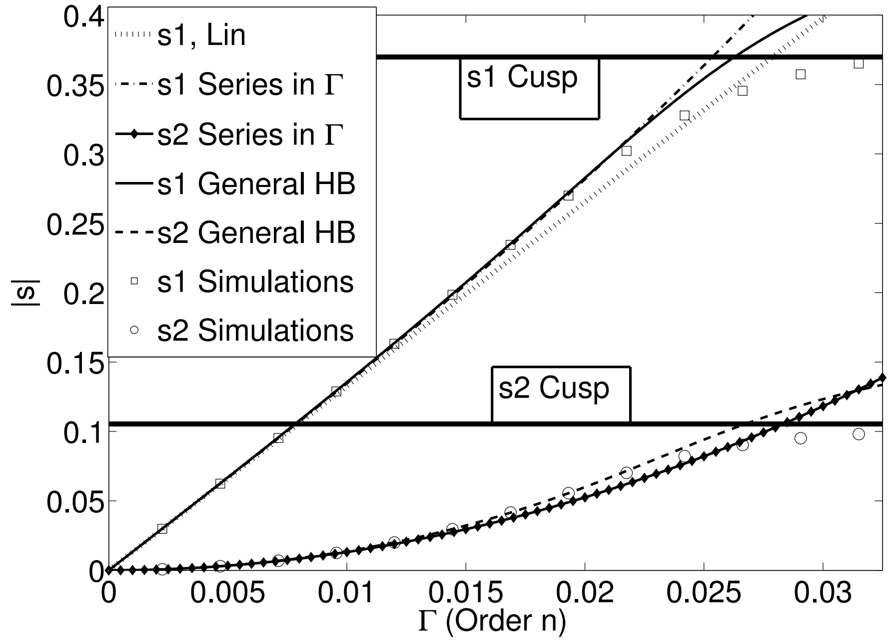

Figure 4.5: Absorber amplitude, $|s|$, vs. amplitude of applied order n torque, Γ_n, from different order harmonic balance (HB) approximations, with numerical simulations, for $\varphi = 0$ (tautochronic epicycloid).

Therefore, the first harmonic approximation for the amplitude of s, out to first order in $\tilde{\Gamma}_n$, that is, $|s|_{\text{lin}}$, is thus given by truncating at $k = 1$ in which

$$(C_1^2 + D_1^2)\tilde{\Gamma}_n^2 = (\frac{\epsilon^2}{\tilde{n}_1^4 + n_1^4(\epsilon - 1)^2 + n^2(2\tilde{n}_1^2(\epsilon - 1) + \mu_a^2\epsilon^2)})\tilde{\Gamma}_n^2.$$

The higher order terms in Γ_n for the absorber amplitude, C_3 and D_3, can also be included and simplified by making the above assumptions to the expressions given in the appendix.

The relationship between Γ_n and the absorber amplitude A_1 obtained from the general harmonic balance method also simplify as follows,

$$\tilde{\Gamma}_n = \frac{32A_1(-2\tilde{n}_1^2 + n^2(2 - 2\epsilon + A_1^2\tilde{n}_1^4\epsilon) + 3A_1^2\epsilon\varphi)}{(-64 + 5A_1^4\tilde{n}_1^4(1 + \tilde{n}_1^2)^2 + 24A_1^2(\tilde{n}_1^2 + \tilde{n}_1^4))\epsilon}, \tag{4.21}$$

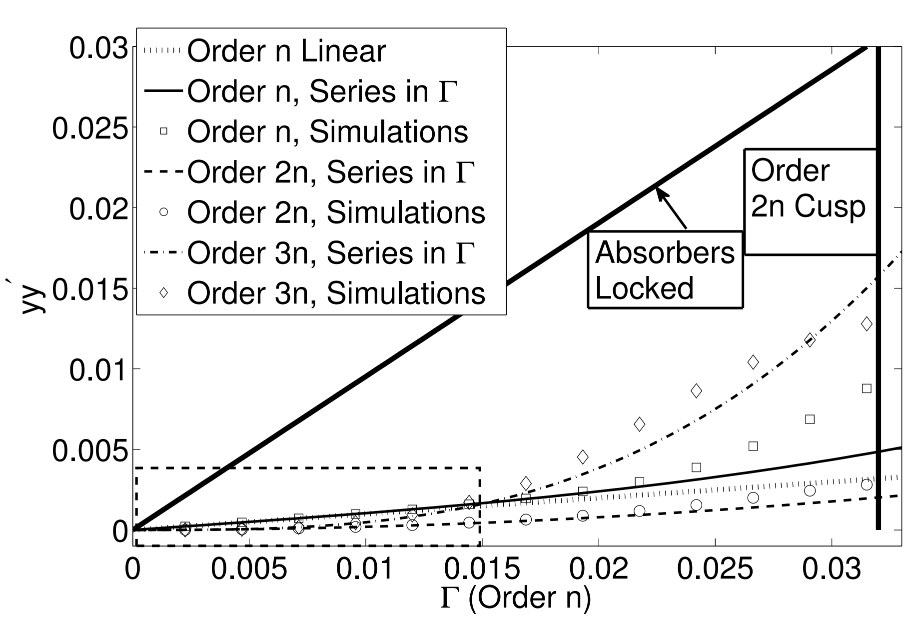

(a)

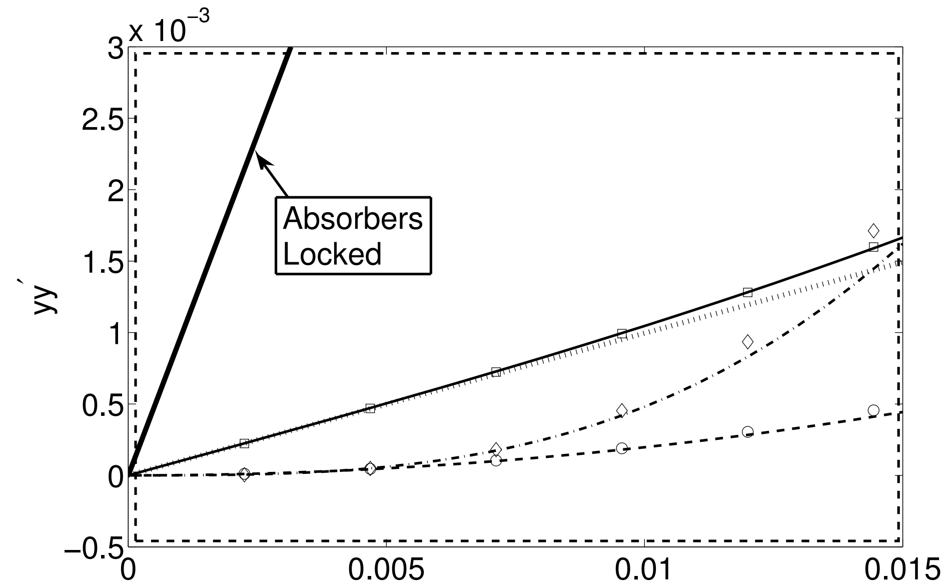

(b)

Figure 4.6: Rotor angular acceleration amplitude approximations using the amplitude expansions, yy', vs. the amplitude of applied order n torque, Γ_n. (a) Full torque range showing approximations out to $O(\Gamma_n^3)$. (b) The zoomed in region near the origin.

and the first three rotor harmonics simplify to,

$$\begin{aligned} w_n' = &\frac{1}{64}(64\tilde{\Gamma}_n - A_1 n^2(-64 + A_1^4\tilde{n}_1^4(1+\tilde{n}_1^2)^2 \\ &+ 8A_1^2(\tilde{n}_1^2+\tilde{n}_1^4))), \end{aligned}$$

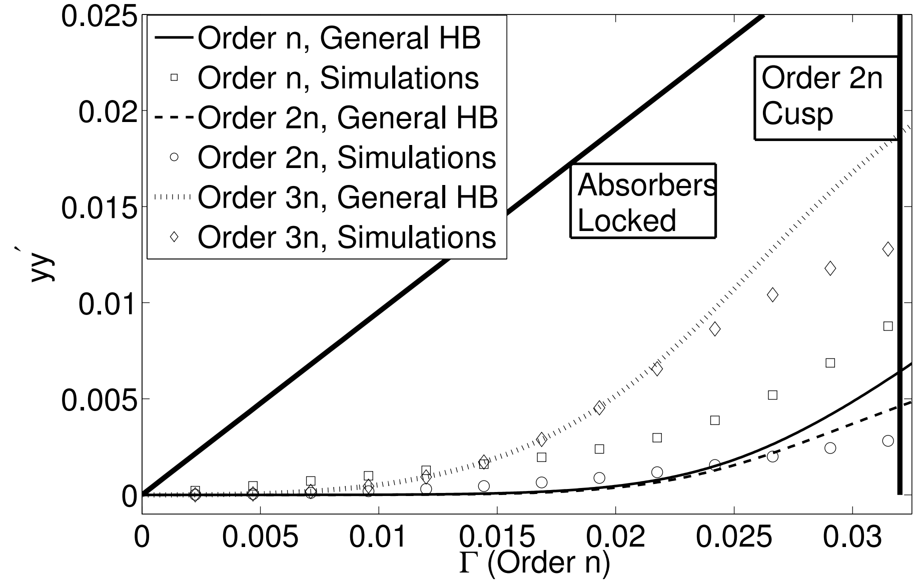

Figure 4.7: Harmonic amplitudes of rotor angular acceleration $|yy'|$ vs. Γ_n, including approximations from the general HB method and simulations, for $\varphi = 0$.

$$w'_{2n} = A_1^2 n\tilde{n}_1^2, \tag{4.22}$$

and,

$$w'_{3n} = \frac{3}{128} A_1^3 n^2 \tilde{n}_1^2 (1 + \tilde{n}_1^2)(16 + 3A_1^2(\tilde{n}_1^2 + \tilde{n}_1^4)). \tag{4.23}$$

The amplitude of the absorber as a function of Γ_n, using the harmonic balance approximations and compared to simulations of the full nonlinear equations of motion is shown in Fig. 4.8. The linear absorber amplitude approximation is accurate here to $\sim 50\%$ of the torque which causes the absorber to reach its amplitude limit, and, in this case, with a single absorber only, the general harmonic balance method is more accurate than the power series in the applied torque method near the amplitude limits. This is due to the breakdown of the expansions in the applied non-dimensional torque near the absorber cusps.

The two HB approximations of the harmonic amplitudes of yy' versus Γ_n, and simulation results, are shown in Figs. 4.9 and 4.10. The linear harmonic balance approximation is again

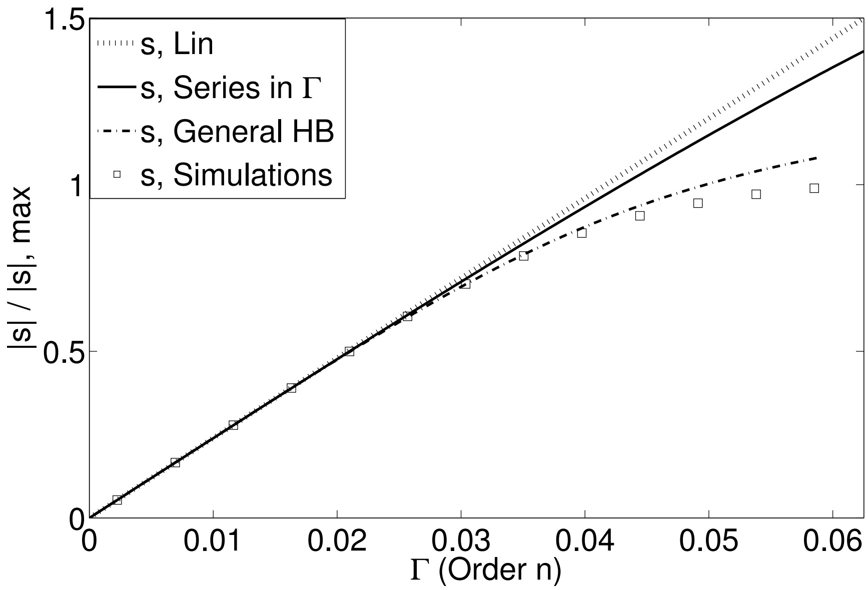

Figure 4.8: Absorber amplitude, $|s|/|s|_{\max}$, vs. Γ_n, from the linear theory, the two nonlinear harmonic balance (HB) approximations, and numerical simulations, for $\varphi = 0$ and $\alpha = 0$.

shown to be in good agreement with the numerical simulations until the torque level approaches around 50% of that which causes the absorbers to reach their cusp limits, following the deviation of the absorber approximations from the simulations. In order to increase the accuracy of the order n approximation, as well as to estimate the amplitudes of the higher harmonics on the rotor, we again must include the higher order terms in the expansions. As shown in Fig. 4.9, the higher order approximations capture some of the nonlinear effects of the order n torque as well as the order $2n$ and $3n$ torques, and provide reliable results out to torque amplitudes at which the absorbers reach $\approx 70\%$ of their cusp amplitude.

4.3.3.1 Non-Tautochronic Paths

The above results show good agreement between the theory and the numerical simulations for the tautochronic path, up to certain torque levels near to where the absorbers reach their cusps. We now investigate the accuracy of the method for non-tautochronic paths,

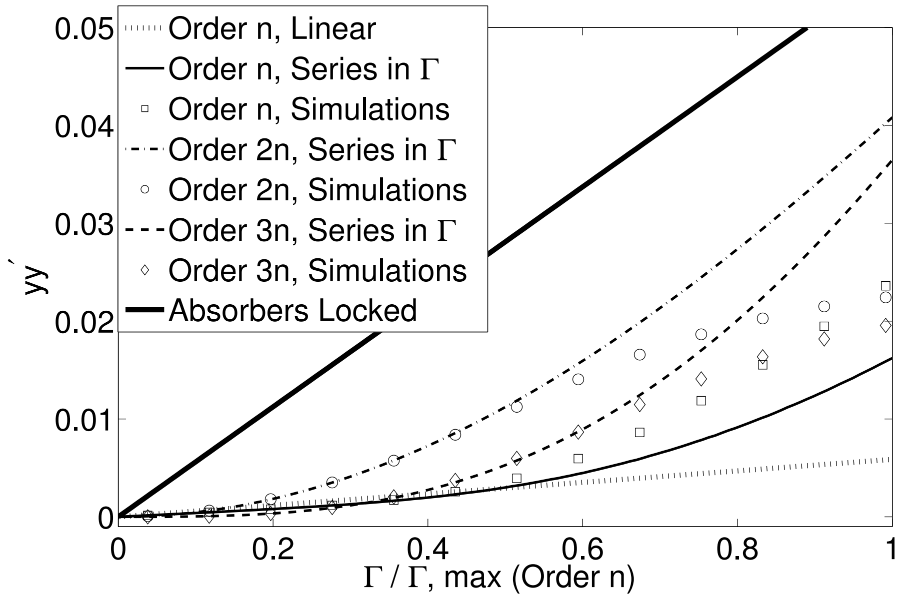

Figure 4.9: Approximations of the harmonic amplitudes of yy' obtained using the amplitude expansions, vs. Γ_n, for $\varphi = 0$ and $\alpha = 0$; comparison with simulation results are also included.

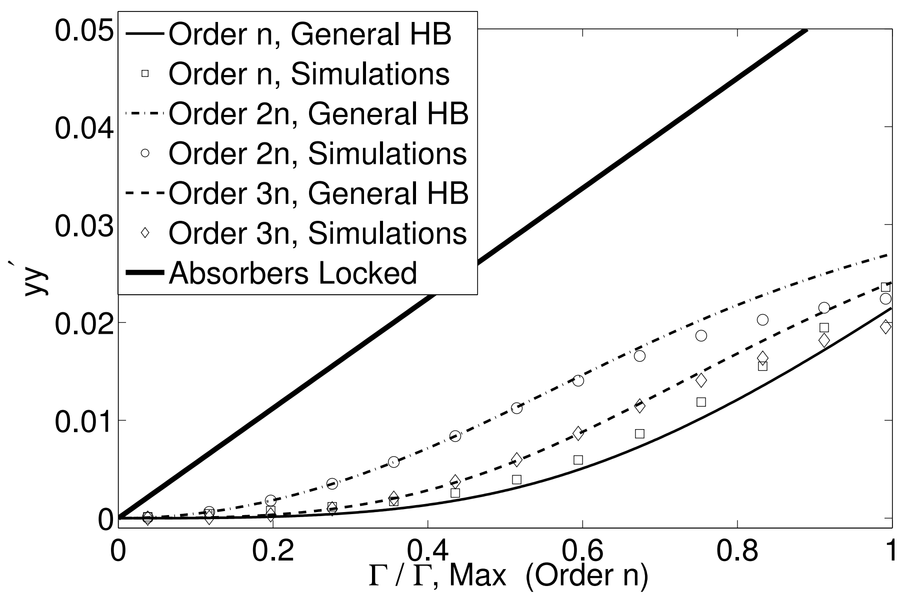

Figure 4.10: Approximations of the harmonic amplitudes of yy' obtained using the general HB method, vs. Γ_n, for $\varphi = 0$ and $\alpha = 0$; comparison with simulation results are also included.

specifically a circle. Utilizing the perturbation away from the tautochrone in the form of $h = \varphi s^4$, we investigate the absorber and rotor responses for a circular path absorber. Shown in Fig. 4.11 is the estimated absorber amplitude versusΓ_n obtained using both harmonic balance approximations. As found by previous researchers, the circular path absorbers exhibit an instability at a certain torque level which causes a jump in their amplitude [36]. This occurs since, when the rotor spins at a constant speed, circular path absorbers behave similar to a softening Duffing oscillator with bistability in the force response. This can be seen in the numerical simulations in Fig. 4.11. However, the results from the power series harmonic balance method fails to capture the large amplitude solution branch; this is expected, since this approach does not allow for multiple solution branches. In contrast, the general harmonic balance approach does capture the bistability, which is due to the fact that the form of the amplitude is not constrained to be of a certain form, thus allowing multiple solutions to be obtained. Figure 4.12 shows the rotor angular acceleration harmonics as a function of Γ_n for the power series HB method along with simulation results. One can see that the numerical simulations capture the amplification of the torsional vibrations due to the absorber jump instability, but, as noted above, this HB approximation fails to capture the jump phenomenon. Figure 4.13 shows the rotor response as estimated from the general HB method along with simulations. This approximation is much more accurate than the power series approach; it captures the jump instability, and is also very accurate in estimating the higher order harmonics. In fact, one can easily calculate the torque level which causes the absorber to go unstable, denoted here by Γ_n^*. This is done by setting the derivative of Eq. (4.21) with respect the absorber amplitude, A_1, equal to zero, solving for the corresponding value of A_1, and inserting it back into Eq. (4.21). Performing these operations for the conditions in Fig. 4.11, it is found that $\Gamma_n^* = 0.0083242$, which matches the numerical simulation data quite well.

It should be noted that in practice absorbers are often overtuned, that is, designed

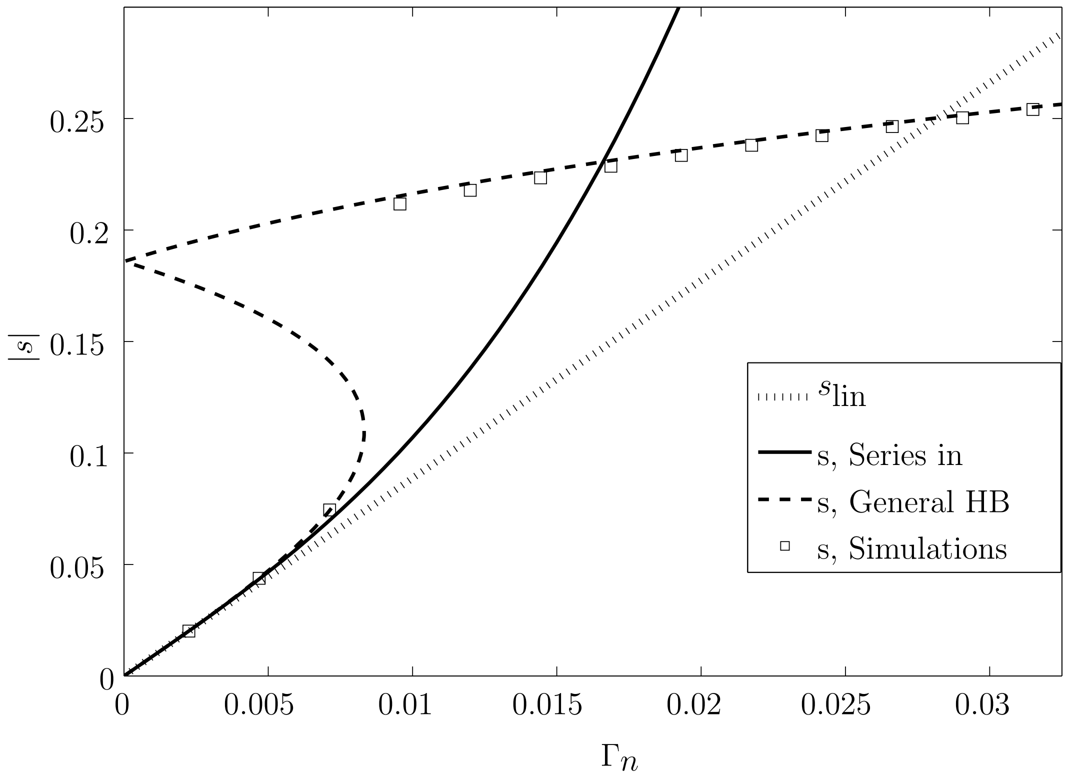

Figure 4.11: Absorber amplitude, $|s|$, vs. Γ_n, from the two HB approximations, along with numerical simulations, for a perfectly tuned circular path absorber.

with $\tilde{n} > n$, in order to alleviate the absorber jump instability [3, 36]. This is especially important for circular path absorbers, where detuning extends the stable torque range, but at the expense of absorber effectiveness [3, 36]. Since increasing the detuning makes the absorber response more linear over a large torque range, the power series HB method likewise improves in accuracy, and becomes quite accurate when the absorber is overtuned as little as 2%. We present an example case for a circular path absorber overtuned by 5%, ($\tilde{n}_1 = 1.575$). The estimated absorber amplitude versus Γ_n for both HB methods, and comparisons with simulations, are shown in Fig. 4.14. With the detuned absorber, the response is stable out to a very large level of applied torque, specifically, about 6.3 times the torque level which caused the perfectly tuned absorber to jump. Both harmonic balance estimations are very accurate

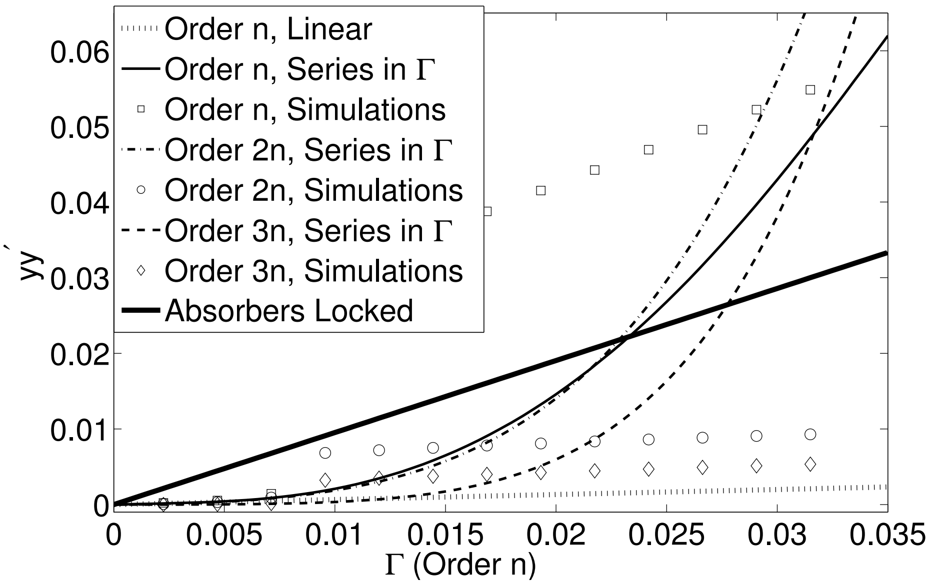

Figure 4.12: Approximations of the harmonic amplitudes of the rotor angular acceleration obtained using the series expansion HB method, vs. Γ_n, along with results from numerical simulations, for a perfectly tuned circular path.

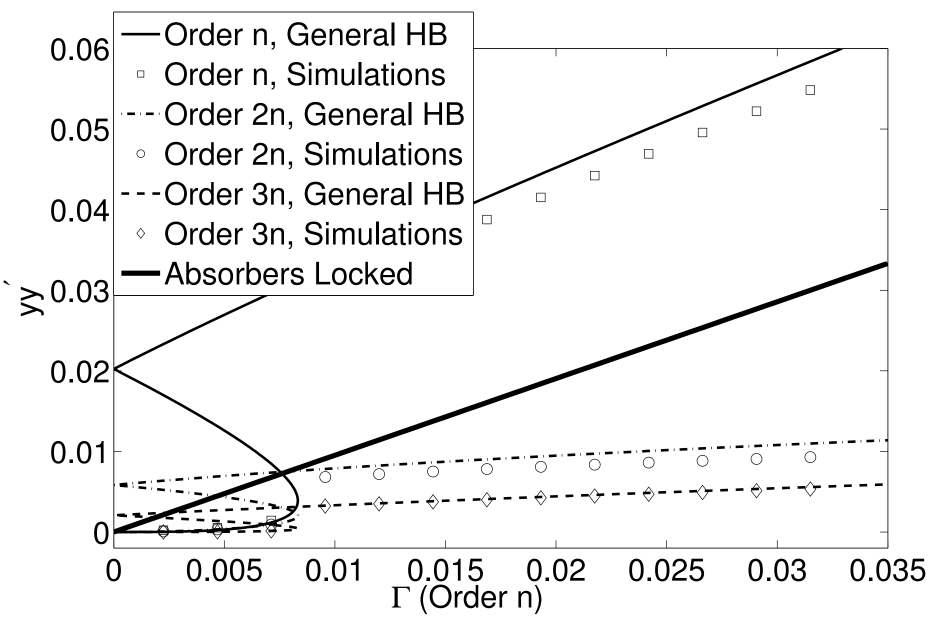

Figure 4.13: Approximations of the harmonic amplitudes of the rotor angular acceleration obtained using the general HB method, vs. Γ_n, along with results from numerical simulations, for a perfectly tuned circular path.

out to large torque amplitudes here, and it can be shown the same accuracy follows for all detuned absorber paths. The rotor response for the power series HB approach is shown in

Fig. 4.15, and for the general HB method in Fig. 4.16. As expected from the accuracy of the absorber response approximations, both methods are very accurate in predicting the rotor harmonic approximations over a large torque range.

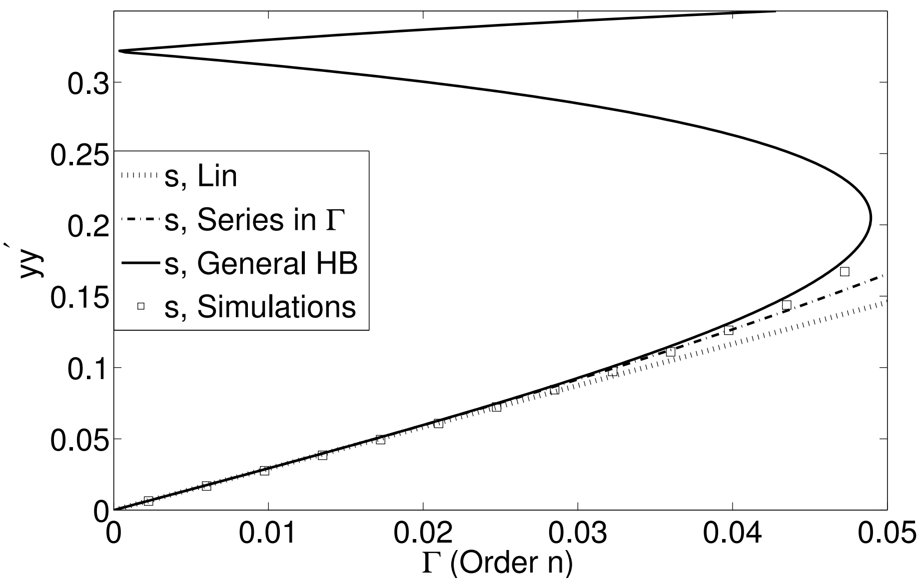

Figure 4.14: Absorber amplitude, $|s|$, vs. Γ_n, obtained using different order HB approximations, along with results from numerical simulations, for a detuned circular path.

4.4 Experimental Testing

Utilizing the experimental setup described in Chapter 2, we investigate the accuracy of the above analytical and numerical approximations. Single order tautochronic and circular path absorber systems are tested, as well as multiple order tautochonic absorbers. The experimental data is found to confirm the accuracy of the harmonic balance approximations developed above for all cases considered. The experimental observations are presented in the same format as the above analytical and numerical investigations, beginning with multiple order absorbers and concluding with single order, non-tautochronic absorbers. When showing experimentally measured quantities we use their normalized versions, matching the

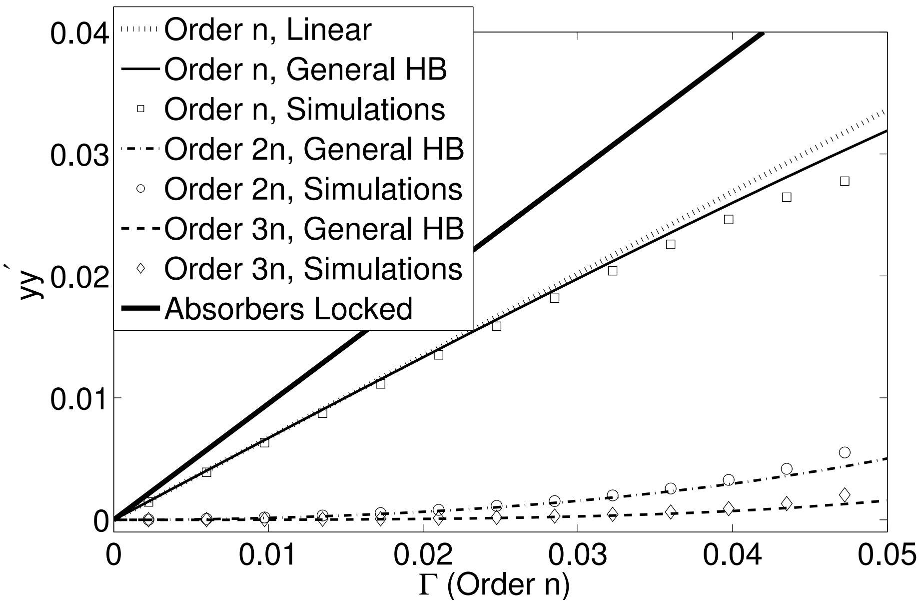

Figure 4.15: Approximations of the harmonic amplitudes of the rotor angular acceleration obtained using the series expansion HB method, vs. Γ_n, along with results from numerical simulations, for a detuned circular path.

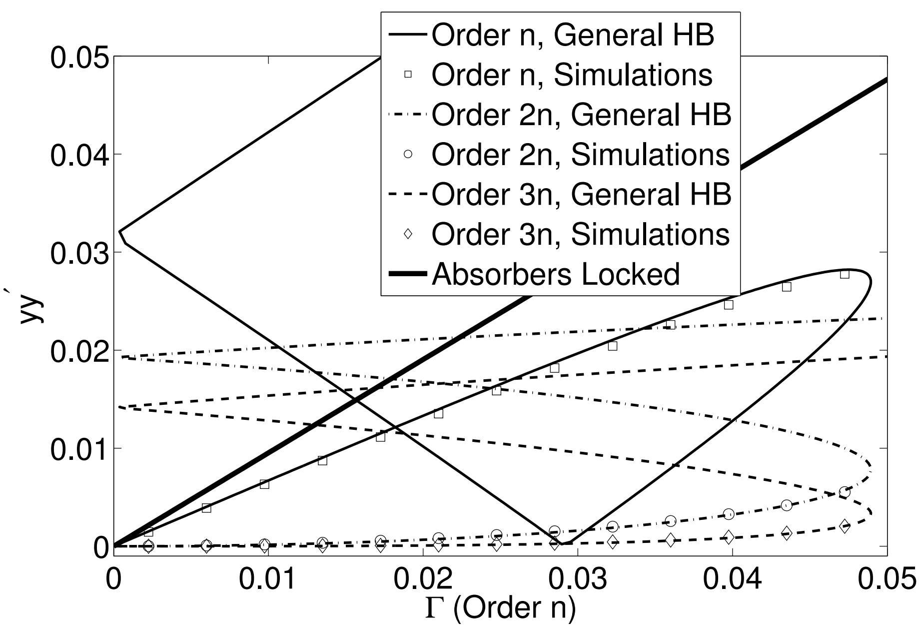

Figure 4.16: Approximations of the harmonic amplitudes of the rotor angular acceleration obtained using the general HB method, vs. Γ_n, along with results from numerical simulations, for a detuned circular path.

non dimensional quantities used in the analysis.

4.4.1 Tautochronic Absorbers at Two Orders

Epicycloidal path absorbers tuned to orders $\tilde{n}_1 = 2.3$ and $\tilde{n}_2 = 4.6$, as described in Chapter 3 are tested to investigate the accuracy of the multiple order harmonic balance methods. The physical parameters used in the subsequent experimental results are summarized in Table 4.1.

Table 4.1: Physical Multiple Order Epicycloidal Path Experimental Parameters.

Physical Parameter	Definition	Value
m_1	Order $\tilde{n}_1$ Absorber mass	0.4313 kg
m_2	Order $\tilde{n}_2$ Absorber mass	0.0482 kg
α	Different order absorber inertia ratio	0.0106
$R_{1,0}$	Rotor center to absorber 1 COM (at vertex) distance	0.12316 m
$R_{2,0}$	Rotor center to absorber 2 COM (at vertex) distance	0.12 m
$\mu_{a,1}$	Absorber 1 viscous damping	0.1
$\mu_{a,2}$	Absorber 2 viscous damping	0.191
ϵ	Absorber to rotor inertia ratio	0.18486
Ω	Rotor mean speed	300 RPMs

Figure 4.17 shows experimental absorber amplitudes versus the amplitude of the fluctuating part of the applied torque. The experimental torque is applied at a single order only, $n = 2.29$, which excites the order $\tilde{n}_1$ absorber resonantly, and the internal $2:1$ resonance drives the order $\tilde{n}_2$ absorber. As visible from Fig. 4.17, both of the harmonic balance methods accurately predict the experimental absorber amplitudes. As expected, the general HB method captures the large amplitude hardening of the order $\tilde{n}_1$ absorber more accurately than the power series HB method, although the power series method is more accurate at lower torque levels, for both absorbers, due to the inclusion of damping in that approach. At low torque levels, both the numerical simulations and the HB approximations differ slightly from the experimental results, which could be due to a number of factors, perhaps most importantly, assumptions made about the absorber damping. As described in Chapter 3,

a constant effective absorber damping value is used for each absorber, whereas in fact the absorber damping is estimated using coupled absorber/rotor free vibration data, and it is known that the damping level depends on amplitude.

Considering the harmonics of rotor angular acceleration, as shown in Figs. 4.18 and 4.19 for the power series HB method and Figs. 4.20 and 4.21 the general HB method, the experimental results track both predictions quite well, with negligible differences between the two methods in terms of approximating the experimental results. Interestingly, recalling Fig. 4.7, the accuracy of the general HB method in approximating the rotor harmonics for a similar system was significantly less than that for the power series HB method. The explanation for the increase in accuracy for the general HB method here can be attributed to the fact that in Fig. 4.7, the order $\tilde{n}_1$ absorber was being forced precisely at its tuning order, whereas here there is a small (0.05%) detuning. Although this detuning is very small, the general HB method improves drastically in accuracy, as noted in Section 4.3.3.1.

There exists some deviation in the order n rotor harmonic approximations at small torque levels, specifically, the experimental data is larger in amplitude than the predictions. This is due to the fact that the absorber amplitude at this level is smaller than the approximations, thus not absorbing as much of the torsional oscillations as the model predicts. Also, near the torque level which causes the order $\tilde{n}_2$ absorber to reach it's cusp, the order $2n$ and $3n$ experimental rotor harmonics are smaller in amplitude than predicted. This can be attributed to two effects. First, the experimental rotor harmonics are computed by taking a digital Fourier Transform of the measured time response of the rotor speed. As not all experimental data samples are taken for the same time period, some leakage of the higher rotor harmonic amplitudes could occur in the Fourier Transform computation, causing one to calculate a lower amplitude of the desired harmonic than measured. Second, when decoupling

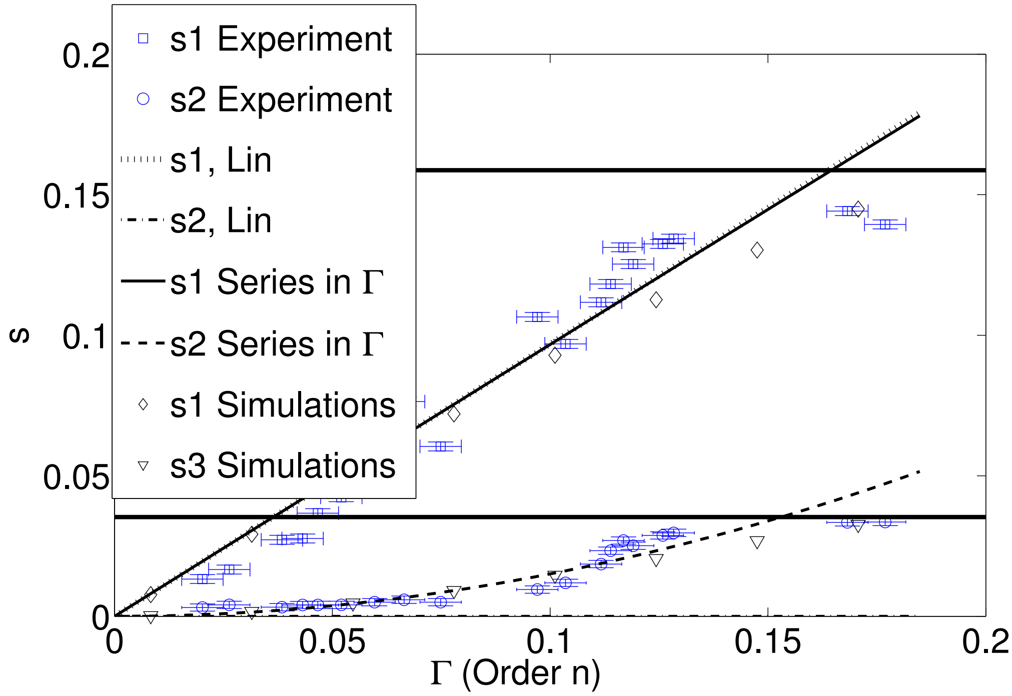

(a)

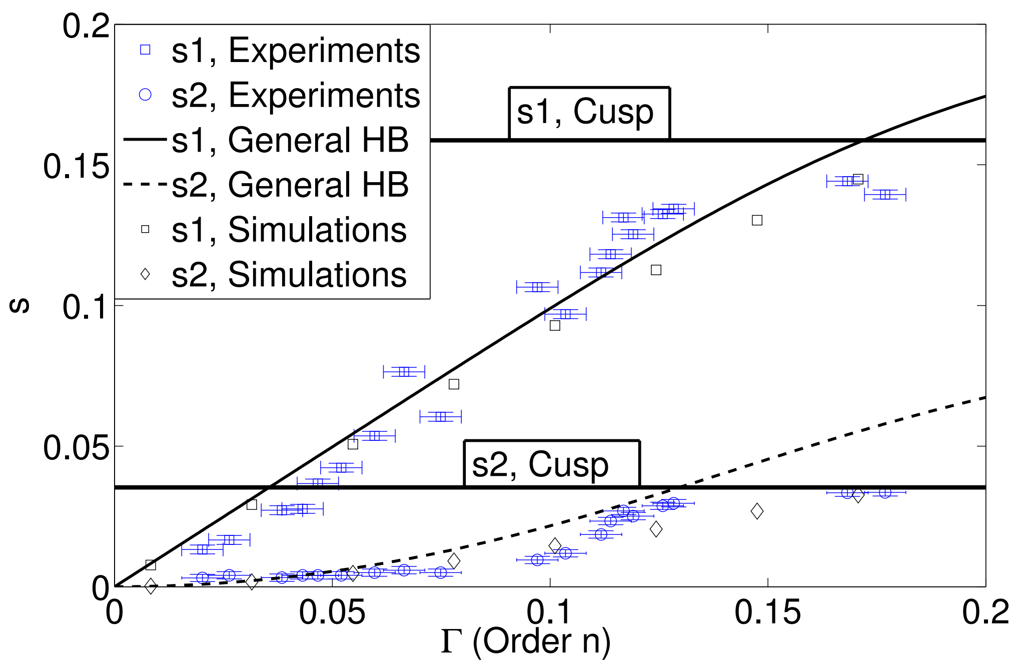

(b)

Figure 4.17: Experimental absorber amplitudes, s, versus the amplitude of order n torque, Γ_n compared against the harmonic balance approximations for multiple order absorbers. (a) Series expansion HB method. (b) General HB method.

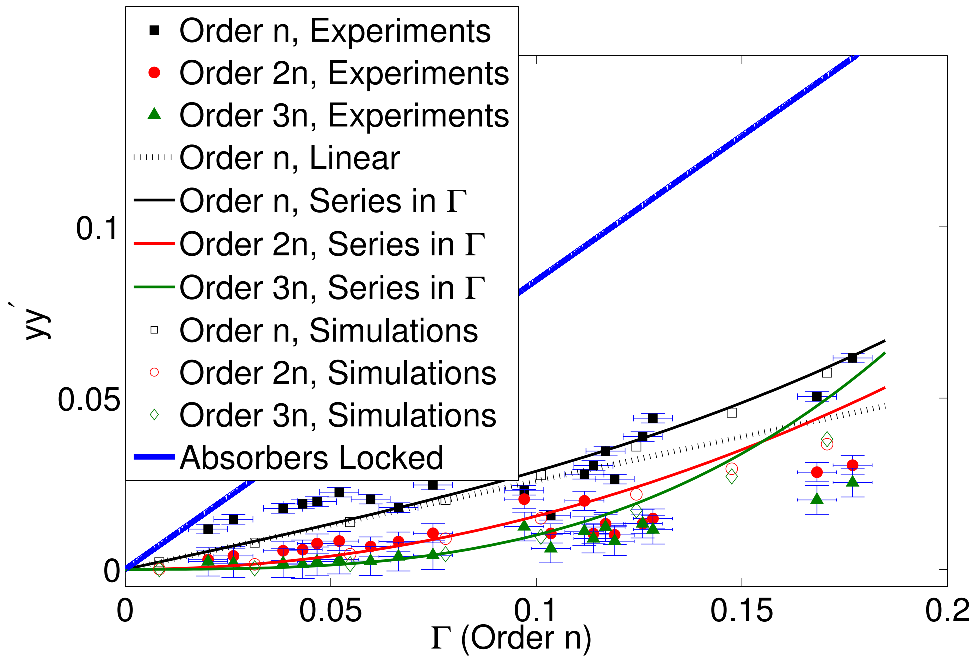

(a)

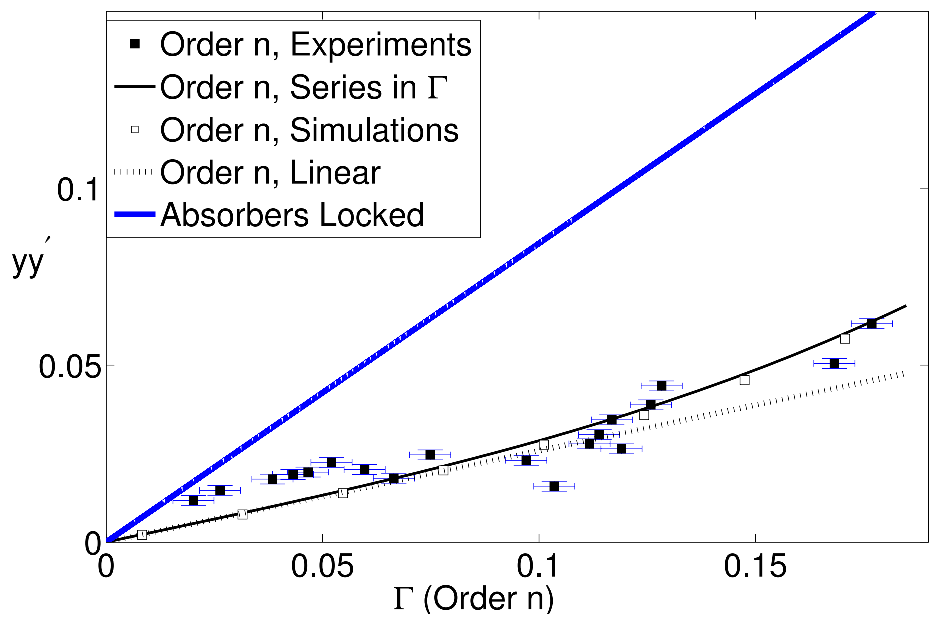

(b)

Figure 4.18: Experimental rotor angular acceleration, yy' vs. Γ_n for multiple order epicycloidal absorbers compared against the power series HB approximation. (a) All three rotor response orders, n, $2n$, $3n$. (b) Order n.

the absorber dynamics from those of the rotor, one must assume that the amplitude of the applied mean torque balances the mean rotor damping torque, that is, $T_0 = c_0\Omega$, thus

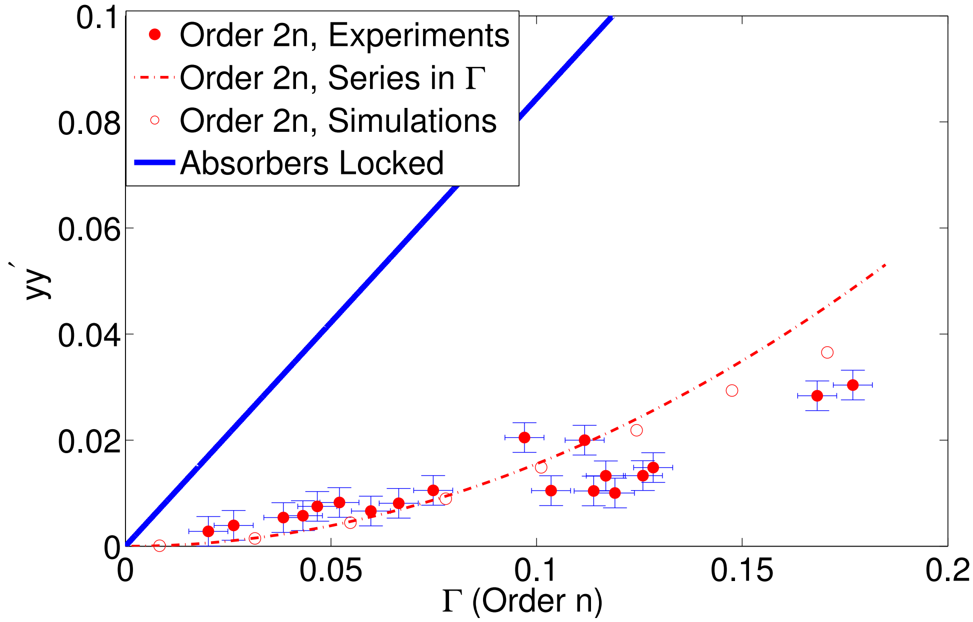

(c)

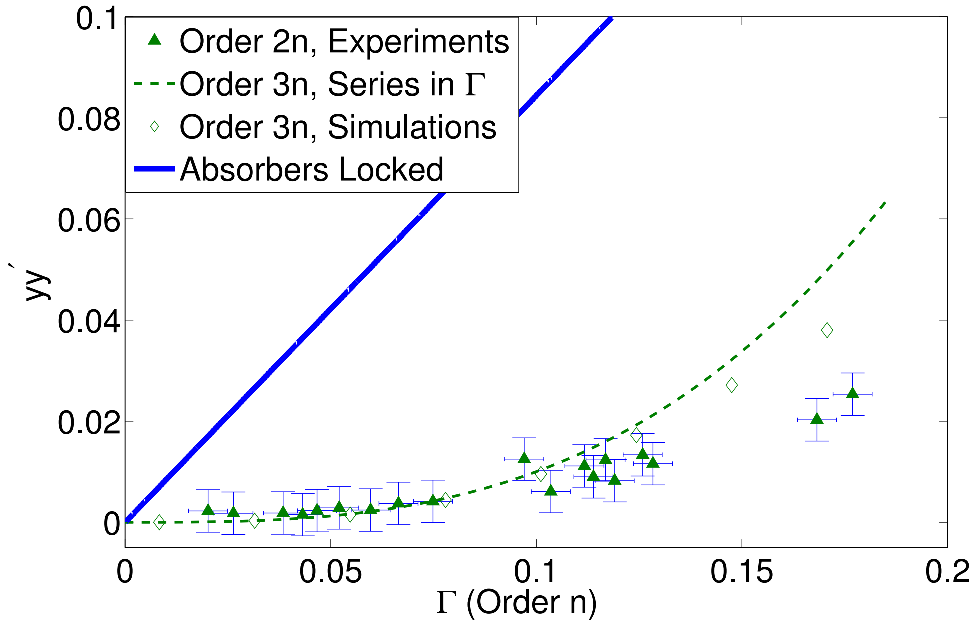

(d)

Figure 4.19: (c) Order $2n$. (d) Order $3n$. Coorsponding with Fig. 4.18

eliminating the effects of the rotor damping from the model. Numerical simulations have shown that if one increases the rotor damping and compensates for this by increasing the mean torque level, the corresponding rotor angular acceleration amplitudes will be lower.

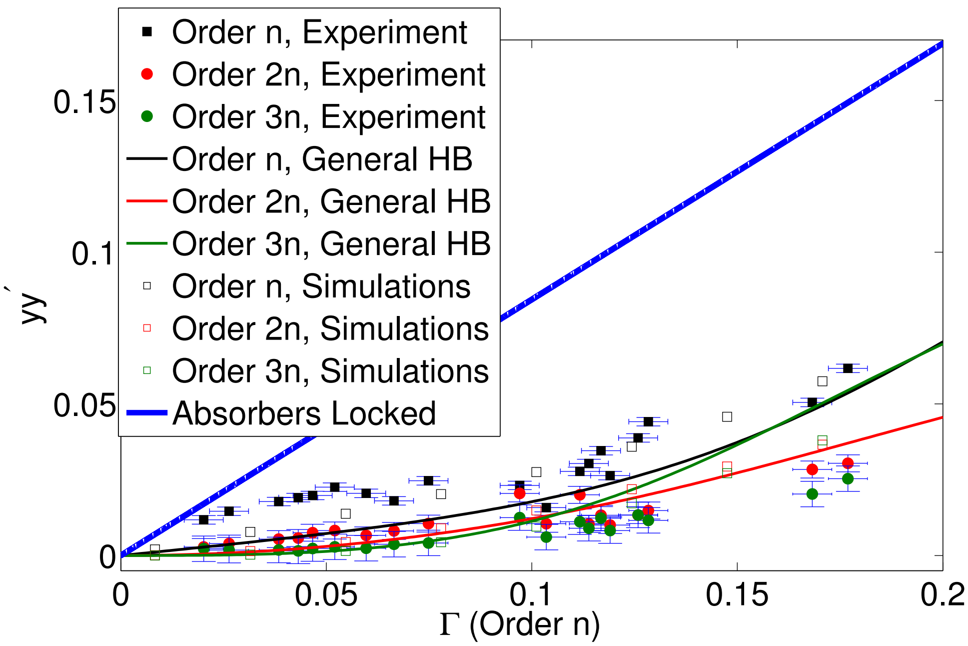

(a)

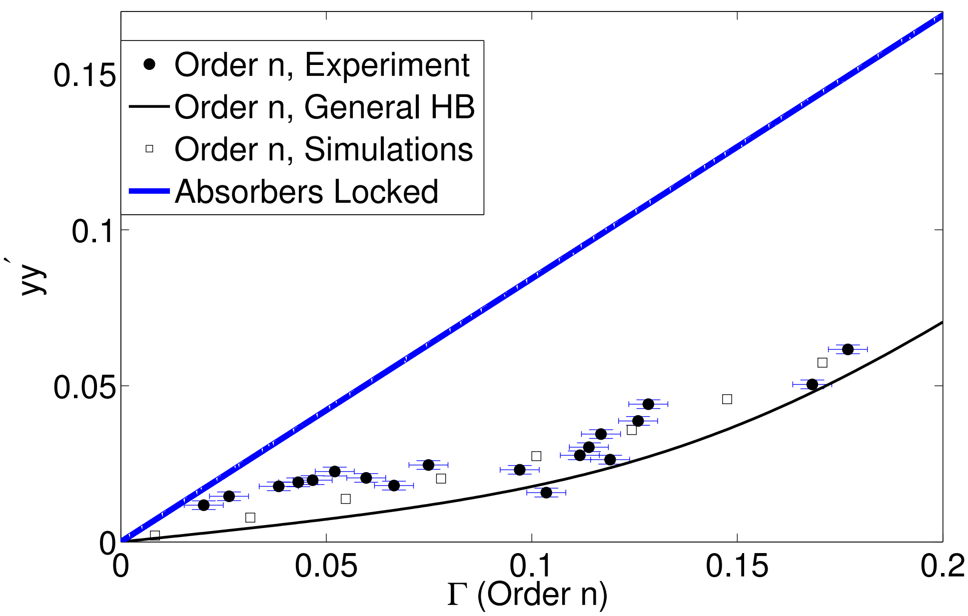

(b)

Figure 4.20: Experimental rotor angular acceleration, yy' vs. Γ_n for multiple order epicycloidal absorbers using the general HB approximation. (a) All three rotor response orders. (b) Order n only.

This is a higher order effect that we do not investigate here, but warrants further study.

Overall, both of the HB methods are accurate in predicting the absorber and rotor

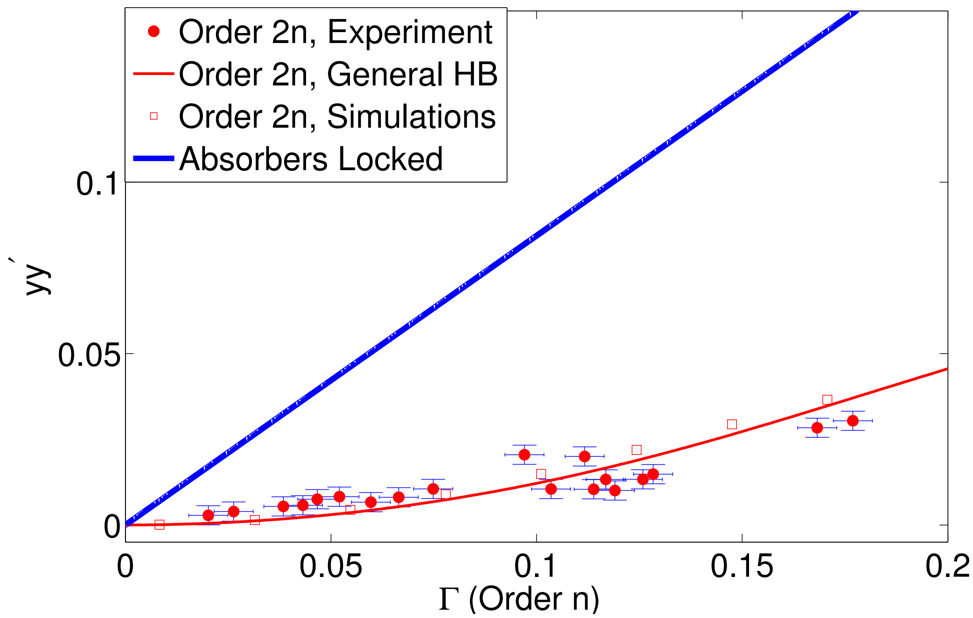

(c)

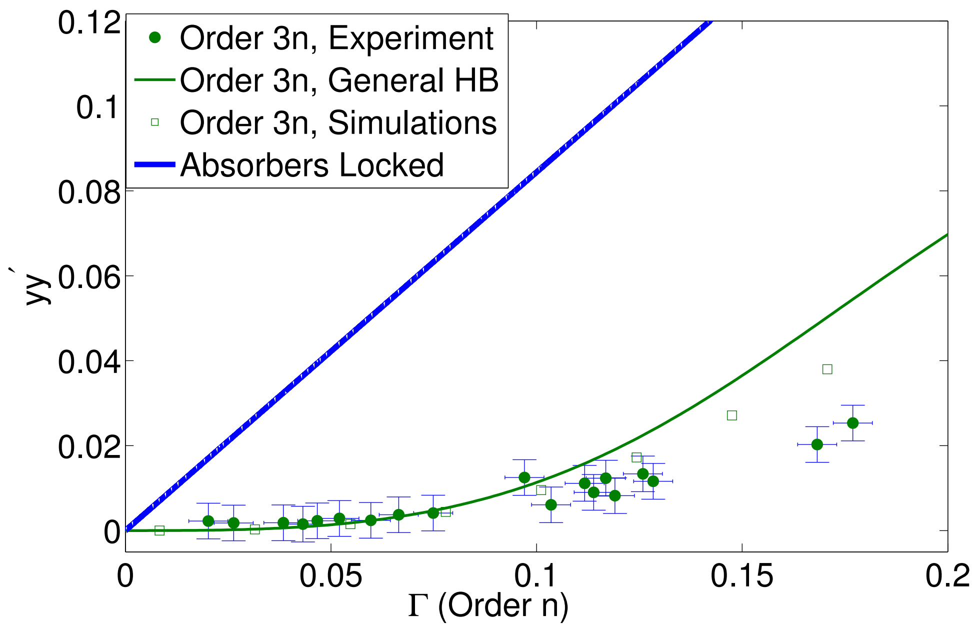

(d)

Figure 4.21: (c) Order 2n only. (d) Order 3n only. Coorsponding with Fig. 4.20

response of a system equipped with internally resonate multiple order absorbers, confirming the utility of the HB methods for designing such systems.

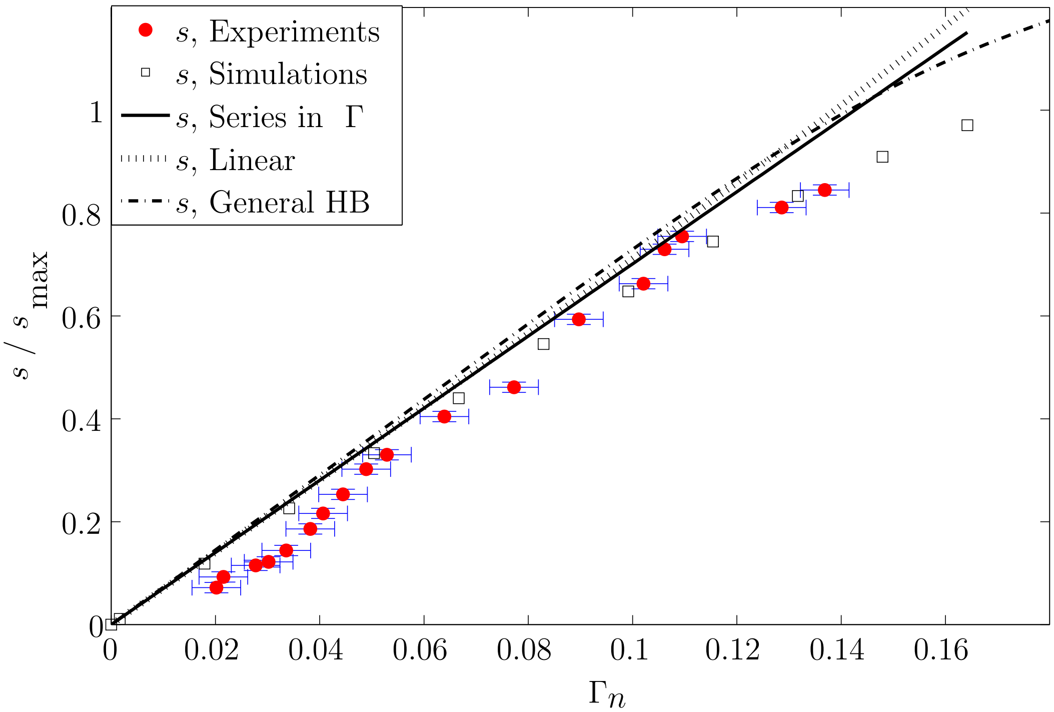

Figure 4.22: Experimental absorber amplitude, s, versus the amplitude of order n torque, Γ_n compared against the harmonic balance approximations for a single order tautochronic absorber.

4.4.2 Single Order Tautochronic Path Absorber

Utilizing the order $\tilde{n}_1$ epicycloidal path absorber used above, with the order $\tilde{n}_2$ absorber locked, we investigate the validity of the HB approximations for a single order tautochonic absorber. The parameters defined in Table 4.1 apply to this case, except for two: first, the inertia ratio which changes to $\epsilon = 0.1642$, due to only one absorber being active and the other locked; and well the order of the applied torque is taken to be exactly at the absorber's tuning order, that is, $n = \tilde{n} = 2.3$.

The experimentally obtained absorber amplitude versus Γ_n is compared against both HB methods and numerical simulations in Fig. 4.22.

Again, both HB methods accurately capture the experimental observations for a wide range of applied torque. The general method better captures some of the absorber hardening near its amplitude limits, but both methods degrade in accuracy at this limit. Just as in the multiple order absorber case, the experimental absorber amplitudes are smaller than the predictions at small torque levels, which is consistent with the previous results. One can see the effect of this error in estimating the absorber amplitude at small torque levels in the corresponding order n rotor harmonic, as shown in Figs. 4.23 and 4.24 for the power series HB method and in Figs. 4.25 and 4.26 for the general HB method.

The fact that the experimentally measured absorber amplitude is smaller than the predictions at the small torque levels again causes a similar error in the order n rotor response. Interestingly, this trend does not seem to carry over to the higher order harmonics, mainly due to their respective amplitudes being relatively small at this torque level. The accuracy of both methods in approximating the higher order rotor harmonics is similar for this system. The accuracy difference between the two methods is visible in the estimation of the order n harmonic, where the accuracy of the general method is much lower than the power series HB method. This is surprising, since in the multiple order absorber case, a .05% detuning causes the general method to be much more accurate in modeling the order n torque, where here we are forcing directly at the absorbers tuning order. Again, both methods are effective overall in predicting the absorber and rotor response. Also, when the absorber is exactly tuned, the absorber damping has a more significant effect, and it is included in the power series method but not in the general method.

4.4.3 Single Order Circular Path Absorber

We now turn to an experimental investigation of circular path absorbers, which exhibit nonlinear behavior at much smaller amplitudes, due to the softening nature of the path. A

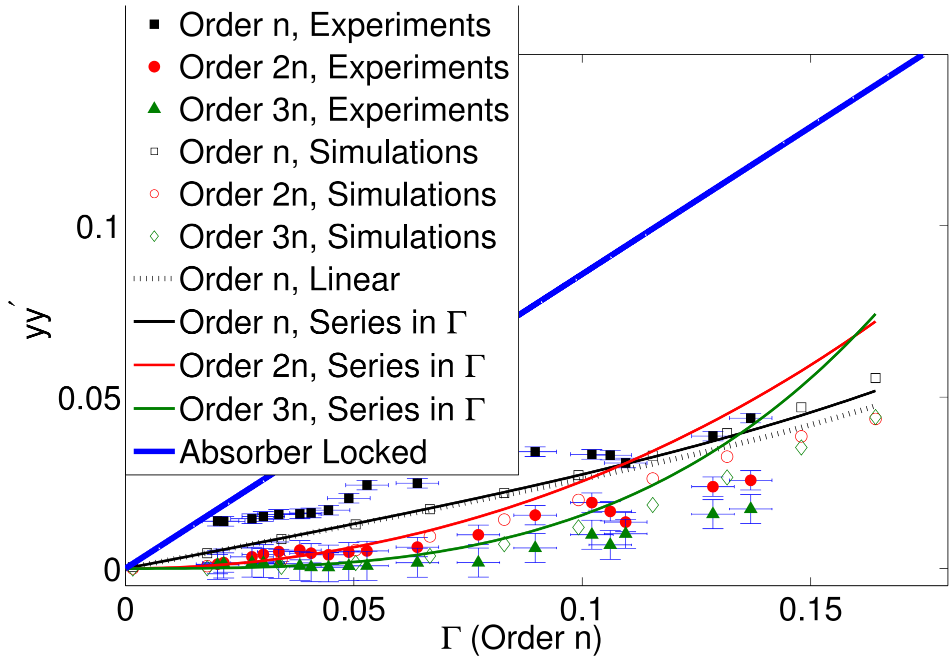

(a)

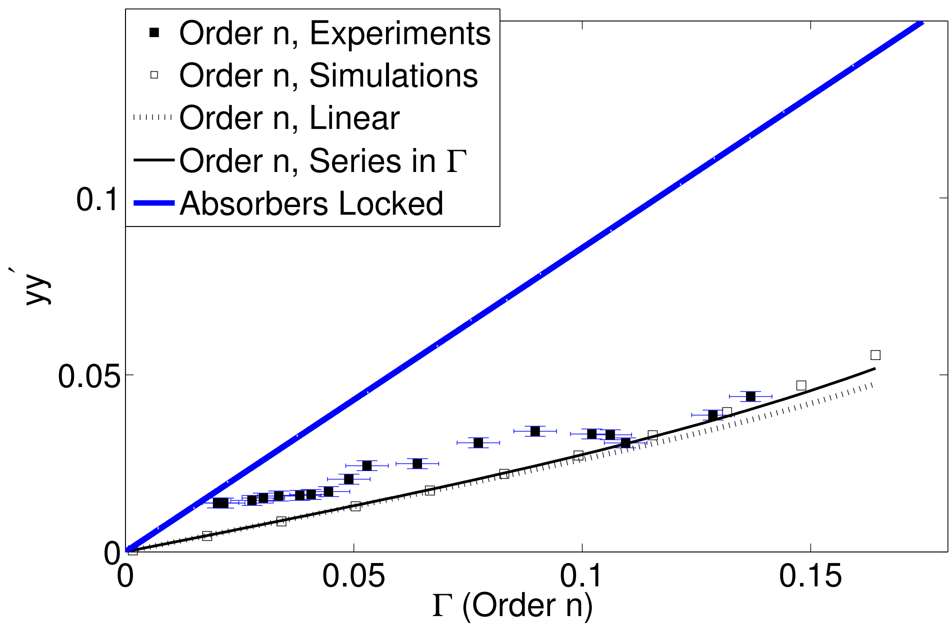

(b)

Figure 4.23: Experimental rotor angular acceleration, yy' vs. Γ_n for a single order epicycloidal absorber compared with the power series HB approximation. (a) All three rotor response orders, n, $2n$, $3n$. (b) Order n.

perfectly tuned circular path absorber is first tested, followed by investigation a detuned circular path absorber for different inertia ratios. In order to experimentally test circular

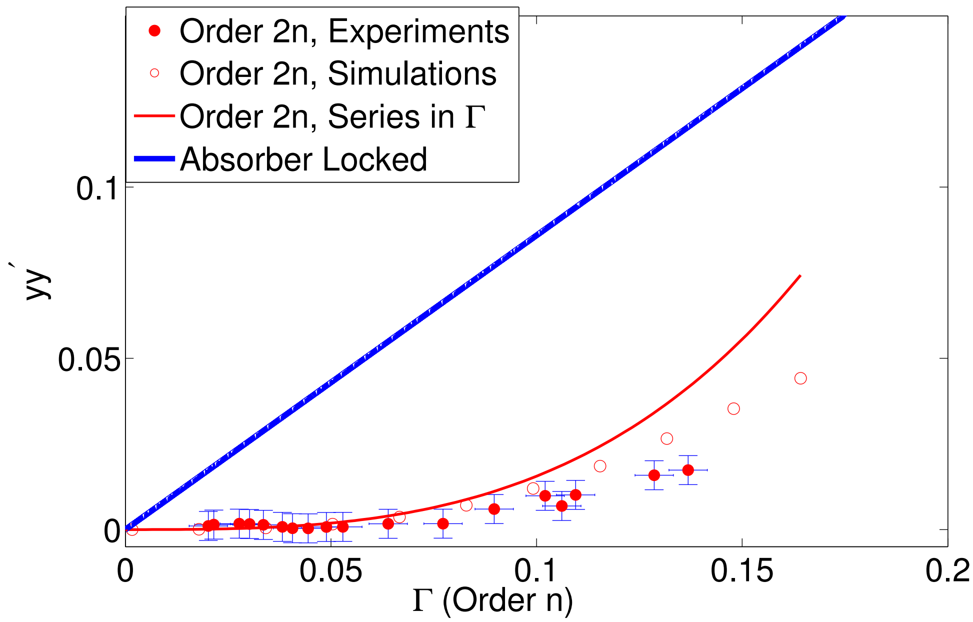

(c)

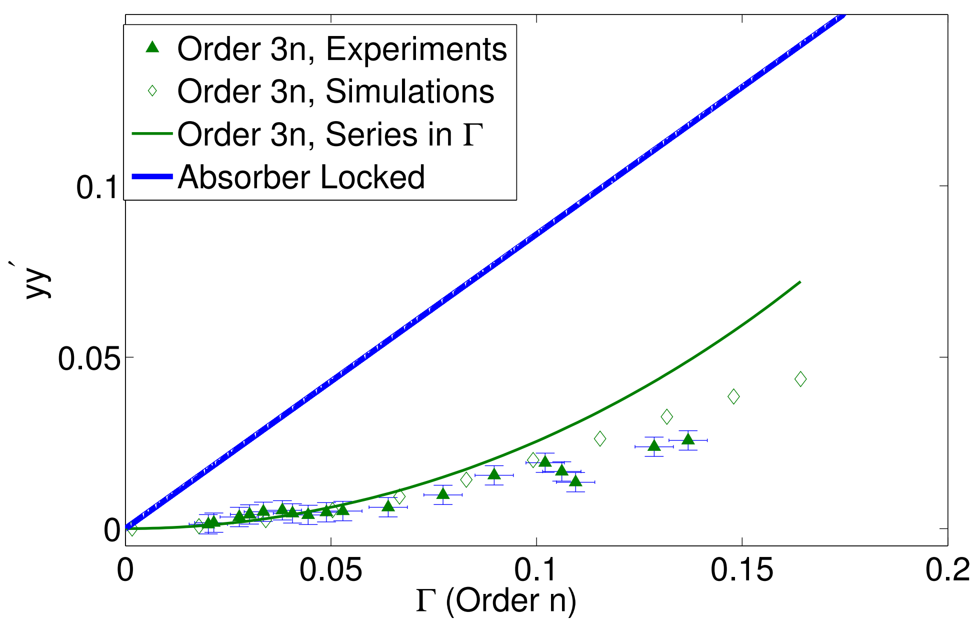

(d)

Figure 4.24: (c) Order $2n$. (d) Order $3n$. Coorsponding with Fig. 4.23

path absorbers, the T-shaped compound pendulum absorber used in [32, 47] and shown in Fig. 4.36 is used. It must be noted here that, unlike bifilar absorber suspensions, this configuration allows the pendulum to rotate with respect to the rotor. One must then include

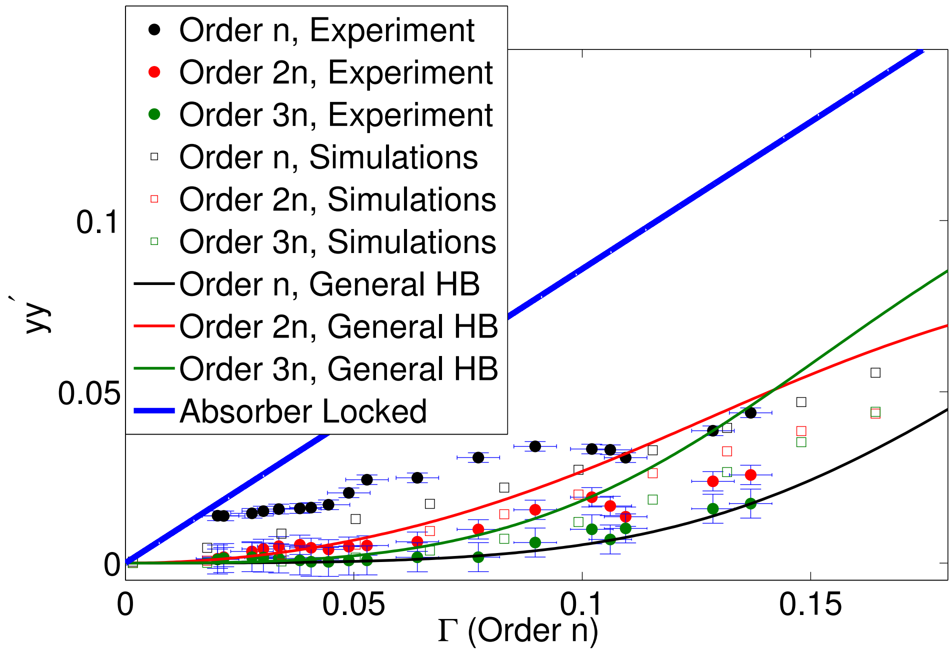

(a)

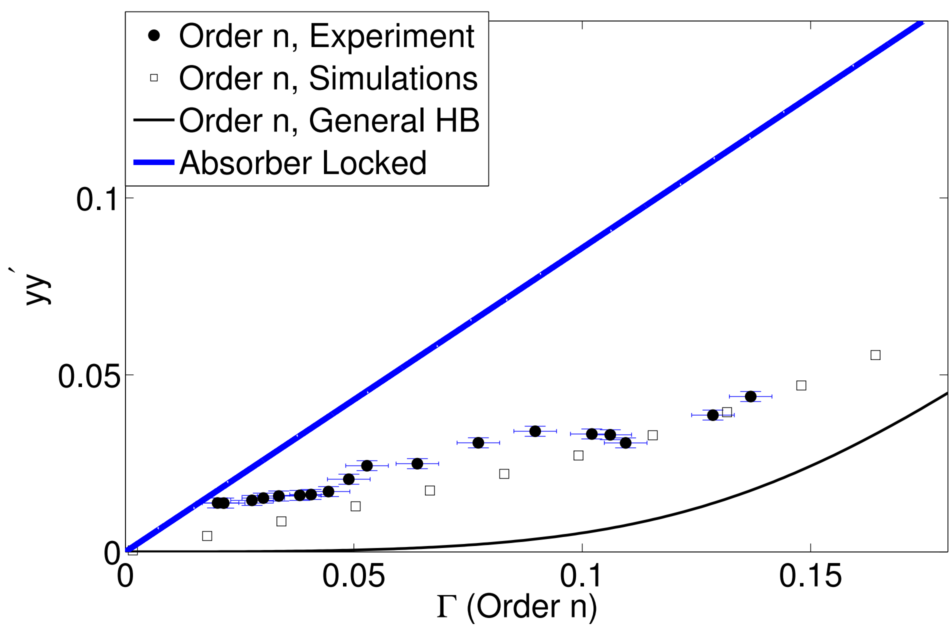

(b)

Figure 4.25: Experimental rotor angular acceleration, yy' vs. Γ_n for a single order epicycloidal absorber compared with the general HB approximation. (a) All three rotor response orders, n, $2n$, $3n$. (b) Order n.

the rotational inertia of the pendulum with respect to its center of mass when defining the

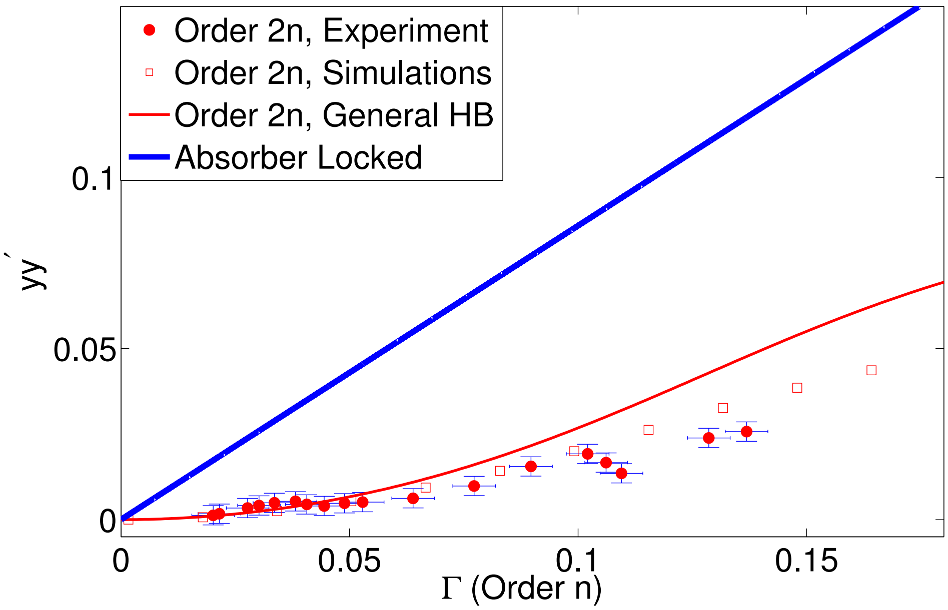

(c)

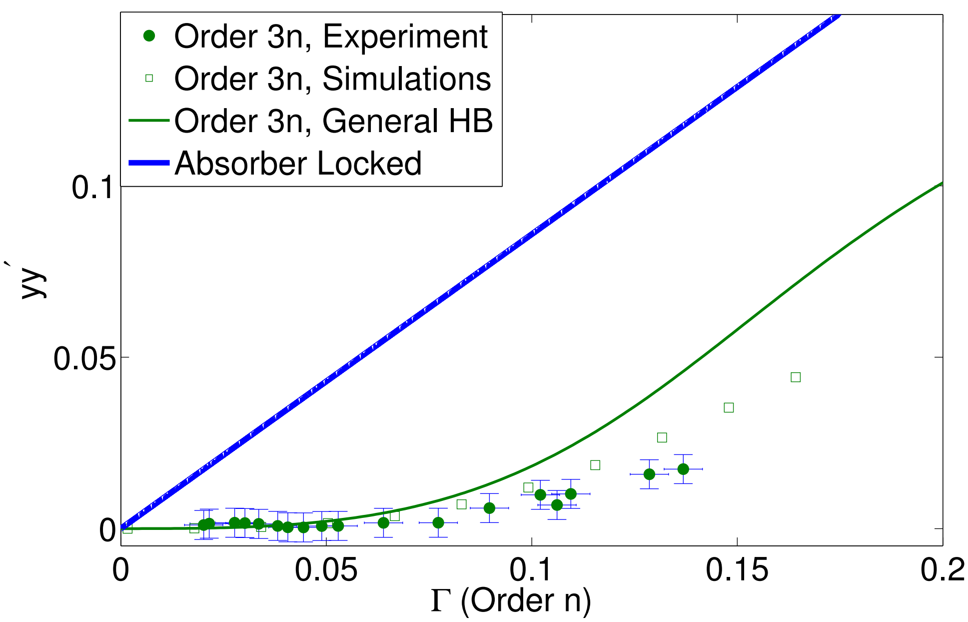

(d)

Figure 4.26: (c) Order $2n$. (d) Order $3n$. Coorsponding with Fig. 4.25

tuning order of the absorber, which can be found to be,

$$\tilde{n} = \sqrt{\frac{RL}{L^2 + \rho^2}},$$

where R is the distance from the rotor center to pivot point of the absorber, L is the distance from the pivot point to the absorber center of mass, and ρ is the pendulums radius of gyration. The analysis presented in the previous sections is adequate for a point mass, or a bifilar design, where the rotational inertia of the absorber with respect to its center of mass can be grouped into the rotor inertia, J. Previous analysis [33, 47] has shown that one can account for this rotational inertia and formulate the non-dimensional absorber and rotor equations of motion in the same form as Eqs. (2.2) and (2.3) by including a simple dimensional scaling constant when describing the non-dimensional absorber arc length, defined as,

$$s = \frac{L\phi}{\beta},$$

where ϕ is angle the absorber swings at with respect to its vertex position, and β is the dimensional scaling constant. One then finds that by choosing $\beta = L(1 + \tilde{n}^2)$, the equations of motion for the compound pendulum absorber can be put into the necessary form for comparison with bifilar absorbers. For the subsequent plots, the experimental physical parameters used for these absorbers are presented in Table 4.2.

Table 4.2: Circular Path Absorber Physical System Parameters.

Circular Path Parameter	Definition	Value
m	Absorber Mass	0.225 kg
R	Rotor Center to Absorber Pivot Point Distance	0.118 m
L	Absorber Pivot Point to Absorber COM Distance	0.051 m
$\tilde{n}$	Absorber Tuning Order	1.315
ρ	Absorber Radius of Gyration	0.03 m^2
μ_a	Absorber Viscous Damping	0.017
Ω	Rotor Mean Speed	300 RPMs

We begin with a circular path absorber driven exactly at its tuning order, with $n = \tilde{n} =$

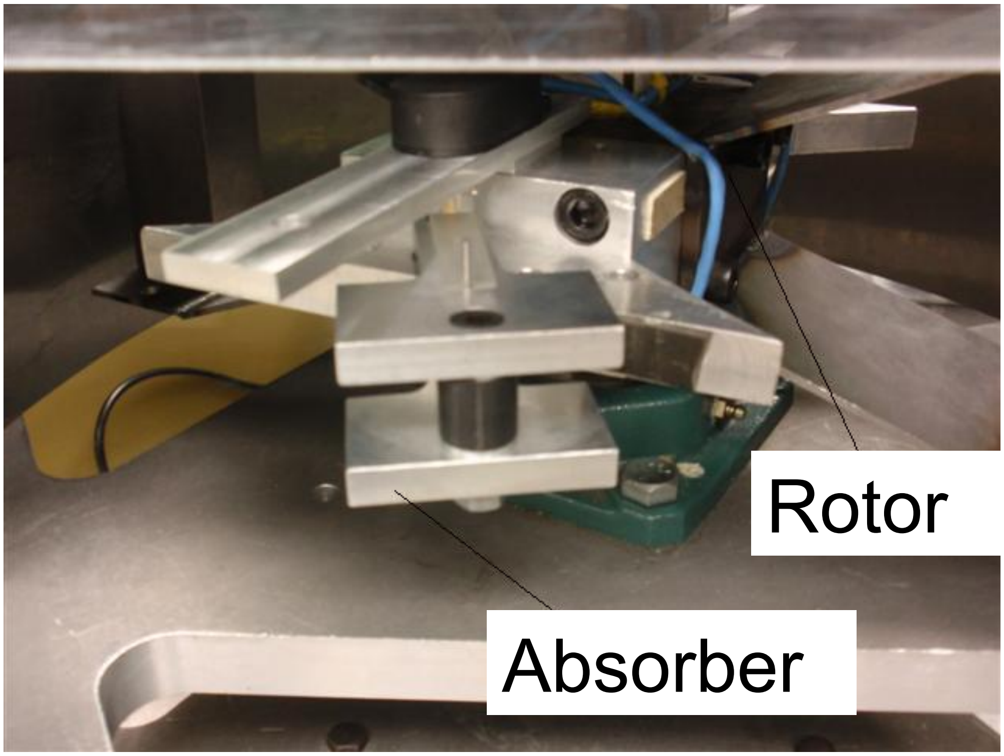

Figure 4.27: Picture of the experimental circular path pendulum “T-shaped” absorber.

1.315, with an inertia ratio of $\epsilon = 0.1045$. Figure 4.29 shows the experimentally obtained absorber amplitude compared against both harmonic balance approximations and numerical simulations versus the amplitude of the applied fluctuating torque, represented by Γ_n.

As with the comparisons with the numerical simulations presented in Section 4.3.3.1 above, the general method tracks the experimental data very accurately and also captures the jump bifurcation. The power series method is accurate up to near the jump bifurcation, but, as noted in Section 4.3.3.1, it fails to capture the bistability, and thus misses the large amplitude response entirely. The corresponding rotor harmonics are presented inFigs. 4.29 to 4.32 and, as expected, the inability of the power series HB method to accurately predict the absorber motion carries over to the rotor harmonics. For all subsequent circular path studies we therefore present only the rotor harmonic approximations obtained from the general HB method.

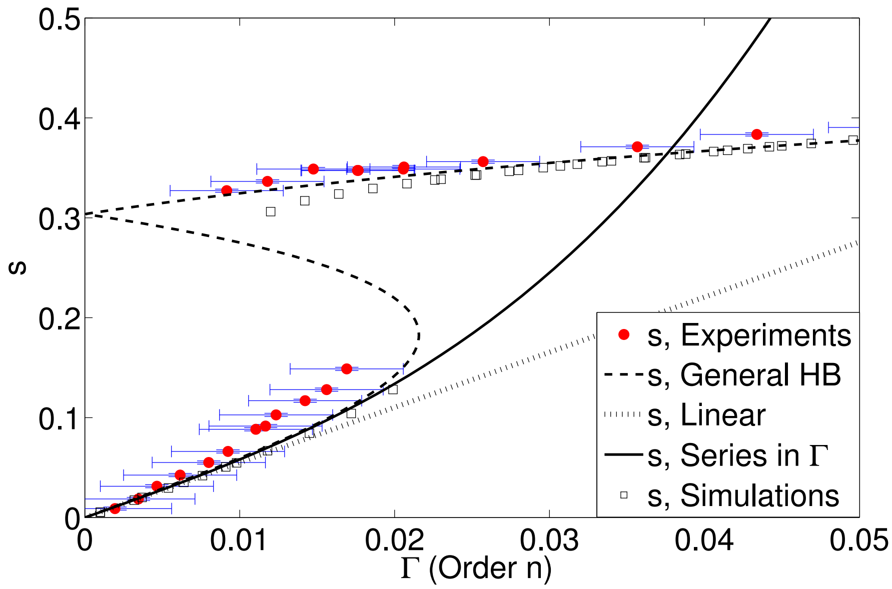

Figure 4.28: Absorber arc length harmonic amplitude, $|s|$ vs. Γ_n for a circular path absorber driven exactly at tuning; experimental results compared with both harmonic balance approximations and simulations.

As evident from Figs. 4.31 and 4.32, the general HB method accurately captures the increase in torsional vibrations due to the jump to the upper response branch of the absorber. On that branch the absorbers are in phase with the applied torque, thus amplifying the rotor torsional vibration at order n. Their exists some error between the HB approximations and the experimental data after the jump occurs, due to the relatively large absorber amplitudes, and the fact that expansions in the absorber amplitude were employed in the analysis.

We now look at the response of a circular path absorber when the applied torque is detuned from the absorber order. We effectively detune the absorber by forcing at an order less than the absorber's tuning order, specifically we take $n = 1.2492$, which results in a detuning of 5%. Shown in Fig. 4.33 is the absorber amplitude versus applied torque for a system with an inertia ratio of $\epsilon = 0.0519$, and again the general HB method accurately predicts the absorber amplitude throughout the torque range. This method also accurately captures the rotor harmonics, as presented in Figs. 4.34 and 4.35, although the experimental data for the order $3n$ harmonic does not exhibit a jump in amplitude as predicted by theory, that is, the amplitudes of this harmonic are the same on both the upper and response branches. The reason for this anomaly is not presently understood.

We now decrease the inertia ratio to, $\epsilon = 0.0189$, by adding weights to the rotor to increase its rotational inertia, in order to investigate the effects this parameter has on the analytical predictions. Figure 4.36 shows the absorber amplitude versus the amplitude of applied fluctuating torque for this case. This added inertia causes the absorber to jump at a lower non-dimensional torque level, but otherwise there is no discernible difference in the accuracy of the HB method. Once again, there is a slight error in the rotor harmonics, as shown in Figs. 4.37 and 4.38, most notably in the order $2n$ and $3n$ harmonics. These errors are not significant, however, as these harmonics are relatively small in this case, since in this case the torque exerted on the rotor by the absorber has a smaller effect on the rotor dynamics relative to that caused by the fluctuating torque.

4.5 Conclusions

Approximate, closed form expressions for pendulum absorbers and the corresponding rotor dynamics have been developed. One form of the assumptions yields approximation predictions for the applied fluctuating torque as a function of absorber amplitudes. The other form of the approximations, using the assumption that the absorber amplitude is a power series in the applied non-dimensional torque, gives predictions for the absorber amplitude as a function of the applied torque. Both methods also give predictions for the harmonically rich rotor dynamics. The methods are found to agree with numerical simulations and experimental results for a wide range of absorber configurations.

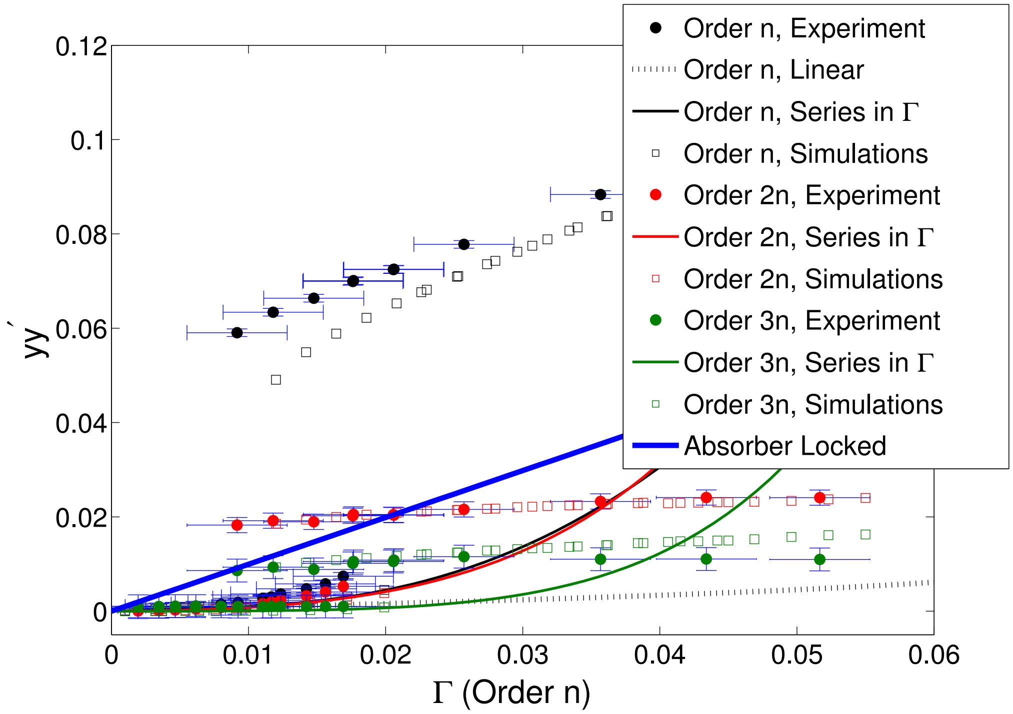

(a)

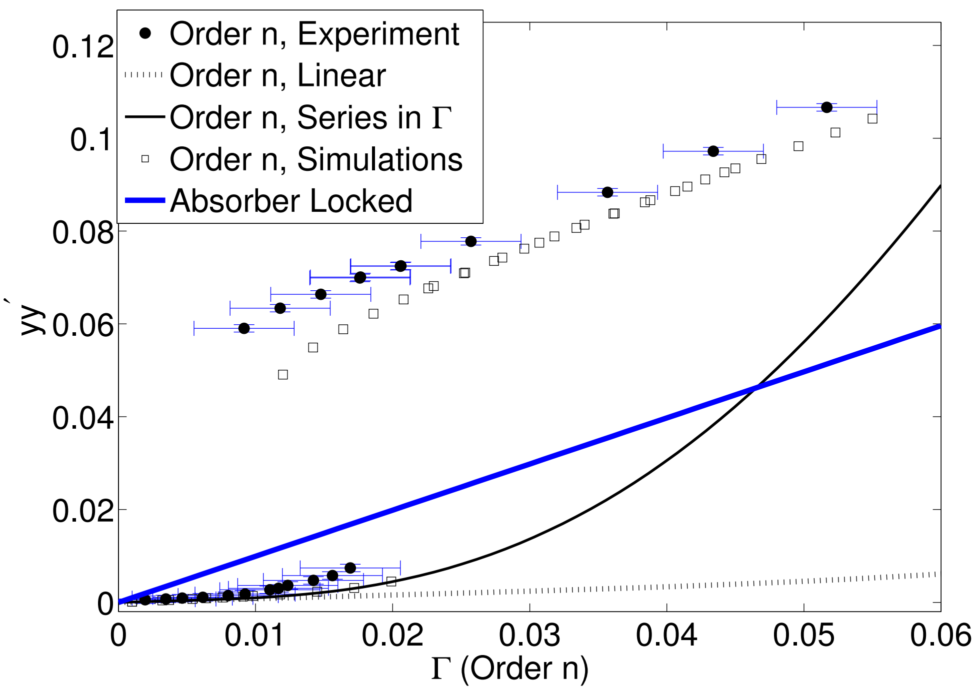

(b)

Figure 4.29: Harmonics of the rotor angular acceleration, yy' vs. Γ_n, for a circular path absorber driven exactly at tuning; experimental results compared against the power series harmonic balance approximation. (a) All three rotor response orders n, $2n$, $3n$. (b) Order n.

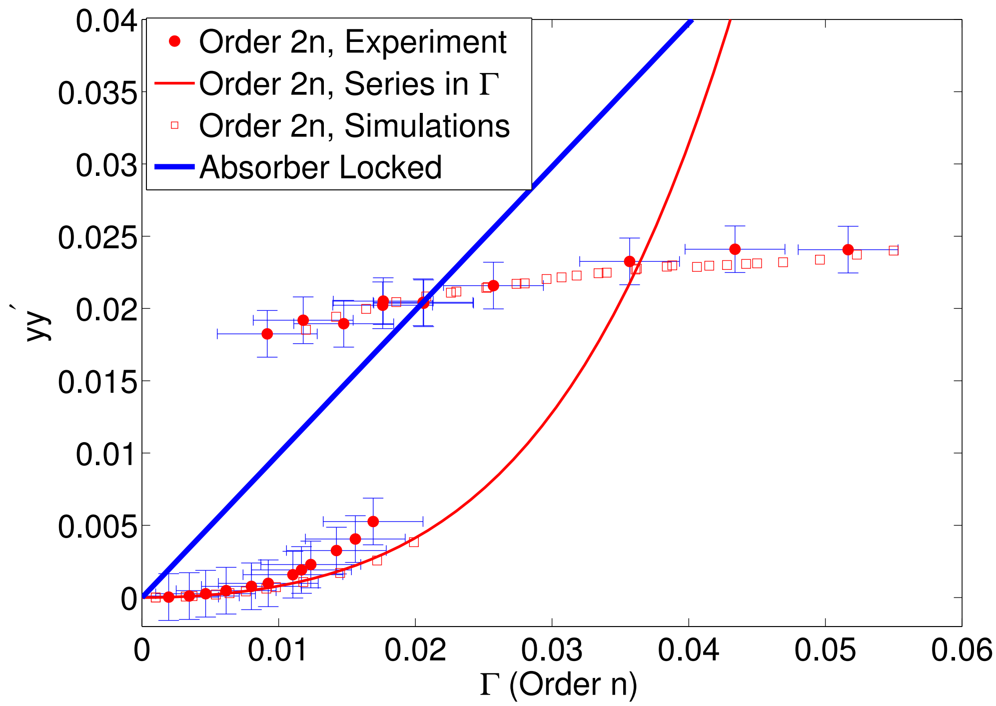

(c)

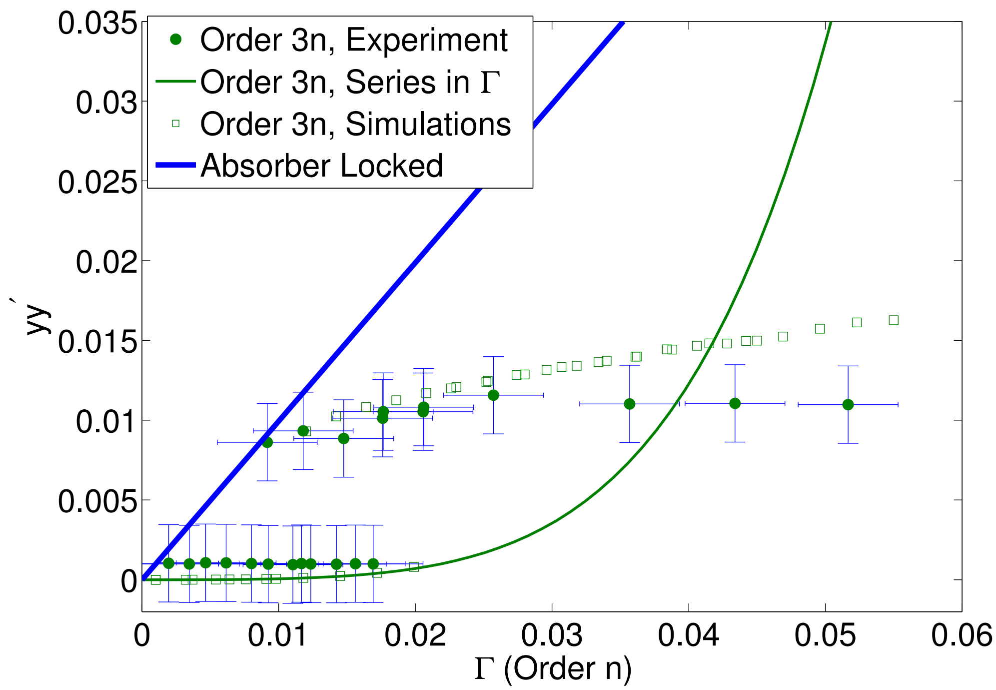

(d)

Figure 4.30: (c) Order $2n$. (d) Order $3n$. Coorsponding with Fig. 4.29

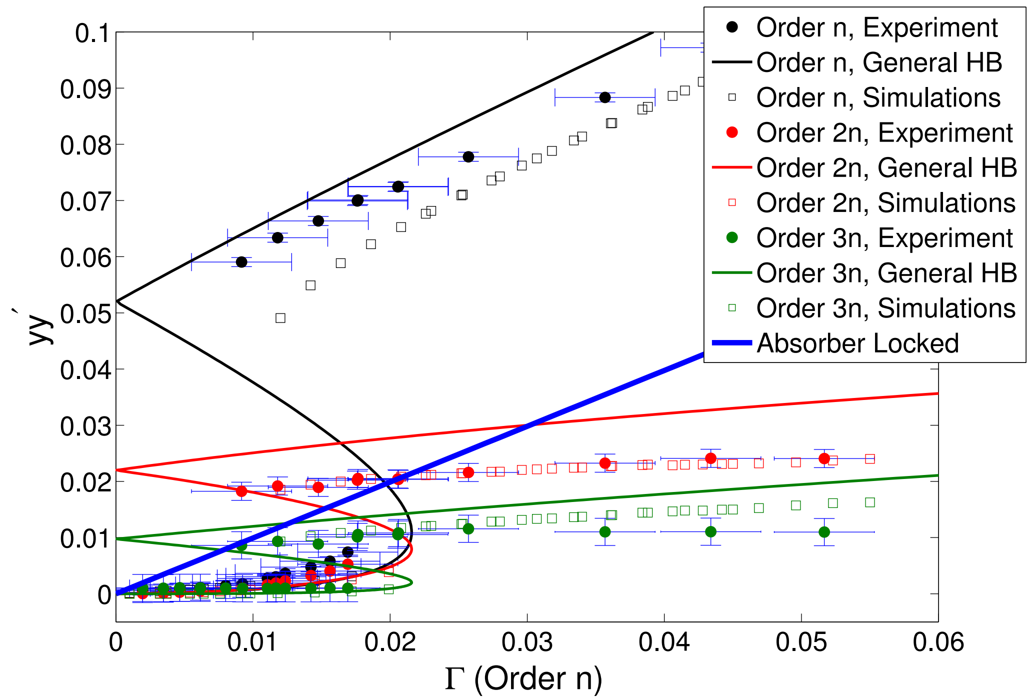

(a)

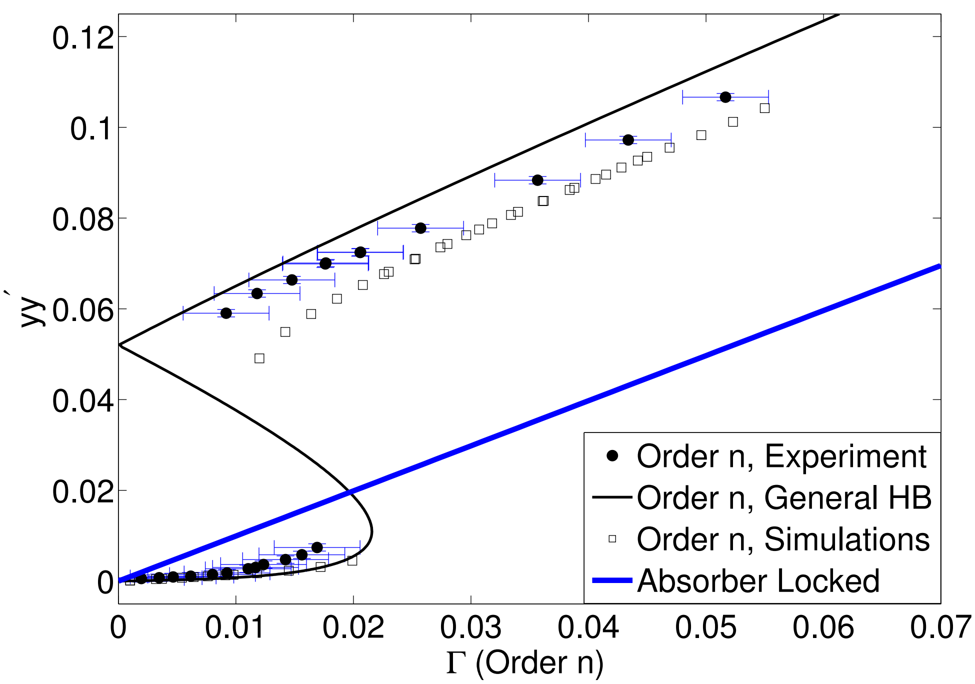

(b)

Figure 4.31: Harmonics of the rotor angular acceleration, yy' vs. Γ_n, for a circular path absorber driven exactly at tuning; experimental results compared against the general harmonic balance approximation. (a) All three rotor response orders n, $2n$, $3n$. (b) Order n.

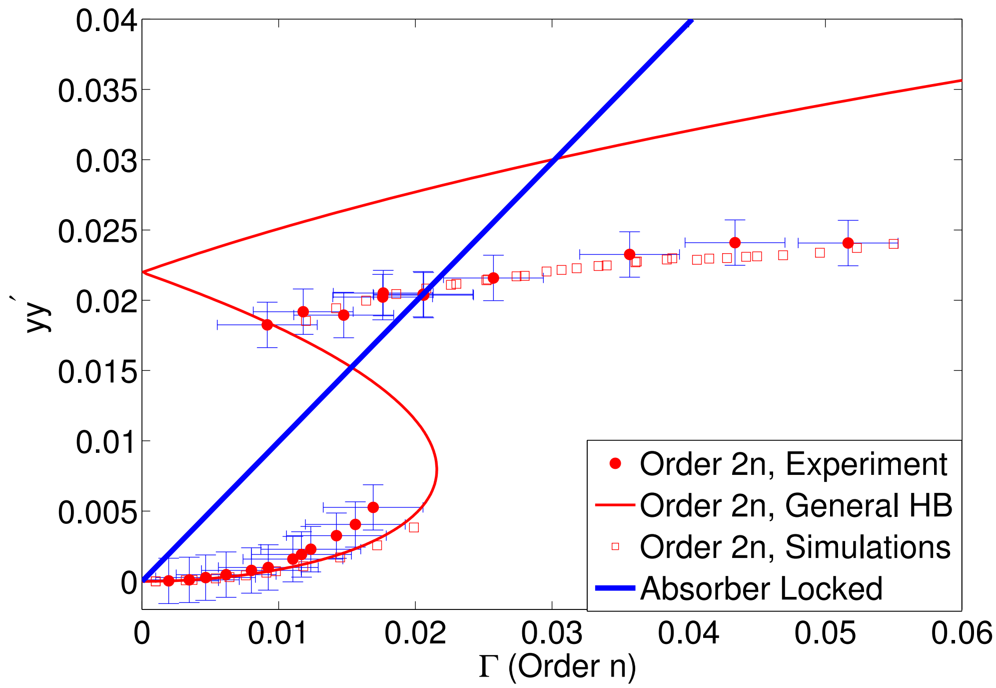

(c)

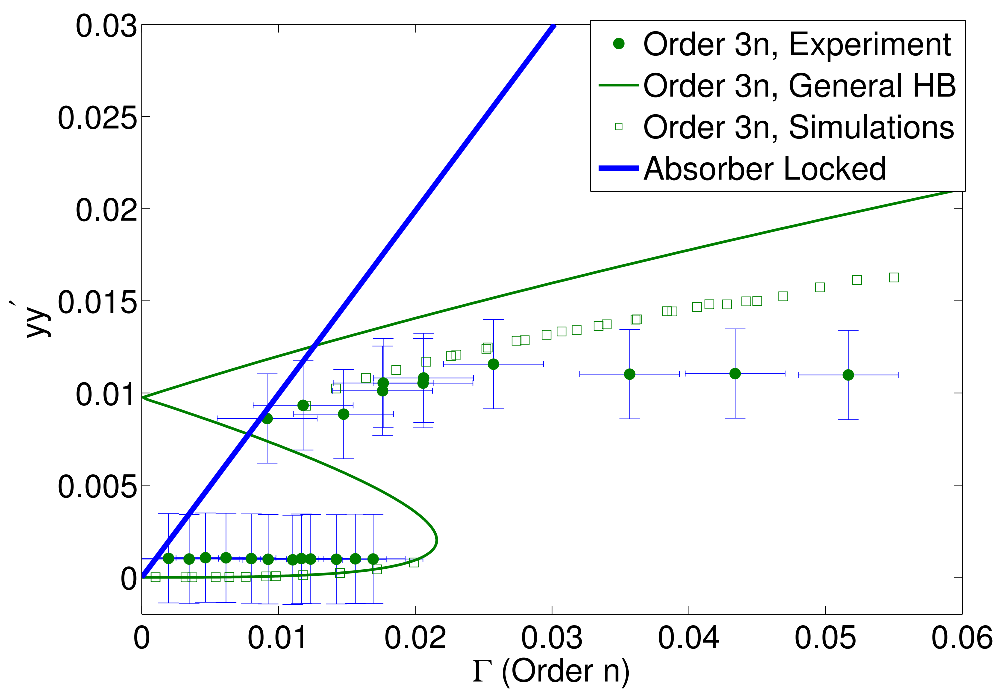

(d)

Figure 4.32: (c) Order $2n$. (d) Order $3n$. Coorsponding with Fig. 4.31

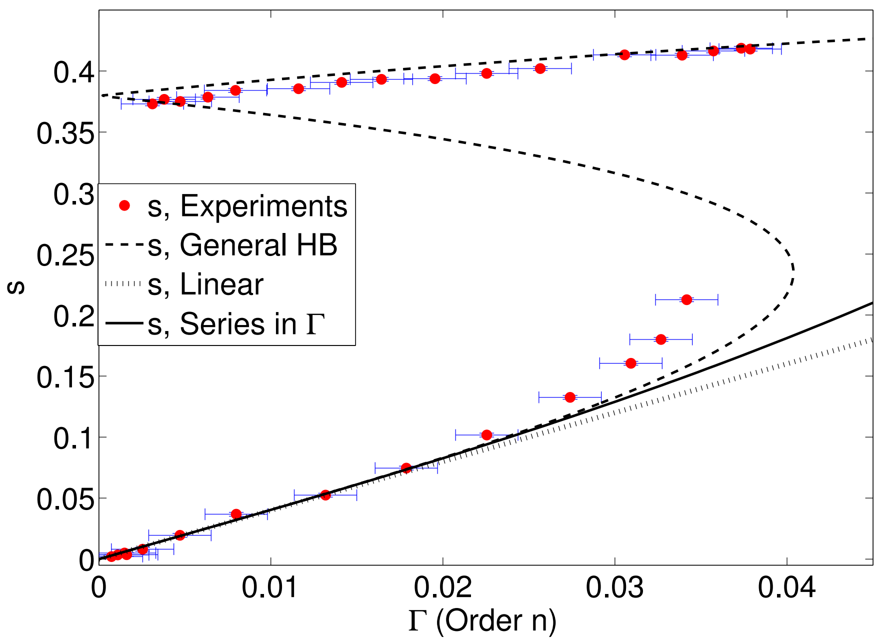

Figure 4.33: Amplitude of the absorber arc length, s vs. Γ_n for a 5% overturned circular path absorber with $\epsilon = 0.0519$; experimental results compared with both harmonic balance approximations and simulations.

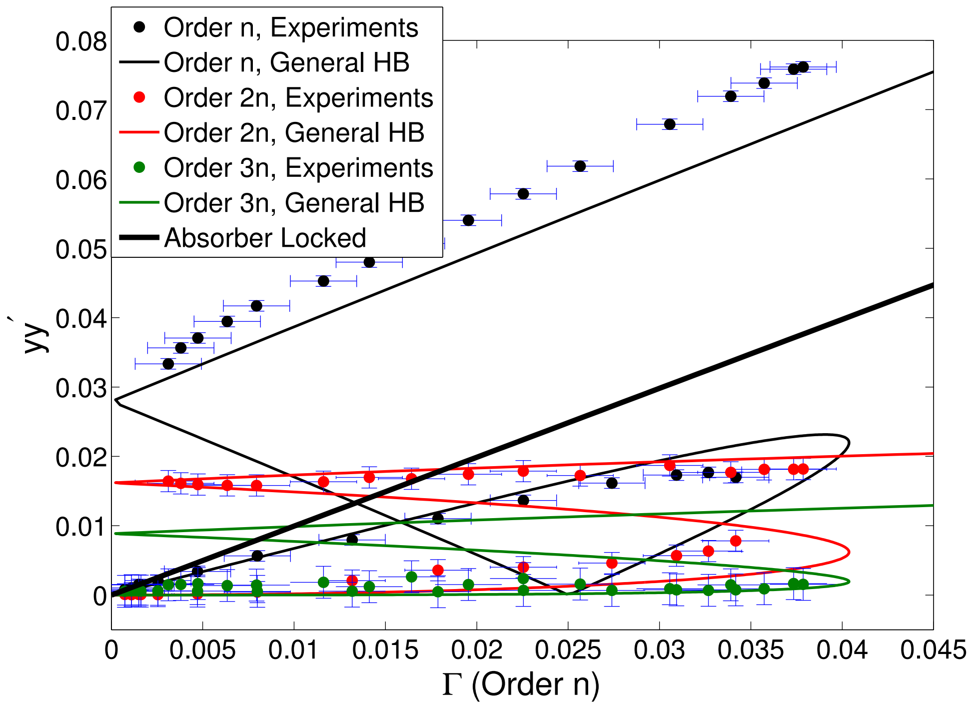

(a)

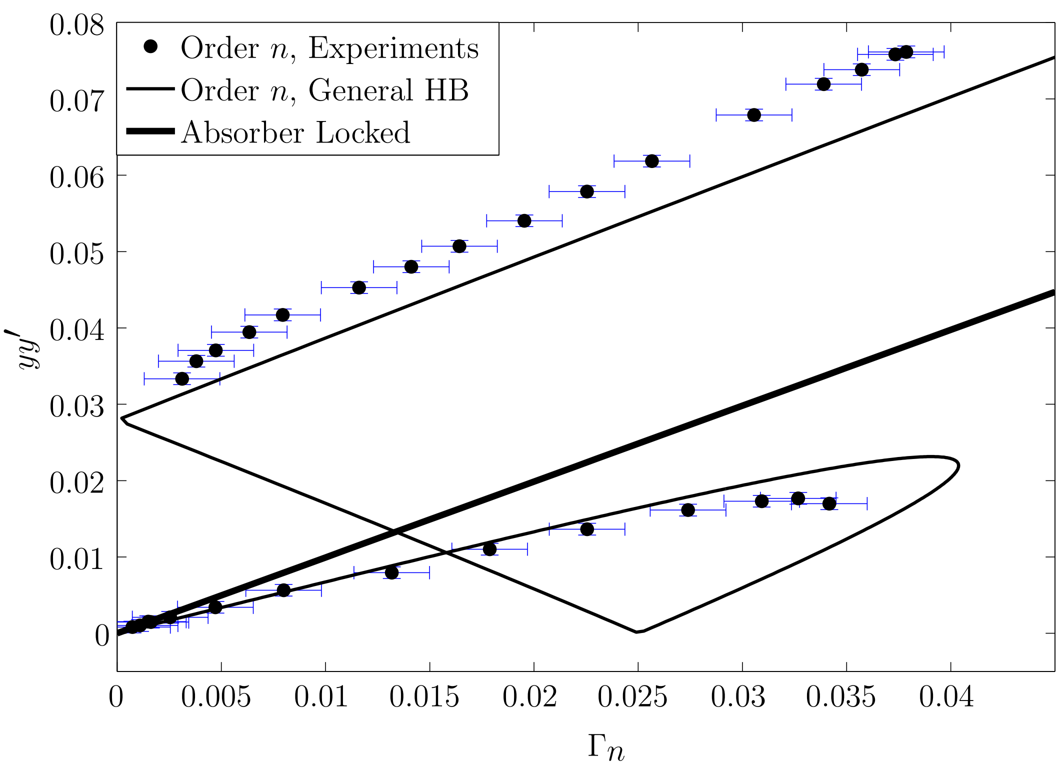

(b)

Figure 4.34: Harmonics of the rotor angular acceleration, yy' vs. Γ_n, for a 5% overturned circular path absorber, with$\epsilon = 0.0519$; experimental results compared against the general harmonic balance approximation. (a) All three rotor response orders n, $2n$, $3n$. (b) Order n.

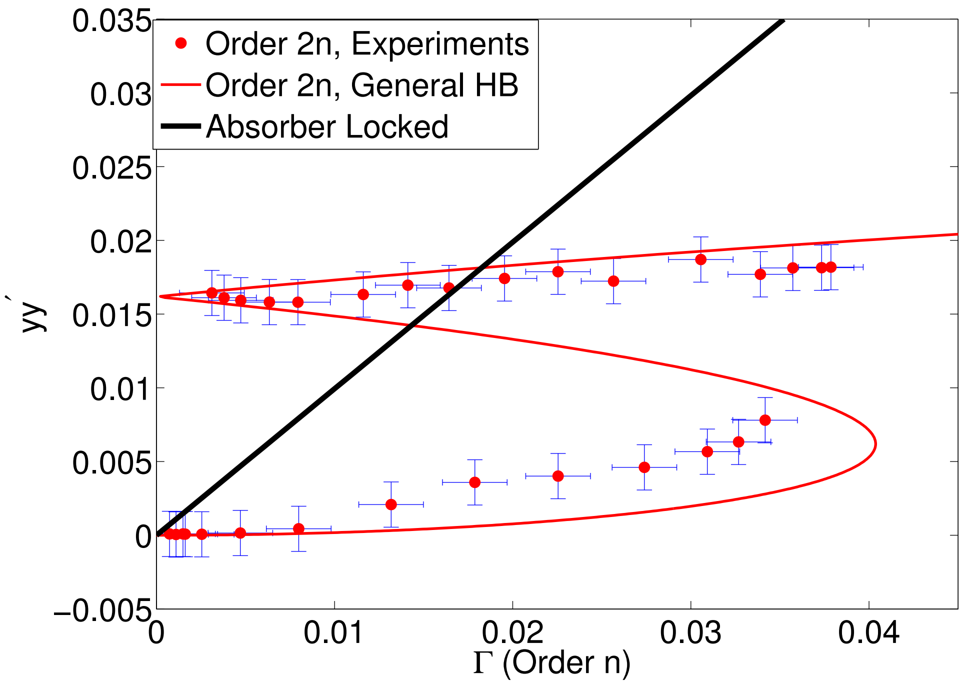

(c)

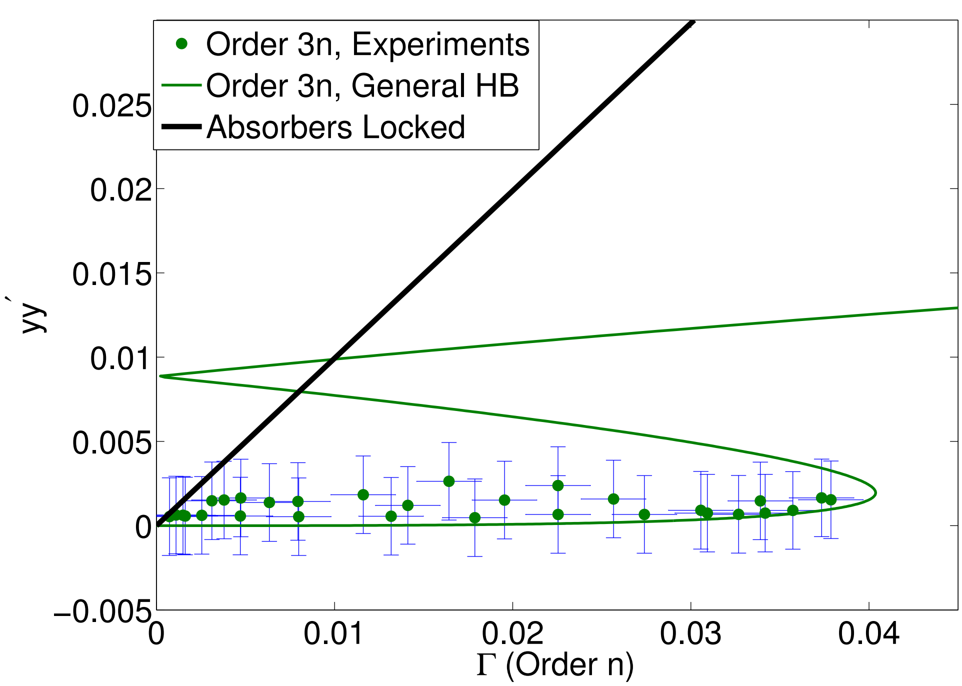

(d)

Figure 4.35: (c) Order $2n$. (d) Order $3n$. Coorsponding with Fig. 4.34

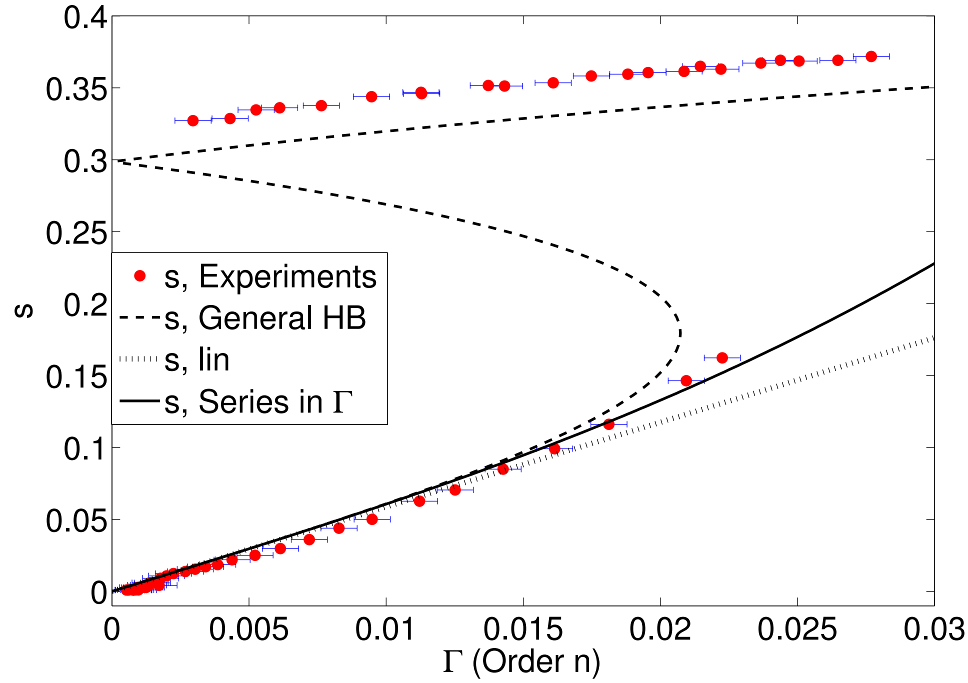

Figure 4.36: Amplitude of the absorber arc length, s vs. Γ_n for a 5% overturned circular path absorber with $\epsilon = 0.0189$; experimental results compared with both harmonic balance approximations and simulations.

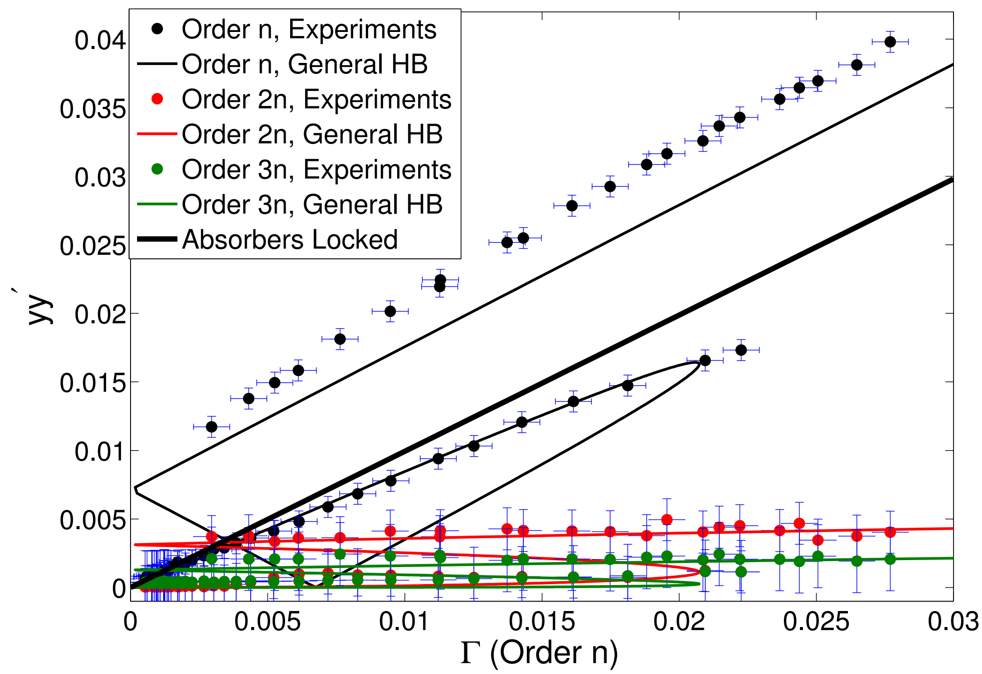

(a)

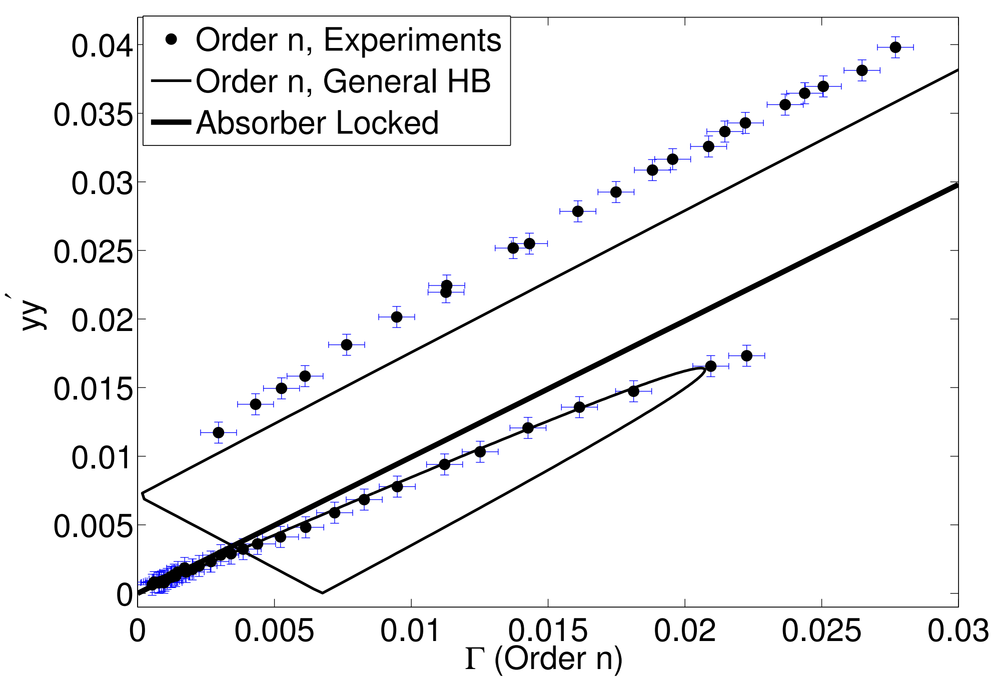

(b)

Figure 4.37: Harmonics of the rotor angular acceleration, yy' vs. Γ_n, for a 5% overturned circular path absorber, with$\epsilon = 0.0189$; experimental results compared against the general harmonic balance approximation. (a) All three rotor response orders n, $2n$, $3n$. (b) Order n.

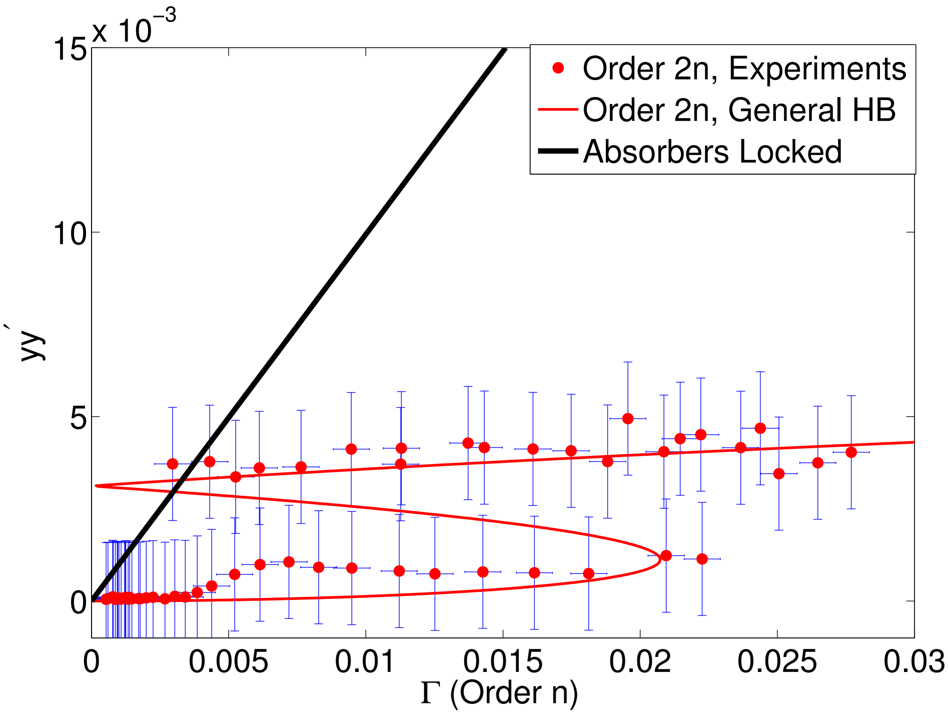

(c)

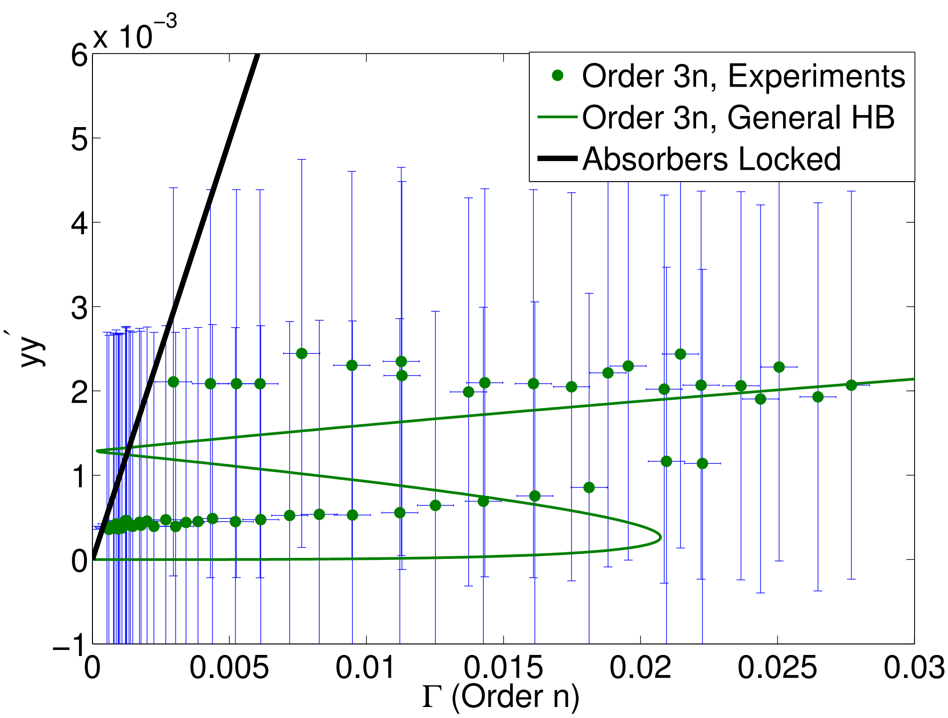

(d)

Figure 4.38: (c) Order $2n$. (d) Order $3n$. Coorsponding with Fig. 4.37

Chapter 5

Conclusions and Recommendations for Future Work

5.1 Summary of Results

In this dissertation, the dynamics of rotational inertias equipped with pendulum-type absorbers tuned to multiple orders were investigated using analysis, simulations, and experiments. To the author's knowledge, this is the first study which maps out the response characteristics of a multiple order absorber system subjected to multiple order torques. It includes important information about the response amplitudes, phases, and stability, of the absorber response, as well as the rich harmonic content of the rotor response. These results are very useful for design strategies that yield optimal performance for rotors fitted with pendulum absorbers.

The analytical findings are based on a dynamic model derived in Chapter 2. Here the differential equations which govern the motion of a system composed of arbitrary numbers of order $\tilde{n}_1$ and order $\tilde{n}_2$ absorbers attached to a rigid rotary inertia that is subjected to multi-order torque harmonics were derived using energy methods. A formulation for the path of the absorbers, which dictate is linear tuning and nonlinear behavior, was employed that allows for small deviations from perfect linear tuning at small amplitudes, as well as from the desirable tautochronic path at large amplitudes. Non-dimensionalization and scaling were employed to simplify the system parameters. Key small parameters were identified, specifically the non-dimensional mean and fluctuating torques, and the absorber and rotor non-dimensional viscous damping, which facilitate analysis, primarily by allowing one to decouple the absorber dynamics to leading order in these parameters. Once the absorber dynamics are determined from these equations, one can substitute these into the rotor equation to obtain its response. Approximate solutions of the absorber equations were solved using perturbation methods (in Chapter 2) and harmonic balance techniques (in Chapter 4).

In Chapter 2 perturbation methods were used to predict and evaluate system response, using an expanded versions of the absorber equations of motion. These perturbation methods yielded equations for the slowly varying absorber amplitudes and phases, which can be used to estimate the steady state response characteristics, including stability. It was shown that these slowly varying absorber amplitude and phase equations accurately captured the effects of the internal resonance resulting when $\tilde{n}_2 \approx 2\tilde{n}_1$, which arises due to the non-linear kinematic coupling between the absorbers and the rotor. Using numerical continuation methods on the perturbed equations, it was shown that a torque of sufficient amplitude applied at order n, with a set of multiple order $\tilde{n}_1$ absorbers tuned close to n, can cause these absorbers to bifurcate to a non-synchronous response. It was also shown that a order $2n$ torque can cause a set of multiple order $\tilde{n}_1$ absorbers, when $2n \approx \tilde{n}_1$, to undergo a period doubling bifurcation, arising from parametric excitation effects, resulting in an unstable response in which the absorbers become non-synchronous and their amplitudes grow until they approach their limiting values. Interestingly, it was shown, by considering a general torque space with both order n and $2n$ excitation harmonics, that these are actually the same bifurcation, since both bifurcations result in non-synchronous behavior of the order $\tilde{n}_1$ absorbers. These instabilities are detrimental to system performance, most importantly since the absorbers reach their limits at lower torques than they would if the response remained synchronous. Another interesting finding of the perturbation investigation is that the addition of absorbers at order $\tilde{n}_2$ generally increases the level of torque which causes the non-synchronous bifurcations. This occurs through the attenuation of the higher order (most notably, order $2n$) harmonics imparted onto the rotor by the nonlinear dynamics of the order $\tilde{n}_1$ absorbers, which move at order n in steady state. This stabilization allows the order $\tilde{n}_1$ absorbers to be tuned closer to resonance, thus increasing their ability to attenuate vibration at order n. The perturbation equations also were shown to allow for a closed form solution of the optimal ratio of inertias between the two different order absorbers, corresponding to the situation in which both sets of absorbers reach their respective amplitude limits at the same level of torque, which maximizes the system's allowable torque range.

In Chapter 3 an experimental spin rig is described, along with results that verify the analytical predictions of Chapter 2. The rig consists of a computer controlled motor driving a rotor to which up to four absorbers can be fitted. For examining the multi-order response and stability results of Chapter 2, two absorbers at order $\tilde{n}_1 = 2.3$ and two at order $\tilde{n}_2 = 4.6$, both with nearly-tautochronic paths, were fitted to the rotor. These absorbers use a bifilar suspension with self-centering rollers, which minimize rubbing friction between the absorbers and their supporting flanges. The motor was programmed to provide a torque composed of two orders, that is, a two term Fourier series, of general form. Steady-state experiments were conducted for one absorber at each order free, in order to compare against the synchronous response theoretical developments. Experimental runs were then made with all four absorbers unlocked, which investigated the non-synchronous instabilities uncovered analytically. The experimental data was shown to agree well with the analytical and numerical predictions, and to the author's knowledge, this is the first time that period doubling sub-harmonic absorber bifurcations were captured experimentally. The response amplitudes and experimental instabilities were found to match the numerical continuation results, proving the utility of these analytical tools in absorber design.

Chapter 4 describes an alternative to numerical simulations and the perturbation analysis for describing the system response, specifically, a harmonic balance (HB) approach. The advantage of this approach over perturbation methods is that it yields simple expressions for response amplitudes and phases, although it cannot provide stability information. Two HB approaches were employed. The general method employed provides accurate predictions of single order absorber and rotor dynamics for a wide range of absorber paths, but requires assumptions which cause the method to decrease in accuracy when analyzing multiple order absorber systems. The other method, which employs expansions in the torque amplitude, yields relatively simple, closed form expressions for the absorber and rotor dynamics as a function of the applied torques, but fails to accurately capture some of the large-amplitude non-linear absorber dynamics. Numerical simulations and experimental tests using the spin rig were employed to verify the accuracy of these closed-form solutions. The data was shown to agree with the predictions provided by these solutions in most cases. Two types of absorbers were consider to experimentally verify the HB results: the epicycloidal path absorbers of one and two orders described above, and simply pivoted circular path absorbers of order $\tilde{n}_1 = 1.315$. The power series HB method provides more accurate comparisons to multiple order, nearly-tautochronic absorber data while the general method is more beneficial when implementing a non-tautochronic path absorber. These closed-form expressions allow designers to quickly and easily investigate the effects of system parameters on absorber performance, which allows for a preliminary design tool for sizing absorbers. Of course, prospective designs should be tested for dynamic stability using either simulations or the perturbation methods of Chapter 2.

5.2 Importance of Results

The results here advance our fundamental understanding of the system's nonlinear dynamics, and these provide guidance for improving their performance. The predictive nature of the results will help shorten the design cycle for absorber systems, and the experimental validation insures the fidelity of the analytical results.

5.3 Future Work

As described in this study, the addition of multiple order absorbers have multiple benefits. They reduce the higher order harmonics generated by single order absorbers, they allow for vibration attenuation of systems subjected to multiple order torques, and, in some cases, they can stabilize the response of multi-order absorber systems. This study investigated absorber tuned to *two* different orders, it would be interesting to examine nonlinear interactions and the potential benefit of adding absorbers tuned to three or more orders (e.g., $\tilde{n}$, $2\tilde{n}$, $3\tilde{n}$). Absorbers of order n generate three harmonics of noticeable magnitude on the rotor, with the first order (n) used to counteract the applied torque, while the others actually add to the overall fluctuations of the rotor response. Second order absorbers have a particular role on the system response, since they affect second harmonics and thus can modulate the effects of parametric excitation. While third order absorbers will not have such a specific role, they may still be beneficial due to the fact that third harmonics are prominent on the rotor. An interesting design problem would be to extend the present analysis to consider the nonlinear interactions in sets of absorbers tuned to three orders, namely, how does one most effectively allocate the available inertia to each order absorber in order to achieve an optimal design, for example, to minimize the root mean square of the rotor response. The two order absorber problem studied in this dissertation borders the line in which perturbation analysis becomes too complicated for the benefit gained, and adding three order absorbers may send the complication over this line. A combined harmonic balance and simulation study of three-order absorber systems would be the approach recommended that the author.

It would also be beneficial to conduct a study where sets of multiple order absorbers are detuned, and map out the benefits and drawbacks such systems. In general, detuned absorbers are more stable but less effective in reducing torsional vibrations. A potentially beneficial setup would incorporate detuned order $\tilde{n}_2$ absorbers, which are implemented purely for stabilization of the order $\tilde{n}_1$ absorbers, but detuned so as to increase the torque range the $\tilde{n}_2$'s can safely operate in.

At the end of Chapter 2, a brief study is carried out on alternatives to the tautochronic path, specifically cycloids. The analysis shows that the accuracy of the perturbation equations is not accurate for low order absorbers, in terms of their ability to capture the large amplitude dynamics. This is due to the hardening nature of the cycloidal path, which causes the absorber nonlinearity to no longer be weak. The accuracy of the perturbation methods increases at the tuning order of the absorber increases, since a cycloid approaches the tautochronic epicycloid as $\tilde{n}$ becomes larger. For an accurate analysis of multiple order cycloidal path absorbers, one must perform a strongly non-linear oscillator analysis, which would be a rather complicated study involving averaging using the system described in terms of action-angle coordinates. Again, it would be recommended to perform a numerical study when investigating these strongly non-linear absorbers.

Currently, several automotive manufacturers are conducting research into the implementation of pendulum absorbers, and the ideas in this study may be put into practice in the near future.

Appendices

A.1 Experimental Error Analysis

In this appendix we will attempt to quantify the experimental measurement error in the CPVA testing device. The main measurements of interest include:

1. Absorber COM position, S
2. The speed of the rotor $\dot{\theta}$
3. The applied torque which includes the mean T_0 and fluctuating T_θ (at order of interest),

where the position of the absorber(s) and the rotor speed are each measured with an encoder. The applied torque on the rotor is measured from a feedback current that the motor outputs. Each of these measurements will be discussed in more detail in the following sections. This document follows the NIST experimental uncertainty guidelines [43].

Uncertainty in Absorber position: A U.S. Digital optical encoder is used to measure absorber position. These encoders contain 4 channels which are A, -A, B, and -B. The two negative channels are literally the negative of A and B, respectively. To eliminate the noise in the encoder signal the positive channel is subtracted from the negative channel and then divided by 2. The encoder has two sets of 360 equally spaced lines. The lines in each set are spaced 90° apart, the so-called quadrature spacing, in order to obtain the direction of rotation. The 360 lines yield 720 measurements for a complete encoder rotation, meaning that with two sets of lines we get $\frac{1}{4}$ degree resolution from this encoder. Therefore, assuming the pulses are equally spaced on the encoder and we don't miss any counts, the uncertainty in the absorber position is

$$u_S = \pm \frac{1^\circ}{4}. \tag{1}$$

Speed of rotor: The encoder on the rotor has 1000 pulses per revolution, which output a frequency corresponding to speed of rotation. This frequency signal is then sent to a frequency to voltage (F2V) converter in order to supply to the analog to digital converter with a usable signal. The F2V converter measures the instantaneous frequency between two pulses in pulses/sec. This frequency is divided by 1000 to obtain the frequency of the rotor in Hz. This device is rated to be able to measure up to 25 kHz between pulses which means approximately 25 Hz for 1000 pulses. An important check here was to make sure the F2V converter could detect the frequency of the rotor during a torsional disturbance. This means the rotor is now rotating at a mean speed with a oscillating part superimposed. In terms of pulses going into the F2V this means that these pulses are no longer evenly spaced along the time axis. Now their time spacing is modulated (i.e. they get closer and further apart, etc.) due to the fluctuation about the mean rotor speed. The bandwidth of the F2V converter turned out to be sufficiently large to resolve the frequency of the rotor pulses. Using the specification sheet from the device manufacturer, the accuracy calibration of the device is given as a maximum ±0.1% of the frequency span to be measured. Since the frequency at the tuning order for the absorbers used in this study is about 10 Hz for mean speeds at 400 rpm, an estimate for the uncertainty in the F2V conversion using a 10 Hz span which corresponds to an output voltage of 3 V (of the 5 V range) is

$$u_{\dot{\theta},F2V} = \pm(3\text{V})(.001) = \pm 3\text{mV}. \tag{2}$$

After the signal leaves the F2V converter it is digitized by the National Instruments DAQ board (PCI-6281). According to the specification sheet, the device has an absolute accuracy of 1.05 mV with the built-in low pass filter turned off. The quantization step size for the 18 bits at $\pm$(10V) range is

$$Q_{NI} = \frac{2 * (10\text{V})}{2^{18} - 1} = 7.6294 * 10^{-5}\text{V}. \tag{3}$$

To obtain the quantization error from this we divide Q in half because at worst our actual signal amplitude could have been exactly in the middle of the quantization step (i.e. $Q/2$), in which case it would be rounded up and anything below is rounded down. Note that this also assumes the maximum amplitude of our signal is approximately 10 volts which is the maximum analog input voltage to the DAQ board. Although, this isn't always the case, we will approximate the quantization error as

$$Q_{NI,error} = Q_{NI}/2 = \pm 0.0381\text{mV}. \tag{4}$$

Since the quantization error is about 3% of the absolute accuracy given in the NI DAQ specification sheet, we will assume that the quantization error was accounted for in this specification. Therefore the uncertainty in digitizing the speed signal u_{DAQ} is

$$u_{\dot{\theta},DAQ} = \pm 1.05\text{mV}. \tag{5}$$

Finally, the last bit of uncertainty is the overall noise floor of the signal's Digital Fourier Transform (DFT). This can be determined simply by taking an DFT of the speed signal in LabView and then plotting the magnitude of the Fourier coefficients. One then estimates the largest amplitude at which white noise is present (i.e. constant amplitude level at all frequencies). This is determined to be

$$u_{\dot{\theta},FFT} = \pm 0.02\text{mV}. \tag{6}$$

The total uncertainty in the rotor speed is

$$u_{\dot{\theta},T} = u_{\dot{\theta},F2V} + u_{\dot{\theta},DAQ} + u_{\dot{\theta},FFT} = \pm 3.07\text{mV}. \tag{7}$$

Torque Uncertainty: The torque measurement comes from a current feedback signal that is multiplied by two calibration constants, one which converts the motor current to a measurable voltage, and another, given by the motor manufacturer, which gives the motor torque in Newton-meters from the inputted current. This signal is digitized by the motor control box and the National Instruments DAQ board. The quantization for the motor control box which is 8 bits at a ±(10V) range is

$$Q_{\text{box}} = \frac{2 * (10\text{V})}{2^8 - 1} = 78.43\text{mV}. \tag{8}$$

Just like before we can approximate the quantization error as

$$Q_{\text{box,error}} = Q_{\text{box}}/2 = \pm 39.22\text{mV}. \tag{9}$$

Digitizing the torque signal with the National Instruments DAQ board will have the same uncertainty as calculated in equation (5). Similar to the rotor speed signal, the white noise level for the torque signal is estimated in the same way. This uncertainty is found to be

$$u_{T_\theta,\mathrm{DFT}} = \pm 2\mathrm{mV}. \tag{10}$$

The total uncertainty in the torque signal is then

$$u_{T_\theta,T} = u_{\dot{\theta},\mathrm{DAQ}} + Q_{\mathrm{box,error}} + u_{T_\theta,\mathrm{DFT}} = \pm 42.27\mathrm{mV}. \tag{11}$$

Combined Uncertainties for the Rotor Angular Acceleration and Rotor Inertia. Using the uncertainties above, this section computes the combined uncertainty for the rotor acceleration and the rotor inertia.

Rotor Angular Acceleration: The rotor angular acceleration at order n is computed as follows

$$\ddot{\theta}_n = n\Omega\dot{\theta}_n, \tag{12}$$

where n is order of excitation, Ω is the mean speed that the fluctuation is about, and $\dot{\theta}_n$ is the magnitude of the DFT of the rotor speed signal at order n. Assuming the fluctuations in Ω and $\dot{\theta}_n$ are uncorrelated, the combined uncertainty for $\ddot{\theta}_n$ is computed following the NIST standards as follows:

$$u_{\ddot{\theta}_n}^2 = \left(\frac{\partial\ddot{\theta}_n}{\partial n}\right)^2 u_n^2 + \left(\frac{\partial\ddot{\theta}_n}{\partial\Omega}\right)^2 u_\Omega^2 + \left(\frac{\partial\ddot{\theta}_n}{\partial\dot{\theta}_n}\right)^2 u_{\dot{\theta}_n}^2, \tag{13}$$

which is essentially a first order Taylor series approximation of a function whose inputs are measured quantities and whose output is the desired quantity one wishes to resolve from the combined measurements. The function is squared in order to yield positive values for the combined uncertainty. We assume here that there is no error in the order of the torque signal $u_n = 0$ which is generated in LabView [1]. To estimate error in the ability of the PID to maintain a constant speed (u_Ω), an experiment is run with the rotor spinning at a constant rate with PID active. The mean and standard deviation of the resulting rotor speed signal is computed using basic statistics and the standard deviation yields u_Ω which is

$$u_\Omega = \pm 2.39\text{mV}. \tag{14}$$

The uncertainty in the rotor speed at order n ($u_{\ddot{\theta}_n}$) had already been calculated in equation (7). Taking the derivatives in equation (13) and using equations (14) and (7), the uncertainty in the angular acceleration at order n is

$$u^2_{\ddot{\theta}_n} = (n\dot{\theta}_n)^2 u^2_\Omega + (n\Omega)^2 u^2_{\dot{\theta},T}, \tag{15}$$

which will provide error bars on a $\ddot{\theta}_n$ measurement of $\pm u_{\ddot{\theta}_n}$.

Rotor Inertia: To compute the rotor inertia we use Newton's law to obtain

$$J = \frac{T_{\theta_n}}{\ddot{\theta}_n}, \tag{16}$$

where T_{θ_n} is the magnitude of the applied fluctuating torque at order n and $\ddot{\theta}_n$ is the angular acceleration of the rotor at order n calculated according to equation (12). Assuming the fluctuations in T_{θ_n} and $\ddot{\theta}_n$ are uncorrelated, the uncertainty in the rotor inertia is

$$u^2_J = \left(\frac{1}{\ddot{\theta}_n}\right)^2 u^2_{T_{\theta_n}} + \left(\frac{T_{\theta_n}}{\ddot{\theta}^2_n}\right)^2 u^2_{\ddot{\theta}_n}, \tag{17}$$

[1] Or the error in the generated order can be included in the deviation of the mean speed, Ω

where $u_{T_{\theta_n}}$ and $u_{\ddot{\theta}_n}$ are the uncertainties calculated in equations (11) and (15), respectively. The error bars on the rotor inertia calculation will then be $\pm u_J$.

B.2 Harmonic Balance Higher Order Approximations

The form of the expressions for the higher order expansions in $\tilde{\Gamma}_{n,2n}$ developed in Section 4.2 in their most general form are found to be as follows:

$$\begin{aligned}
E_2 = {} & (4n\tilde{n}_1^2\epsilon((C_1^2 - D_1^2)(-8\mu_{a,2}n(1+\alpha) + G_1\tilde{\Gamma}_{2n}^2\tilde{n}_2^2 \\
& \times (1+\alpha+\tilde{n}_2^2(1+\alpha+16H_1n^2\alpha)))\epsilon + 2C_1D_1 \\
& \times (\tilde{n}_2^2(1+\alpha)(-4+3\tilde{\Gamma}_{2n}^2H_1(1+\tilde{n}_2^2)\epsilon) + 8n^2 \\
& \times (2+\alpha(2+(-2+G_1^2\tilde{\Gamma}_{2n}^2\tilde{n}_2^4 + 3\tilde{\Gamma}_{2n}^2H_1^2\tilde{n}_2^4)\epsilon)))))(\frac{1}{Q}),
\end{aligned}$$

$$\begin{aligned}
& F_2 = \\
& (\frac{2C_1D_1}{-8\tilde{\mu}_{a,2}n(1+\alpha) + G_1\tilde{\Gamma}_{2n}^2\tilde{n}_2^2(1+\alpha+\tilde{n}_2^2(1+\alpha+16H_1n^2\alpha))} \\
& + ((\tilde{n}_2^2(1+\alpha)(-4+\tilde{\Gamma}_{2n}^2H_1(1+\tilde{n}_2^2)\epsilon) + 8n^2(2+\alpha(2+(-2 \\
& + 3G_1^2\tilde{\Gamma}_{2n}^2\tilde{n}_2^4 + \tilde{\Gamma}_{2n}^2H_1^2\tilde{n}_2^4)\epsilon)))((C_1^2 - D_1^2)(-8\tilde{\mu}_{a,2}n(1+\alpha) \\
& + G_1\tilde{\Gamma}_{2n}^2\tilde{n}_2^2(1+\alpha+\tilde{n}_2^2(1+\alpha+16H_1n^2\alpha)))\epsilon + 2C_1D_1(\tilde{n}_2^2 \\
& \times (1+\alpha)(-4+3\tilde{\Gamma}_{2n}^2H_1(1+\tilde{n}_2^2)\epsilon) + 8n^2(2+\alpha(2 \\
& + (-2+G_1^2\tilde{\Gamma}_{2n}^2\tilde{n}_2^4 + 3\tilde{\Gamma}_{2n}^2H_1^2\tilde{n}_2^4)\epsilon)))))\frac{4n\tilde{n}_1^2}{Q},
\end{aligned}$$

where,

$$Q = ((8\tilde{\mu}_{a,2}n(1+\alpha) - G_1\tilde{\Gamma}_{2n}^2\tilde{n}_2^2(1+\alpha+\tilde{n}_2^2(1+\alpha$$
$$+ 16H_1n^2\alpha)))(8\tilde{\mu}_{a,2}n(1+\alpha) + G_1\tilde{\Gamma}_{2n}^2\tilde{n}_2^2(1+\alpha$$
$$+ \tilde{n}_2^2(1+\alpha+16H_1n^2\alpha)))\epsilon^2 + (\tilde{n}_2^2(1+\alpha)(-4+\tilde{\Gamma}_{2n}^2$$
$$\times H_1(1+\tilde{n}_2^2)\epsilon) + 8n^2(2+\alpha(2+(-2+3G_1^2$$
$$\times \tilde{\Gamma}_{2n}^2\tilde{n}_2^4 + \tilde{\Gamma}_{2n}^2H_1^2\tilde{n}_2^4)\epsilon)))(\tilde{n}_2^2(1+\alpha)(-4+3\tilde{\Gamma}_{2n}^2H_1(1+\tilde{n}_2^2)\epsilon)$$
$$+ 8n^2(2+\alpha(2+(-2+G_1^2\tilde{\Gamma}_{2n}^2\tilde{n}_2^4 + 3\tilde{\Gamma}_{2n}^2H_1^2\tilde{n}_2^4)\epsilon)))).$$

$$C_3 = -(2\tilde{\Gamma}_{2n}(G_1+\tilde{\Gamma}_{2n}^2G_3)n^2(16C_1E_2n^3\alpha - C_1^2(\tilde{n}_1^2(1+\alpha)$$
$$+ \tilde{n}_1^4(1+4D_1n^2+\alpha) + 12D_1(1+\alpha)\varphi_1) - D_1(-16F_2n^3\alpha$$
$$+ 3D_1\tilde{n}_1^2(1+\tilde{n}_1^2)(1+\alpha) + 4D_1^2(n^2\tilde{n}_1^4 + 3(1+\alpha)\varphi_1)))\epsilon$$
$$- (C_1n((C_1^2+D_1^2)\tilde{n}_1^2(1+\tilde{n}_1^2) + 4F_2(-2n+\tilde{\Gamma}_{2n}$$
$$\times (H_1+\tilde{\Gamma}_{2n}^2H_3)\tilde{n}_2^2(1+\tilde{n}_2^2))) + 4E_2(2D_1n^2 + C_1\tilde{\Gamma}_{2n}(G_1+\tilde{\Gamma}_{2n}^2G_3)$$
$$\times n\tilde{n}_2^2(1+\tilde{n}_2^2) + 2(1+\alpha)))(2\tilde{n}_1^2(1+\alpha) - 2n^2(1+\alpha-\epsilon)$$
$$+ 4\tilde{\Gamma}_{2n}(H_1+\tilde{\Gamma}_{2n}^2H_3)n^3\alpha\epsilon + \tilde{\Gamma}_{2n}n(1+\alpha)\epsilon))\frac{1}{P_3},$$

$$
\begin{aligned}
D_3 = {} & ((1+\alpha)\epsilon(C_1^2\tilde{n}_1^2 + 3D_1^2\tilde{n}_1^2 + C_1^2\tilde{n}_1^4 + 3D_1^2\tilde{n}_1^4 + \frac{4C_1^2 D_1 n^2\tilde{n}_1^4}{1+\alpha} \\
& + \frac{4D_1^3 n^2\tilde{n}_1^4}{1+\alpha} - \frac{16C_1 E_2 n^3\alpha}{1+\alpha} - \frac{16D_1 F_2 n^3\alpha}{1+\alpha} + 12C_1^2 D_1\varphi_1 \\
& + 12D_1^3\gamma 1 + (4(2\tilde{\Gamma}_{2n}(G_1 + \tilde{\Gamma}_{2n}^2 G_3)n^2\alpha - \tilde{\mu}_{a,1}(1+\alpha)) \\
& \times (2\tilde{\Gamma}_{2n}(G_1 + \tilde{\Gamma}_{2n}^2 G_3)n^2(16C_1 E_2 n^3\alpha - C_1^2(\tilde{n}_1^2(1+\alpha) \\
& + \tilde{n}_1^4(1 + 4D_1 n^2 + \alpha) + 12D_1(1+\alpha)\varphi_1) - D_1(-16F_2 n^3\alpha \\
& + 3D_1\tilde{n}_1^2(1+\tilde{n}_1^2)(1+\alpha) + 4D_1^2(n^2\tilde{n}_1^4 + 3(1+\alpha)\varphi_1)))\epsilon \\
& - (C_1 n((C_1^2 + D_1^2)\tilde{n}_1^2(1+\tilde{n}_1^2) + 4F_2(-2n + \tilde{\Gamma}_{2n}(H_1 + \tilde{\Gamma}_{2n}^2 H_3) \\
& \times \tilde{n}_2^2(1+\tilde{n}_2^2))) + 4E_2(2D_1 n^2 + C_1\tilde{\Gamma}_{2n}(G_1 + \tilde{\Gamma}_{2n}^2 G_3)n\tilde{n}_2^2(1+\tilde{n}_2^2) \\
& + 2(1+\alpha)))(2\tilde{n}_1^2(1+\alpha) - 2n^2(1+\alpha-\epsilon) + 4\tilde{\Gamma}_{2n}(H_1 + \tilde{\Gamma}_{2n}^2 H_3) \\
& \times n^3\alpha\epsilon + \tilde{\Gamma}_{2n} n(1+\alpha)\epsilon)))\frac{1}{P_3},
\end{aligned}
$$

where,

$$
\begin{aligned}
G_3 = {} & (\epsilon(G_1(H_1\tilde{n}_2^2(1+\tilde{n}_2^2)(1+\alpha) + 2G_1^2(4n^2\tilde{n}_2^4\alpha + 3(1+\alpha)\varphi_2) \\
& + H_1^2(8n^2\tilde{n}_2^4\alpha + 6(1+\alpha)\varphi_2))(\tilde{n}_2^2(1+\alpha) + 4n^2(-1+\alpha(-1+\epsilon))) \\
& - \tilde{\mu}_{a,2} n(1+\alpha)(G_1^2(\tilde{n}_2^2(1+\alpha) + \tilde{n}_2^4(1+\alpha+16H_1 n^2\alpha) \\
& + 12H_1(1+\alpha)\varphi_2) + H_1^2(3\tilde{n}_2^2(1+\alpha) + \tilde{n}_2^4(3+3\alpha+16H_1 n^2\alpha) \\
& + 12H_1(1+\alpha)\varphi_2))\epsilon))\frac{1}{4R_3}
\end{aligned}
$$

$$
\begin{aligned}
H_3 = {} & \frac{1}{8\tilde{\mu}_{a,2}n}(G_1 H_1 \tilde{n}_2^2 + G_1 H_1 \tilde{n}_2^4 + \frac{8G_1^3 n^2 \tilde{n}_2^4 \alpha}{1+\alpha} + \frac{8G_1 H_1^2 n^2 \tilde{n}_2^4 \alpha}{1+\alpha} \\
& + 6G_1^3 \varphi_2 + 6G_1 H_1^2 \varphi_2 - ((G_1(H_1 \tilde{n}_2^2(1+\tilde{n}_2^2)(1+\alpha) + 2G_1^2 \\
& \times (4n^2 \tilde{n}_2^4 \alpha + 3(1+\alpha)\varphi_2) + H_1^2(8n^2 \tilde{n}_2^4 \alpha + 6(1+\alpha)\varphi_2))(\tilde{n}_2^2(1+\alpha) \\
& + 4n^2(-1+\alpha(-1+\epsilon))) - \tilde{\mu}_{a,2} n(1+\alpha)(G_1^2(\tilde{n}_2^2(1+\alpha) + \tilde{n}_2^4 \\
& \times (1+\alpha+16H_1 n^2 \alpha) + 12H_1(1+\alpha)\varphi_2) + H_1^2(3\tilde{n}_2^2(1+\alpha) \\
& + \tilde{n}_2^4(3+3\alpha+16H_1 n^2 \alpha) + 12H_1(1+\alpha)\varphi_2))\epsilon)(\tilde{n}_2^2 + n^2(-4 + \frac{4\alpha\epsilon}{1+\alpha})))\frac{1}{R_3},
\end{aligned}
$$

where,

$$
R_3 = ((1+\alpha)^2(4\tilde{\mu}_{a,2}^2 n^2 \epsilon^2 + (\tilde{n}_2^2 + n^2(-4 + \frac{4\alpha\epsilon}{1+\alpha}))^2)))
$$

The first through third harmonics in the rotor response are defined as,

$$
\begin{aligned}
yy'_n = {} & \frac{1}{64(1+\alpha)^2}\tilde{\Gamma}_n^2(n^4(-8\mathrm{C}3\tilde{\Gamma}_n^2 + C_1^3 \tilde{\Gamma}_n^2 \tilde{n}_1^2(1+\tilde{n}_1^2) \\
& + C_1(-8 + D_1^2 \tilde{\Gamma}_n^2 \tilde{n}_1^2(1+\tilde{n}_1^2)))^2 + (D_1^3 \tilde{\Gamma}_n^2 n^2 \tilde{n}_1^2(1+\tilde{n}_1^2) \\
& + D_1 n^2(-8 + C_1^2 \tilde{\Gamma}_n^2 \tilde{n}_1^2(1+\tilde{n}_1^2)) - 8(1 + D_3 \tilde{\Gamma}_n^2 n^2 + \alpha))^2),
\end{aligned}
$$

$$
\begin{aligned}
yy'_{2n} = {} & \frac{1}{4(1+\alpha)^2}(n^2(-4C_1 D_1 \tilde{\Gamma}_n^2 \tilde{n}_1^2 + n(E_2 \tilde{\Gamma}_n^2(-8 \\
& + 3G_1^2 \tilde{\Gamma}_{2n}^2 \tilde{n}_2^2(1+\tilde{n}_2^2) + \tilde{\Gamma}_{2n}^2 H_1^2 \tilde{n}_2^2(1+\tilde{n}_2^2)) + \tilde{\Gamma}_{2n}(-8\tilde{\Gamma}_{2n}^2 G_3 \\
& + G_1^3 \tilde{\Gamma}_{2n}^2 \tilde{n}_2^2(1+\tilde{n}_2^2) + G_1(-8 + 2F_2 \tilde{\Gamma}_n^2 \tilde{\Gamma}_{2n} H_1 \tilde{n}_2^2(1+\tilde{n}_2^2) \\
& + \tilde{\Gamma}_{2n}^2 H_1^2 \tilde{n}_2^2(1+\tilde{n}_2^2))))\alpha)^2 + (-\tilde{\Gamma}_n^2 \tilde{\Gamma}_{2n}^2(2E_2 G_1 H_1 + F_2(G_1^2 + 3H_1^2)) \\
& \times n^2 \tilde{n}_2^2(1+\tilde{n}_2^2)\alpha + \tilde{\Gamma}_{2n}^3 n^2(8H_3 - H_1(G_1^2 + H_1^2)\tilde{n}_2^2(1+\tilde{n}_2^2))\alpha \\
& + 2\tilde{\Gamma}_n^2 n(-C_1^2 \tilde{n}_1^2 + D_1^2 \tilde{n}_1^2 + 4F_2 n\alpha) + 2\tilde{\Gamma}_{2n}(1+\alpha+4H_1 n^2 \alpha))^2),
\end{aligned}
$$

and

$$yy'_{3n} = \frac{9(C_1^2 + D_1^2)^3 \tilde{\Gamma}_n^6 n^4 \tilde{n}_1^4 (1 + \tilde{n}_1^2)^2}{64(1+\alpha)^2}.$$

BIBLIOGRAPHY

BIBLIOGRAPHY

[1] Engine-cylinder deactivation saves fuel. `http://www.jdpower.com/content/detail.htm?jdpaArticleId=925`, 2012.

[2] B. Aldasouqi and B. J. Vidmar. The design of self-centering rollers. Technical report, Michigan State University, 2012.

[3] A. Alsuwaiyan and S. W. Shaw. Performance and dynamic stability of general-path centrifugal pendulum vibration absorbers. *Journal of Sound and Vibration*, 252:791–815, 2002.

[4] A. Alsuwaiyan and S. W. Shaw. Steady-state responses of systems of nearly-identical torsional vibration absorbers. *Journal of Vibration and Acoustics*, 125:80–87, 2003.

[5] Abdallah Saleh Alsuwaiyan. *Performance, Stability, and Localization of Systems of Vibration Absorbers*. PhD thesis, Michigan State University, 1999.

[6] V. J. Borowski, S. W. Shaw, H.H. Denman, D. L. Cronin, J.P. Hanisko, L.T. Brooks, D.A. Mikulec, W.B. Crum, and M.P. Anderson. Reducing vibration of reciprocating engines with crankshaft pendulum absorbers. *1991 SAE Technical Paper 911876*, 1991.

[7] C. P. Chao. *The Performance of Multiple Pendulum Vibration Absorbers Applied to Rotating Systems*. PhD thesis, Michigan State University, 1997.

[8] C. P. Chao and S. W. Shaw. Stability of the unison response for a rotating system with multiple centrifugal pendulum vibration absorbers. *Journal of Applied Mechanics*, 204(5):769–794, 1997.

[9] C. P. Chao and S. W. Shaw. The dynamic response of multiple pairs of subharmonic torsional vibration absorbers. *Journal of Sound and Vibration*, 231:411–431, 2000.

[10] D. L. Cronin. Shake reduction in an automobile engine by means of crankshaft-mounted pendulums. *Mechanism and Machine Theory*, 27:517–533, 1992.

[11] J. P. Den Hartog. Vibration in industry. *Journal of Applied Physics*, 8:76–83, 1937.

[12] J. P. Den Hartog. Tuned pendulums as torsional vibration eliminators. *Stephen Timoshenko 60th Anniversary Volume*, pages 17–26, 1938.

[13] J. P. Den Hartog. *Mechanical Vibrations*. Dover Publications, Inc. New York, 1985.

[14] H. H. Denman. Tautochronic bifilar pendulum torsion absorbers for reciprocating engines. *Journal of Sound and Vibration*, 159:251–277, 1992.

[15] Eusebius Doedel. Auto [software]. `http://cmvl.cs.concordia.ca/auto/`, 1996.

[16] Bard Ermentrout. Xppaut [software]. `http://www.math.pitt.edu/~bard/xpp/xpp.html`, 2002.

[17] B. K. Geist. Small displacement high torque engines. personal communication, 2012.

[18] R. J. Gilmore and M. B. Steer. Nonlinear circuit analysis using the method of harmonic balance-A review of the art. Part I. Introductory concepts. *International Journal of RF and Microwave Computer-Aided Engineering*, 1(1):22–37, 1991.

[19] A. G. Haddow and S. W. Shaw. Centrifugal pendulum vibration absorbers: An experimental and theoretical investigation. *Nonlinear Dynamics*, 34:293–307, 2003.

[20] C. M. Harris and C. E. Crede. *Shock and Vibration Handbook*. McGraw-Hill Book Co., 1976.

[21] KerWilson. *Practical Solutions of Torsional Vibration Problems*. Chapman and Hall, Ltd., London, 1968.

[22] C.-T. Lee, S. W. Shaw, and V. T. Coppola. A subharmonic vibration absorber for rotating machinery. *ASME Journal of Vibration and Acoustics*, 119:590–595, 1997.

[23] C. T. Lee and S.W. Shaw. Nonlinear dynamic response of paired centrifugal pendulum vibration absorbers. *Journal of Sound and Vibration*, 203:731–743, 1997.

[24] C.T. Lee and S.W. Shaw. On the couteraction of periodic torques in rotating systems using centrifugally driven vibration absorbers. *Journal of Sound and Vibration*, 191:695–719, 1996.

[25] J. Madden. Constant frequency bifilar vibration absorber. Technical report, United States Patent No. 4218187, 1980.

[26] K. D. McCutchen. No short days. the struggle to develop the r-2800 "double wasp" crankshaft. *Journal of the American Aviation Historical Society*, Summer:124–146, 2001.

[27] R. Monroe and S.W. Shaw. Transient dynamics of centrifugal pendulum vibration absorbers. In *The 2011 ASME International Design Engineering Technical Conferences*, 2011.

[28] R. J. Monroe. *Transient dynamics of nonlinear oscillators with applications to centrifugal pendulum vibration absorbers*. PhD thesis, Michigan State University, 2011.

[29] R. J. Monroe, S. W. Shaw, A. G. Haddow, and B. K. Geist. Accounting for roller dynamics in the design of bifilar torsional vibration absorbers. *Journal of Vibration and Acoustics*, 133, 2011.

[30] A. Nayfeh. *Nonlinear Interactions: Analytical, Computational, and Experimental Methods.* John Wiley & Sons, 2000.

[31] A. H. Nayfeh and D. T. Mook. *Nonlinear Oscillations*. Wiley-Interscience, 1979.

[32] T. Nester, A. H. Haddow, S. W. Shaw, J Brevick, and V. J Borowski. Vibration reduction in variable displacement engines using pendulum absorbers.

[33] T.M. Nester, A.G. Haddow, S.W. Shaw, J.E. Brevick, and V.J. Borowski. Vibration reduction in variable displacement engines using pendulum absorbers. In *Proceedings of the SAE Noise and Vibration Conference and Exhibition*, 2003.

[34] Tyler M. Nester. Experimental investigation of circular path centrifugal pendulum vibration absorbers. Master's thesis, Michigan State University, 2002.

[35] E. J. Nestorides. *A Handbook on Torsional Vibration*. Cambridge University Press, 1958.

[36] D. E Newland. Nonlinear aspects of the performance of centrifugal pendulum vibration absorbers. *ASME Journal of Engineering for Industry*, 86:257–263, 1964.

[37] B. Salomon, 1933.

[38] R. R. Sarazin, 1932.

[39] S. W. Shaw and B. K. Geist. Tuning for performance and stability in systems of nearly-tautochronic torsional vibration absorbers. *Journal of Vibration and Acoustics*, 132, 2010.

[40] S. W. Shaw, P. M. Schmitz, and A. G. Haddow. Dynamics of tautochronic pendulum vibration absorbers: Theory and experiment. *Journal of Computational and Nonlinear Dynamics*, 1:283–293, 2006.

[41] S.W. Shaw, M.B. Orlowski, A.G. Haddow, and B. Geist. Transient dynamics of centrifugal pendulum vibration absorbers. In *Proceedings of the 12th International Symposium on Transport Phenomena and Dynamics of Rotating Machinery*, number 2008-20119, Honolulu, HA, 2008.

[42] M. Swank and P. Lindemann. Dynamic absorbers for modern powertrains. *SAE Technical Paper*, (2011-01-1554), 2011.

[43] B. N. Taylor and C. E. Kuyatt. Guidelines for evaluating and expressing the uncertainty of NIST measurement results. `http://physics.nist.gov/Pubs/guidelines/TN1297/tn1297s.pdf`, 1994.

[44] T. Theisen. Gravity's effect on centrifugal pendulum vibration absorbers. Master's thesis, Michigan State University, 2011.

[45] W. T. Thomson and M. D. Dahleh. *Theory of Vibration*. Prentice Hall, 1998.

[46] B. J. Vidmar, S. W. Shaw, B. F. Feeny, and B. K. Geist. Analysis and design of multiple order centrifugal pendulum vibration absorbers. In *The 2012 ASME International Design Engineering Technical Conferences*, 2012.

[47] B.J. Vidmar, B.F. Feeny, S.W. Shaw, A.G. Haddow, B. Geist, and N.J. Verhanovitz. The effects of Coulomb friction on the performance of centrifugal pendulum vibration absorbers. *Nonlinear Dynamics*, 69(1-2):589–600, 2011.